Optical Biosensors; New Aspects in Surface Plasmon Fluorescence Spectroscopy

Amal Kasry

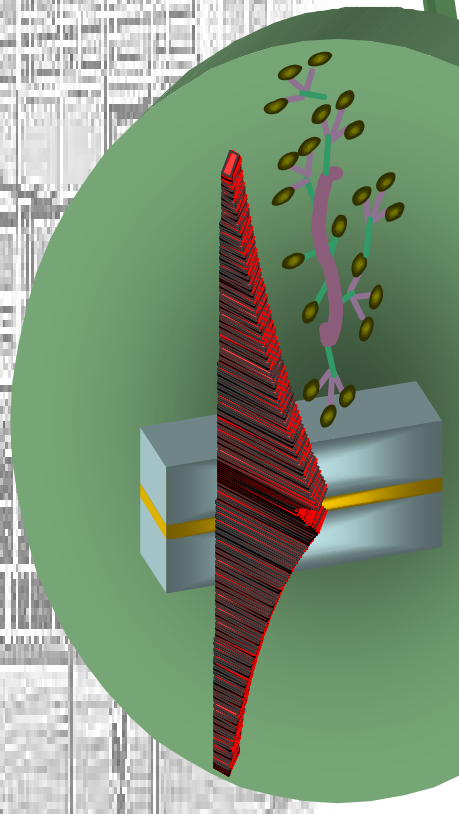

Max Planck Institut für Polymerforschung

Optical Biosensors; New Aspects in Surface Plasmon Fluorescence Spectroscopy

Dissertation zur Erlangung des Grades
'Doktor der Naturwissenschaft'

am Fachbereich Biologie
der Johannes Gutenberg-Universität
in Mainz

vorgelegt von

Amal Kasry
Geboren in Bani-Suef, Egypt

Mainz, February 2006

Dekan: Prof. Dr. H. Paulson

1. Berichterstatter: Prof. Dr. W. Knoll
2. Berichterstatter: Prof. Dr. H. Paulson
3. Berichterstatter: Prof. Dr. H. Decker

Tag der mündlichen Prüfung: 10, Feb. 2006

Die vorliegende Arbeit wurde unter Betreuung von Herrn Prof. Dr. W. Knoll im Zeitraum zwischen Januar 2003 bis Febrauer 2006 am Max-Planck-Institute für Polymerforschung, Mainz,
Deutschland angefergt.

The highest happiness of man... is to have probed what is knowable and quietly to revere what is unknowable.

John Kenneth Gilbraith

To my mother, whose love and support kept me going, and to my father's soul who loved science and made me a science lover!

CONTENTS

Chapter -1-

INTRODUCTION

1. INTRODUCTION

1.1 Biosensors

Biosensors are powerful tools aimed at providing selective identification of toxic chemical compounds at ultra-trace levels in industrial products, chemical substances, environmental samples (e.g., air, soil, and water) or biological systems (e.g., bacteria, virus, or tissue components) for biomedical diagnosis. Combining the exquisite specificity of biological recognition probes and the excellent sensitivity of laser-based optical detection, biosensors are capable of detecting and differentiating big/chemical constituents of complex systems in order to provide unambiguous identification and accurate quantification.

This new technology has many applications, especially in health and medical fields. In health, biosensors can effectively be used to monitor the glucose levels in diabetic patients [1-1]. And in drug discovery, where they can detect the interaction between a particular target and a possible drug without using markers or the detection of colour changes or fluorescence [1-2]. In pathogen detection in food, Biosensor technology can significantly reduce the detection time as well as detect even smaller amounts of pathogens with fewer false positives [1-3]. All these important applications pushed biosensors strongly in the market; the global market for biosensors and other bioelectronics is projected to grow from $6.1 billion in 2004 to $8.2 billion in 2009, at an AAGR (average annual growth rate) of about 6.3% [fig. (1.1)] [1-4].

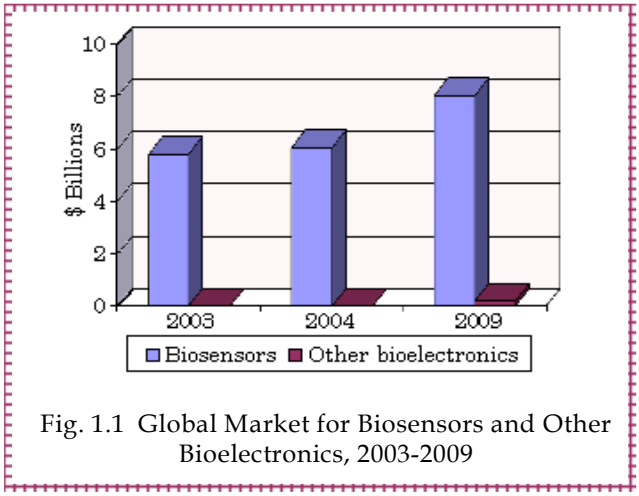

Fig. 1.1 Global Market for Biosensors and Other Bioelectronics, 2003-2009

1-1. "Biosensors & Bioelectronics Abstracts." Biosensors & Bioelectronics". 1997, 12 (1), v - xvi
1-2. Cooper, M A, Nat Rev Drug Discov. 2002, 1(7), p. 515-528
1-3. Cush, R. et al. Biosensors and Bioelectronics 1993, 8, p. 347-354
1-4. Business communications company report, http://www.bccresearch.com/editors/RB-159R.html

A biosensor is simply an analytical device incorporating a biological material that can recognize biological or chemical analytes in solution or in the atmosphere with a physicochemical transducer that produces either discrete or continuous electronic signals proportional to the analyte, this is schematically represented in the figure below.

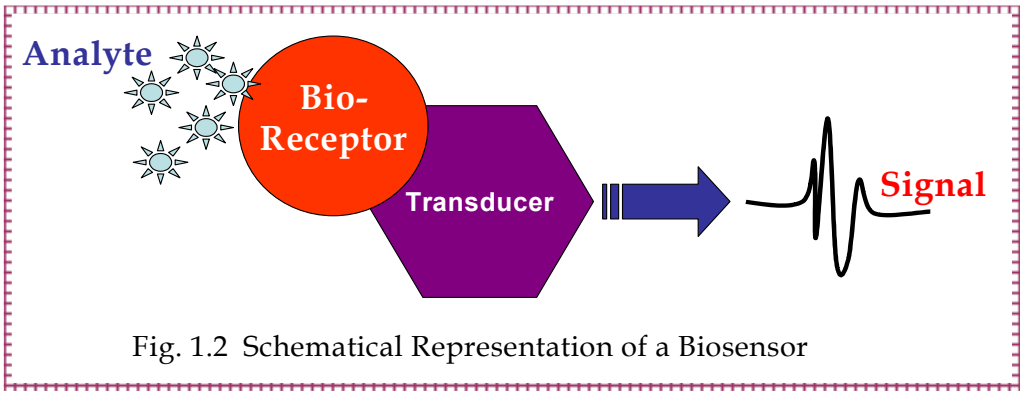

Fig. 1.2 Schematical Representation of a Biosensor

Several basic physical properties of the measuring system, as well as those of the media surrounding the system dictate the optimum design of a biosensor. Some of the most important properties of an ideal biosensor are listed as follows: [1-5]

- Highly sensitive
- Easily calibrated
- Perfectly linear; has a constant sensitivity over different concentration range
- Able to detect lower concentrations
- Has a low background signal
- Highly reversible; should not be affected by its past history of measurements
- Stable; has a constant sensitivity for its entire lifetime
- Selective; responds only to changes in concentration of the target analyte

1.2 Surface Plasmon Sensors

Surface plasmon resonance biosensors are optical sensors exploiting a special electromagnetic waves to probe interactions between an analyte in solution and a biomolecular recognition element immobilized on the surface [1-6]. Surface plasmons are waves that propagate at the interface between a metal and a dielectric according to electron oscillations in the metal. These waves have a combined surface charge and electromagnetic characters; this combined character leads the field perpendicular to the surface to be enhanced near the surface and then decays exponentially at further distances. This field is called evanescent field reflecting the

1-5. Buerk, D.G., *Biosensors: Theory and Applications*. 1993: Technomic Publishing Company.
1-6. Homola, J., *Anal Bioanal Chem*., 2003. 377, p. 528-539.

localized nature of the surface plasmon waves. Based on the fact of the field enhancement at the interface, SPR can be used to measure the change in the refractive index of the media close to the sensor surface, where the change in the refractive index changes the coupling point between the surface plasmons and the incident light.

In addition, the field enhancement at the interface gave the opportunity to use fluorescence molecules placed near the interface, where the fluorescence intensity emitted from the chromophore depends on the optical excitation field and on the probability of the radiative decay from the excited state to the ground state. This was investigated by Liebermann and Knoll at 2000 (1-7). The enhanced localized field was not only used in fluorescence spectroscopy but also in different kinds of spectroscopies, like Raman scattering (1-8), infrared absorption (1-9), and diffraction (1-10).

1.3 Aim of the work

Based on surface plasmon fluorescence spectroscopy in biosensors, this work is divided into two main parts; the first part was concentrating on using grating couplers as biosensors. An easy and fast technique was used to fabricate gratings by embossing, where they were characterized by AFM and SPR. To study the ability of using these gratings as biosensors, it was convenient to study the field enhancement effect on the fluorescence intensity. This effect was studied before in our group on a planar surface, using total internal reflection, the system was studied where the chromophore is placed at different distances and the intensity was measured against air. In our work, the fluorescence intensity was measured in aqueous medium. Since grating couplers have a very high back ground signal, which gives a high bulk signal compared to the surface one in DNA detection, this was the motivation to find a way to eliminate or reduce the bulk signal using the principle of fluorescence resonance energy transfer.

The second part of this work was a detailed investigation of long range surface plasmon resonance spectroscopy, or long range surface plasmon fluorescence spectroscopy. LRSPR was studied before more than 20 years ago as a system that can be of high resolution. The high resolution did not give the system any advantage, but the big advantage was the field intensity at the interface, which is higher than in case of the conventional SPR, and from this point, the idea was that placing chromophores in the vicinity of this high field could give much

1-7. Liebermann, T. and Knoll, W. *Colloids and Surfaces*, 2000 171, p. 115-130
1-8. Campion, A. and Kambhampati, P. *Chem. Soc. Rev.* 1998 27, p. 241-250
1-9. Osawa, M. *Top. Appl. Phys.*2001 81, p. 163-187
1-10. Rothenhäusler, B. and Knoll, W. *Opt. Commun.* 1987 63, p. 301-304

higher fluorescence intensity which means having a very high sensitive system. The sensitivity was proved to be about 10 times higher than in the normal SPR. Another important difference is the decay length of the evanescent field where in LRSPR it can be in the range of 400-800 nm, depending on the refractive index of the first dielectric layer; this long decay length gives the ability of using extended matrices for protein binding. Using an extended matrix of Dextran in the range of 100 nm was also used before in our group in cooperation with Biacore, where 800 aM was reached as a limit of detection of this system. As we found that the signal in case of LRSPR is much higher, we expect that we can reach much lower concentrations with the LRSPR.

2.1 Preface

The fundamental electronic properties of the solid state can be described by the analogy of single electrons moving in a periodic array of atoms. Another different way to go through the solid-state properties is the plasma concept; the word plasma came from treating the free electrons of a metal as an electron liquid of high density of about 10^{23} cm^{-3}, ignoring the lattice in a first approximation.

Surface plasmons can be described in details by Maxwell's theory, which shows that electromagnetic surface waves can propagate along metallic films with a broad spectrum. The dispersion relation of these plasmons lies right of the light line, i.e. the surface plasmons have a longer wavevector than light waves of the same energy, propagating along the surface. These plasmons are called "nonradiative" according to the fluctuations of the surface electron density. Their electromagnetic fields decay exponentially into the medium above the surface, having their maximum at the surface; these waves are called evanescent reflecting their nonradiative nature of them. This is briefly shown in the schematic graph in fig. 2.1 (2-1).

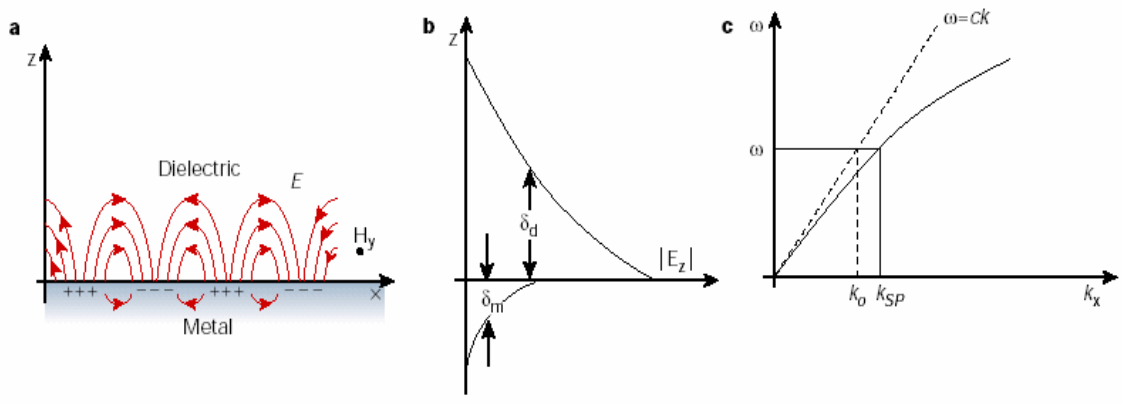

Fig. 2.1 (a) The combined electromagnetic and surface charge character of surface plasmons, (b) the evanescent field decay in the medium above the metal, (c) the mismatch between the wave vectors of the surface plasmons and that of the incident light.

2-1. Barnes et al. *Nature 2003* 424 (6950), P. 824-830

2.2 Surface Plasmon on Smooth Surfaces [2-2]

2.2.1 Fundamental Properties

Talking about surface plasmons cannot be completely understood without talking first about Maxwell's equations, which are related to the dielectric flux density [$\vec{D}$ (cm^{-2})] and magnetic flux density [$\vec{B}$ ($NA^{-1}m^{-1}$)/Tesla], Maxwell's equations are:

$$\nabla \cdot \vec{D} = 0 \quad \nabla \times \vec{E} = -\frac{\partial \vec{B}}{\partial t}$$
$$\nabla \cdot \vec{B} = 0 \quad \nabla \times \vec{H} = \frac{\partial \vec{D}}{\partial t} \qquad \text{-------►} \ \mathbf{2.1}$$

Where,

$$\vec{D} = \varepsilon\varepsilon_0 \vec{E}$$
$$\vec{B} = \mu\mu_0 \vec{H} \qquad \text{-------►} \ \mathbf{2.2}$$

Where ε and ε_o are the dielectric constant and the electric permittivity of free space respectively. μ and μ_o are the magnetic permeability (of the medium) and that of free space, respectively.

The coherent fluctuations of electrons on a metal interface, which are called surface plasma oscillations, were studied by Ritchie [2-3]. The frequency **ω** of these oscillations is tied to its wave vector $\boldsymbol{K_x}$ by a dispersion relation $\boldsymbol{\omega(K_x)}$. As mentioned before, these waves are localized in the z direction and accompanied by a transversal electromagnetic field that disappears as z goes to infinity. This field is described by:

$$E = E_o \exp.\ [\pm i\ (k_x x + k_z z - \omega t)] \qquad \text{-------►} \ \mathbf{2.3}$$

Where + is for $z \geq 0$, and – is for $z \leq 0$, $\boldsymbol{E_z}$ decays exponentially due to the imaginary part $\boldsymbol{K_z}$. $\boldsymbol{K_x} = 2\pi/\lambda_p$ where λ_p is the wavelength of the plasma oscillation. Maxwell's equations yield the retarded dispersion relation for the plane surface with the dielectric function $\boldsymbol{(\varepsilon_1 = \varepsilon'' + i\,\varepsilon''_1)}$ adjacent to a medium $\boldsymbol{\varepsilon_2}$ as air or vacuum.

$$Do = [k_{z1}/\varepsilon_1] + [k_{z2}/\varepsilon_2] = 0 \qquad \text{-------►} \ \mathbf{2.4}$$

$$\varepsilon_i\,(\omega/c)^2 = k_x^2 + k_{zi}^2 \qquad \text{-------►} \ \mathbf{2.5}$$

2-2. Rather, H. *Surface Plasmons* 1988 Springer-Verlag Berlin Heidelberg
2-3. Ritchie, R. H. *Phys. Rev. 1957* 106, P. 874

K_x is continuous through the interface; its dispersion relation is derived as follows:

$z>0$ $H_2 = (0, H_{y2}, 0) \exp i\,(k_{x2}x + k_{z2}z - \omega t)$
$E_2 = (E_{x2}, 0, 0\ E_{z2}) \exp i\,(k_{x2}x + k_{z2}z - \omega t)$

$z<0$ $H_1 = (0, H_{y1}, 0) \exp i\,(k_{x1}x + k_{z1}z - \omega t)$
$E_1 = (E_{x1}, 0, 0\ E_{z1}) \exp i\,(k_{x1}x + k_{z1}z - \omega t)$ ⟶ **2.6**

Where k_{x1} and k_{x2} are the wave vectors in the x direction and k_{z1} and k_{z2} are those in the z direction. Considering the continuity relations:

$E_{x1} = E_{x2}$ ⟶ **2.7**

$H_{y1} = H_{y2}$ ⟶ **2.8**

$\boldsymbol{\varepsilon_1} E_{z1} = \boldsymbol{\varepsilon_2} E_{z2}$ ⟶ **2.9**

Inserting the last three equations in 2.6, we obtain:

$k_{x1} = k_{x2} = k_x$

in vacuum (or air as a first approximation), **$\varepsilon=1$, $\mu=1$ and $\lambda = 2\pi c/\omega$, $k = 2\pi/\lambda = \omega/c$**, then:

$$c = 1/\sqrt{\mu_0 \varepsilon_0}$$ ⟶ **2.10**

Equation 2.10 together with 2.6 can be inserted in 2.1 to give:

$$+k_{z1} H_{y1} = -\frac{\omega}{c}\varepsilon_1 E_{x1}$$

$$+k_{z2} H_{y2} = +\frac{\omega}{c}\varepsilon_2 E_{x2}$$ ⟶ **2.11**

To obtain a solution, the determinant D_o has to be zero

$$\frac{k_{z1}}{\varepsilon_1} + \frac{k_{z2}}{\varepsilon_2} = 0$$ ⟶ **2.12**

From eqn. 2.12, it is revealed that SP can exist at the boundary between two materials having dielectric constants of opposite signs, and together with the continuity relation, we can get:

$$k_x^{\,2} + k_{zi}^{\,2} = \varepsilon_i \left(\frac{\omega}{c}\right)^2 \qquad \text{-------►} \quad \mathbf{2.13}$$

Now, the dispersion relation can be derived to be:

$$k_x = \frac{\omega}{c}\left(\frac{\varepsilon_1 \varepsilon_2}{\varepsilon_1 + \varepsilon_2}\right)^{1/2} \qquad \text{-------►} \quad \mathbf{2.14}$$

In the case of the dielectric ($\varepsilon_1 > 0$, medium 1)/metal ($\varepsilon_2 = \varepsilon_2' + i\,\varepsilon_2''$, medium 2) interface, and assuming $\boldsymbol{\varepsilon_2'' < |\,\varepsilon_2'\,|}$, the complex kx is expressed by:

$$k_x = k_x' + i k_x'' \qquad \text{-------►} \quad \mathbf{2.15}$$

$$k_x' = \frac{\omega}{c}\left(\frac{\varepsilon_1 \varepsilon_2'}{\varepsilon_1 + \varepsilon_2'}\right)^{1/2} \qquad \text{-------►} \quad \mathbf{2.16}$$

$$k_x'' = \frac{\omega}{c}\left(\frac{\varepsilon_1 \varepsilon_2'}{\varepsilon_1 + \varepsilon_2'}\right)^{3/2} \frac{\varepsilon_2''}{2\varepsilon_2'^{2}} \qquad \text{-------►} \quad \mathbf{2.17}$$

2.2.2 Spatial Extension of SP Fields

From the dispersion relation mentioned above, and assuming that $\boldsymbol{|\,\varepsilon_2'\,| > \varepsilon_1}$:

$$k_{z1}^{\,2} \approx \left(\frac{\omega}{c}\right)^2 \left(\frac{\varepsilon_1^{\,2}}{\varepsilon_1 + \varepsilon_2'}\right) \qquad \text{-------►} \quad \mathbf{2.18}$$

$$k_{z2}^{\,2} \approx \left(\frac{\omega}{c}\right)^2 \left(\frac{\varepsilon_2'^{2}}{\varepsilon_1 + \varepsilon_2'}\right) \qquad \text{-------►} \quad \mathbf{2.19}$$

The wave vectors k_{z2} and k_{z1} are imaginary due to the relations $\boldsymbol{(\omega/c) < k_x}$ and $\boldsymbol{\varepsilon_1' < 0}$, so that the field amplitude of the SP's decreases exponentially as $\boldsymbol{\exp(-|k_{zi}||z|)}$, normal to the surface. The value of the skin depth at which the field falls to 1/e, becomes

$$\hat{z} = \frac{1}{|k_{zi}|} \qquad \text{-------►} \quad \mathbf{2.20}$$

The intensity of SPs propagating along the metal/dielectric interface (x-axis) decreases as

$$E_x \propto e^{-2|k_x''|x}$$

Therefore, the propagation length $\mathbf{L_x}$ is:

$$L_x = \frac{1}{2|k_x''|} \qquad \text{-------▶ 2.21}$$

2.3 Excitation of Surface Plasmons by Light

The most remarkable difficulty to excite SP by photons is that the dispersion relation lies right to the light line **(k_x > ω/c)**. At a given photon energy, the **ħω**, the wave vector **ħω/c** has to be increased by **Δk_x** value in order to transform the photons into SPs. To achieve this, there are two methods [2-4]:

2.3.1 Excitation of Sp by Total Internal Reflection

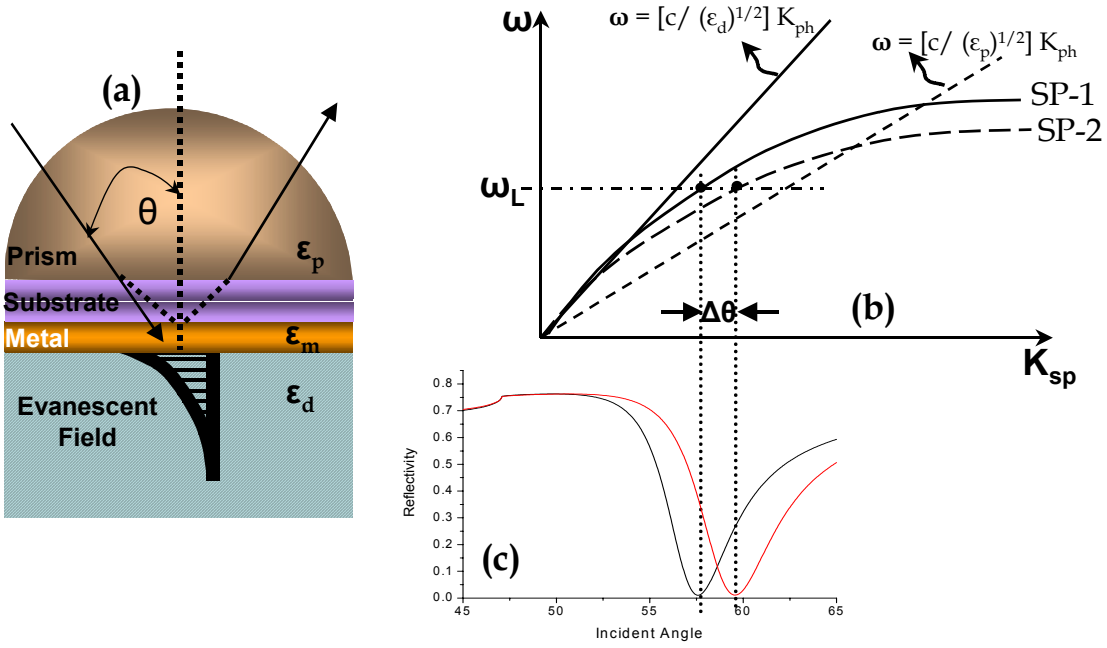

Fig. 2.2 (a) Attenuated total reflection construct for the Kretschmann-Raether configuration with a refractive-index-mismatch between the prism and the substrate, (b) The dispersion relation of free photons in a dielectric and in a coupling prism, and that of SP before (SP-1) and after (SP-2) adsorption, (c) The reflectivity as a function of the incident angle representing the resonant coupling

2-4. Knoll, W. *Annu. Rev. Phys.* Chem. 1998, 49, P. 569-638

To overcome the problem of momentum mismatch, two different prism configurations were introduced, Otto-configuration [2-5], where photons are not coupled directly to the metal dielectric interface but via the evanescent tail of light totally internally reflected at the base of a high index prism **($\varepsilon_p > \varepsilon_d$)**, this light is characterized by a larger momentum. This means that by choosing the appropriate incident angle, resonant coupling between evanescent photons and surface plasmons can be obtained.

The resonant coupling can be observed experimentally by monitoring the intensity of the reflected light from the base of the prism as a function of the angle of incidence, this would be shown as a sharp minimum (fig. 2.2 (c)).

Kretschmann and Rather introduced the other prism configuration [2-6], In this technique, the high momentum photons in the prism couple through a very thin metal layer (45-50 nm thick) evaporated onto the base of the prism or onto a glass slide index matched to the prism base (fig. 2.2 (a)). The increase of the momentum of the light is shown as the dashed line in fig. 2.2 (b). The thickness of the metal layer influences the coupling angle as well as the coupling efficiency, e.g., the minimum reflectivity. This dependence can be simulated by Fresnel's equations. In case of adsorption of molecules of different refractive index on the metal surface, the surface plasmon wave vector changes leading to the change of the resonant coupling. This leads to different minimum angle of reflectivity, also shown in fig. 2.2 (b and c).

2.3.2 Excitation of Sp by Grating Couplers

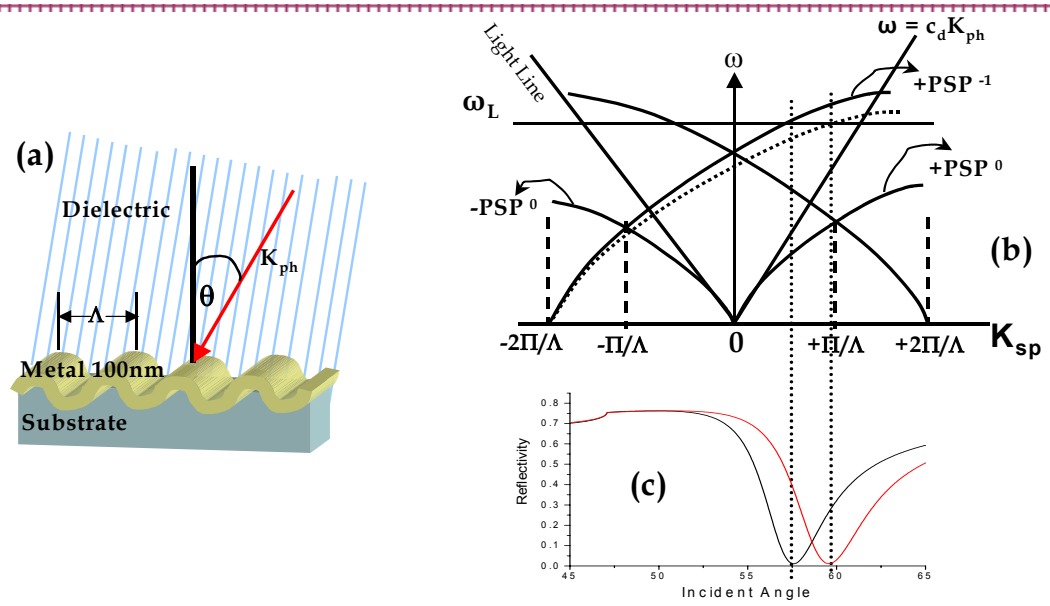

Fig. 2.3 (a) Coupling of photon with wave vector $\mathbf{K_{ph}}$ to a metallic grating with Λ grating constant, (b) the dispersion relation of the surface plasmons on metallic gratings showing the dispersion branches **+PSP ^{0} and -PSP ^{0}** at $\mathbf{K_{sp}} = 0$, (c) the change in the coupling point accompanied with resonance angle shift due to surface absorption

2-5. Otto, A. *Z. Phys.* 1968, 216, P. 398-409
2-6. Kretschmann, E and Raether, H *Z. Naturforsch. Teil. A* 1968, 23, P. 2135-2136

Another configuration to overcome the momentum mismatch problem is the coupling mechanism in a metal/ dielectric interface that is periodically corrugated. Such a metallic grating structure is used in spectrometers as the dispersive element where it optically excites PSP, known as Wood's anomaly [2-2].

As indicated mathematically by a Rayleigh expansion (approximation for shallow grating [2-7]), the surface periodic structure can also enhance the wave vector of the incident light for resonance coupling. As shown in Figure 2.3, light ($k_{ph}= \omega/c$) from the dielectric (ε_d) hits a metallic grating (ε_m) with a grating constant Λ at an incident angle θ. Assuming the dispersion property of the SP wave is not disturbed by the corrugated surface, the momentum matching condition can be written as:

$$k_x = k_{ph,x} \pm mg = \frac{\omega}{c}\sqrt{\varepsilon_d}\sin\theta \pm mg = \frac{\omega}{c}\sqrt{\frac{\varepsilon_d \varepsilon_m}{\varepsilon_d + \varepsilon_m}} = k_{sp,x} \qquad \text{-------} \blacktriangleright \quad \mathbf{2.22}$$

Where m the order of diffraction and ($g = 2\pi/\Lambda = k_g$) is the grating wave vector. The resonance can be also observed as a minimum in the reflected light when monitored as a function of incident angle or wavelength. It is important to notice that the grating constant should be in the same order of magnitude as the wavelength of the incoming light.

The reverse process can also take place. SPs propagating along a grating or a rough surface can reduce their wave vector k_x by ΔK_x so that the SP is transformed into light. This is shown in fig. 2.4. This coupling of photon with SP via roughness plays an important rule as reported by Teng and Stern [2-8], where this radiation can be used as a detector for SPs; if the SP is excited to its maximum value, the emitted intensity passes a maximum too.

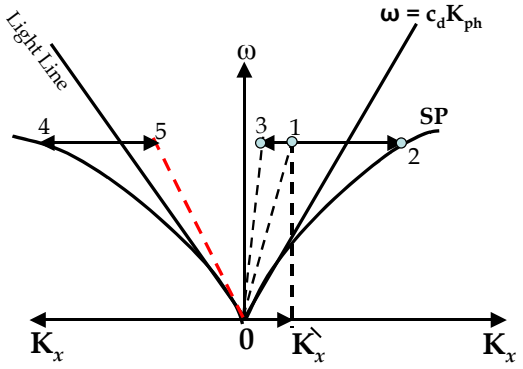

Fig. 2.4 The process 1→2 is the transformation of the incoming light into surface plasmons, the interaction 1→3 via roughness leads to light scattering inside the light cone. The process 4→5 describes the decay of SP into light via ΔK_x, it is the reverse of 1→2.

2-7. Kazandjian, L. *Phys. Rev.* 1996, E 54, P. 6902-6815.
2-8. Teng, Y. and Stern, E. A. *Phys. Rev. Lett.* 1967, 19, P. 511

2.4 Field Enhancement Due to SPs

At the incident angle where the reflectivity has its lowest value, the intensity of the electromagnetic field reaches its maximum at the interface. The enhancement value is given by the ratio of the field intensity on the metal at the air/dielectric $|\mathbf{H_y(2/1)}|^2$ side divided by the incoming field intensity $|\mathbf{H_{y0}(0/1)}|^2$

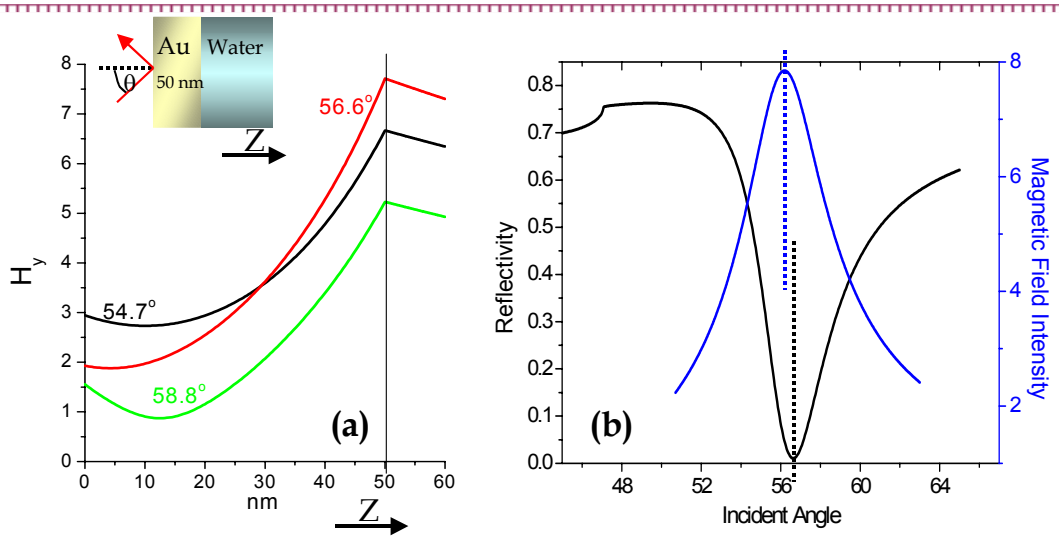

Fig. 2.5 (a) The electromagnetic field intensity (H_y) inside the metal layer (Au 50 nm) at different incident angles, the field enhancement at the interface is maximum at the resonance angle, (b) The enhancement factor of Au 50 nm

Fig. 2.5 (a) shows the field intensity at the interface at different angle of incidence, and it shows that the field has its maximum value at the resonance angle. In general, the interest is more in the maximum enhancement of the electric field intensity, which is obtained from:

$$\left(\frac{|H_y(2/1)|^2}{|H_{y0}(0/1)|^2} \right)_{max} \quad \frac{\varepsilon_2}{\varepsilon_1} \left(\frac{|E(2/1)|^2}{|E0(0/1)|^2} \right)_{max} \qquad \text{-------} \blacktriangleright \ \mathbf{2.23}$$

Fig. 2.5 (b) shows the enhancement factor in case of calculating the field intensity at the interface as a function of the incident angle, where it is obvious that the field is maximum if the reflectivity is in its minimum value. The enhancement can also be derived in an obvious manner by applying energy conversation [2-9].

An interesting observation is the slight shift of the maximum field intensity toward a smaller angle than the minimum reflectivity. This phenomenon can be explained by considering the system as a resonator driven by the incoming light [2-10, 2-11]. The metal imaginary part of the dielectric constant ($\boldsymbol{\varepsilon''}$) is the lossy

2-9. Weber, W. H. and Ford, G. W. *Optics Letters* 1981, 6, P. 122
2-10. Liebermann, T. and Knoll, W. *Colloid Surf. A.* 2000, 171, P. 115–130.
2-11. Nemetz, A. and Knoll, W. *J. Raman Spectrosc.* 1996, 27, P. 587–592.

component of the resonator which separates the coincidence of the resonance. The larger the ε″, the greater the angle shift.

2.5 Fluorescence

There has been a remarkable growth in the use of fluorescence in the biological science. Fluorescence spectroscopy is primarily research tool in biochemistry and biophysics, but now it is also used in environmental monitoring, DNA sequencing, and genetic analysis by fluorescence in situ hybridisation.

2.5.1 Phenomenon of Fluorescence

Luminescence is the emission of light from any substance and occurs from electronically excited states. The processes, which occur between the absorption and emission of light, are usually illustrated by a Jablonski diagram [2-12].

A Jablonski diagram is shown in fig. 2.6. The singlet ground, first and second electronic states are represented by S_0, S_1, and S_2 respectively. Following light absorption, several processes take place. The fluorophore is excited to a higher vibrational level of either S_1 or S_2. Molecules in condensed phases rapidly relax to the lowest vibrational level of S_1, this process is called internal conversion and it occurs in 10^{-12} s or less. Since fluorescence lifetimes are typically 10-8 s, internal conversion is completed prior to emission. Hence, fluorescence emission generally results from a thermally equilibrated excited state, that is, the lowest energy vibrational state of S_1.

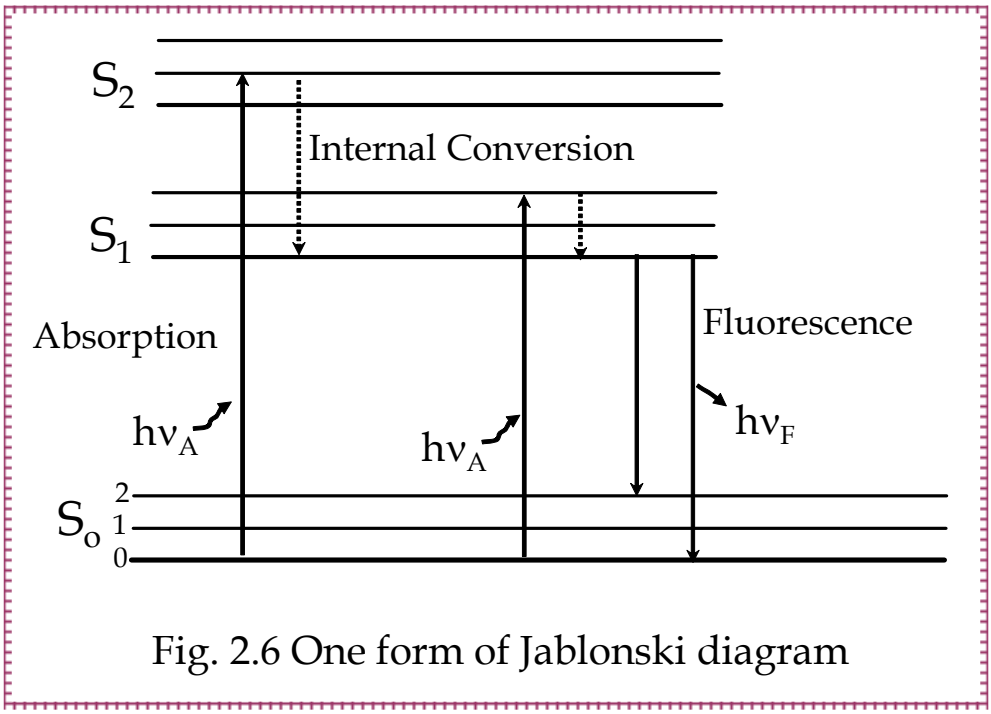

Fig. 2.6 One form of Jablonski diagram

2-12. Joseph R. Lakowicz *Principles of Fluorescence Spectroscopy* 1999 (2nd edition) Kluwer Academic/Plenum Publishers, New York.

Return to the ground state typically occurs to a higher excited vibrational ground state level, which quickly reaches thermal equilibrium. An interesting consequence of emission to higher vibrational ground states is that the emission spectrum is typically a mirror image of the absorption spectrum of the $S_o \rightarrow S_1$ transition. The similarity occurs because electronic excitation does not greatly alter the nuclear geometry. Hence, the spacing of the vibrational energy levels of the excited states is similar to that of the ground state. As a result, the vibrational structures seen in the absorption and emission spectra are similar. Examination of the Jablonski diagram reveals that the emission energy is typically less than the absorption one, so fluorescence occurs at lower energies or longer wavelengths.

The most important characteristics of a fluorophore are the fluorescence lifetime and quantum yield. Quantum yield is the number of emitted photons relative to the number of absorbed photons. This process is governed by the emissive rate of fluorophore (Γ) and the rate of nonradiative decay to S_0 (K_{nr}). The quantum yield is given by:

$$Q = \frac{\Gamma}{\Gamma + K_{nr}} \qquad \text{-------▶ } \mathbf{2.24}$$

The life time is also important as it determines the time available for the fluorophore to interact with its environment, in other words, it can be defined as the average time the molecule spends in the excited state prior to return to the ground state. Generally, fluorescence lifetimes are near 10 ns. The life time can be given by:

$$\tau = \frac{1}{\Gamma + K_{nr}} \qquad \text{-------▶ } \mathbf{2.25}$$

2.5.2 Fluorescence Quenching

Quenching is the decrease of the fluorescence intensity due to a wide variety of processes. Quenching can be collisional or static. Collisional quenching occurs when the excited state fluorophore is deactivated by contact with some other molecule in solution, which is called the quencher. For this kind of quenching, the decrease in intensity is described by the Stern-Volmer equation:

$$I_o/I = 1 + K\,(Q) = 1 + K_q \tau_o\,(Q) \qquad \text{-------▶ } \mathbf{2.26}$$

Where I_o is the fluorescence intensity in the absence of the quencher, I is the intensity in the presence of the quencher at concentration Q. K_q is the rate of collisional quenching and τ is the life time.

Static quenching occurs when fluorophores form nonfluorescent complexes with quenchers. This process occurs in the ground state and does not rely on diffusion or molecular collisions.

2.5.3 Fluorescence Resonance Energy Transfer

An important process that occurs in the excited state is the fluorescence resonance energy transfer (FRET). This process occurs whenever the emission spectrum of a fluorophore (the donor) overlaps with the absorption spectrum of another molecule (the acceptor). The acceptor does not need to be fluorescent; RET does not involve emission of light by the donor. There is not intermediate photon in RET, the donor and acceptor are coupled by dipole-dipole interaction. The extent of energy transfer is determined by the distance between the donor and the acceptor and the extent of the spectral overlap. The spectral overlap is descried in terms of the Förster distance (R_o). The rate of energy transfer $K_T(r)$ is given by:

$$K_T(r) = \frac{1}{\tau_D}\left(\frac{R_o}{r}\right)^6 \qquad \text{-------▶ 2.27}$$

Where r is the distance between the donor and the acceptor, and τ_D is the life time of donor in the absence of energy transfer. The efficiency of energy transfer for a single donor-acceptor pair at a fixed distance is:

$$E = \frac{R_o^6}{R_o^6 + r^6} \qquad \text{-------▶ 2.28}$$

The Förster distances are comparable in size to biological macromolecules, so energy transfer can be used as a spectroscopic ruler for measurements of distance between sites on proteins. FRET is concisely represented in fig. 2.7.

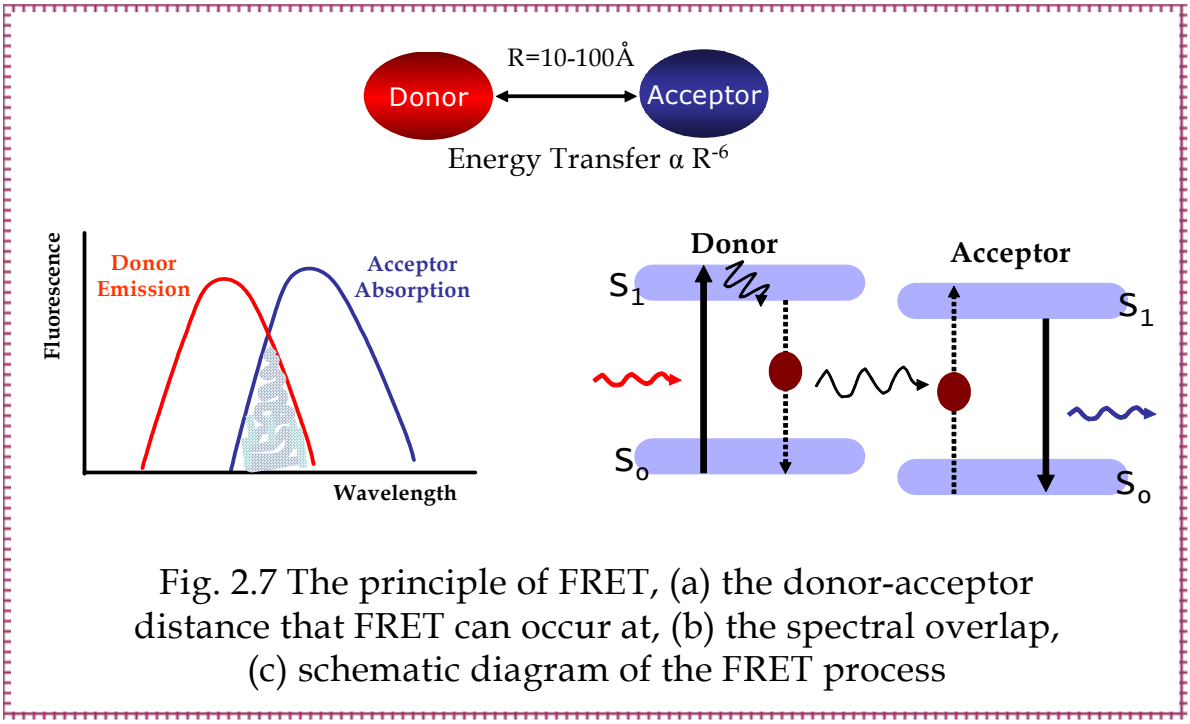

Fig. 2.7 The principle of FRET, (a) the donor-acceptor distance that FRET can occur at, (b) the spectral overlap, (c) schematic diagram of the FRET process

2.5.4 Photobleaching

Photobleaching is a process referred to the decrease in the emission intensity of the fluorophore due to going through numbers of excitation-relaxation cycles. Generally speaking, the photobleaching involves the generation of reactive oxygen molecules, thus it is sometimes useful to introduce antioxidants or to use anoxic conditions. On the other hand, the rate of the photobleaching is often proportional to the intensity of illumination.

2.5.5 Combining Fluorescence with SPR

As explained previously, the excitation of SP is accompanied by electromagnetic field enhancement at the interface and exponential decay at further distances. This means that a fluorophore can be excited, if placed in the vicinity of this field. The fluorophore should be within the decay length of the evanescent field which is several tens to hundreds of nanometers depending on the wavelength. This makes the detection to be surface sensitive and this is the category where SPFS [2-10] and TIRF [2-13] belong to.

Using surface plasmon evanescent waves to excite the fluorophores located at the interface has two advantages. Firstly, the enhanced evanescent field excited by SPR exhibits greatly enhanced intensity. Secondly, the semitransparent metal film acts as an efficient blocker to reduce the background contribution from the excitation light source. However, introducing the metal layer alters the way an excited fluorophore loses its energy. As reviewed, there are additional decay channels which are contributing to the decrease of the radiative quantum yield of the emitters (fluorophores) and they take place at different dye-metal separations (fig. 2.8) [2-14].

If the dye is placed within 10 nm distance from the metal, the dominating process is the nonradiative decay of fluorescence. The excitation is assumed to be due to dipole-dipole interaction, where the Förster model, depending on the dye-metal separation, applies to. The transferred energy dissipated by the metal is converted into heat.

At an intermediate-distance regime (a few nm up to ~20 nm), a significant fraction of excited fluorescence couples back to surface plasmon polaritons, by fulfilling momentum-matching conditions. SPP modes can be converted again into photons by a coupling-prism or a grating, which allows for the monitoring of SPP decay channel [2-15].

2-13. Axelrod, D. et al. *Annu. Rev. Biophys. Bio.* 1984, 13, P. 247-268.
2-14. Barnes, W. L. *J. Mod. Optics* 1998, 45, P. 661-699
2-15. Knobloch, H. et al. *J. Chem. Phys.* 1993, 98, P. 10093-10095.

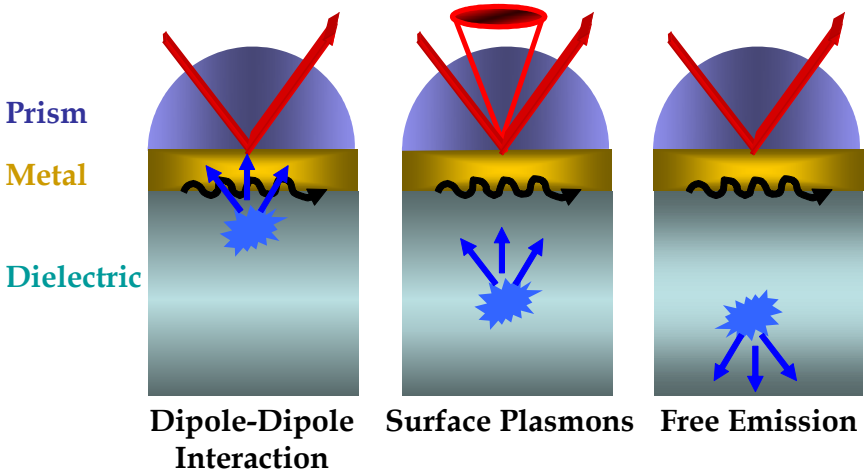

Fig. 2.8 A schematic representation of the behavior of a fluorophore close to a metal-dielectric interface, different decay channels take place at different distances from the metal

At separation distances (>20 nm), the dominating process is the free emission of the dyes. However, in this distance, two important parameters should be taken into consideration. The first one is the oscillation of the fluorescence emission with increasing distance from the metal, and this is because the metal reflects the fluorescence field and introduces light interference. The second one is the weakness of the evanescent field as the distance increases, which, as a consequence, decreases the fluorescence intensity.

2.6 Kinetic Interaction Analysis

The evanescent wave biosensors offer the possibility of monitoring the kinetics of a biomolecule in a solution interacting with another biomolecule immobilized on the surface. The treatment of this situation starts from a simple 1:1 interaction model [2-16] based on the Langmuir adsorption isotherm [2-17]. This isotherm is based on three basic assumptions:

- A monolayer is homogenously covering the surface
- All sites are equivalent and the surface is uniform
- The ability of a molecule to adsorb at a given site is independent of the occupation of the neighboring sites.

Based on these assumptions, the dynamic equilibrium would be:

2-16. Schuckannu, P. *Rev. Biophys. Biomol. Struct.* 1997 26, P. 541–566.
2-17. Atkins, P. W. *Physical Chemistry. 6th edition* 1998, P. 858-859.

$$A + B \underset{k_{off}}{\overset{k_{on}}{\Leftrightarrow}} AB \qquad \text{------►} \quad \textbf{2.29}$$

Where A and B are the molecules in solution and on the surface respectively. The forward and reverse rate are described by the adsorption or association rate constant (K_{on}) and desorption or dissociation rate constant K_{off}.
The association rate is:

$$\frac{d[AB]}{dt} = k_{on}[A][B] \qquad \text{------►} \quad \textbf{2.30}$$

and the dissociation rate is:

$$-\frac{d[AB]}{dt} = k_{off}[AB] \qquad \text{------►} \quad \textbf{2.31}$$

Because of the dynamic equilibrium of both processes, both rates are equal to each other:

$$k_{on}[A][B] = k_{off}[AB] \qquad \text{------►} \quad \textbf{2.32}$$

From this, the equilibrium constants can be expressed by two constants:
The dissociation constant K_D

$$K_D = \frac{[A][B]}{[AB]} = \frac{k_{off}}{k_{on}} \qquad \text{------►} \quad \textbf{2.33}$$

and the affinity constant K_A

$$K_A = \frac{[AB]}{[A][B]} = \frac{k_{on}}{k_{off}} \qquad \text{------►} \quad \textbf{2.34}$$

Beside the interaction between A and B, there is also the transport of A from the solid to the interface (diffusion and convection) which should be taken into account. A simple model for a biomolecular interaction at the solid-water interface is shown below.

$$\xrightarrow{k_f}$$

$$A_{bulk} \underset{k_m}{\overset{k_m}{\Leftrightarrow}} A_{surface} + B \underset{k_{off}}{\overset{k_{on}}{\Leftrightarrow}} AB$$

$$\xleftarrow{k_r}$$

2.7 Description of SPR Instrument

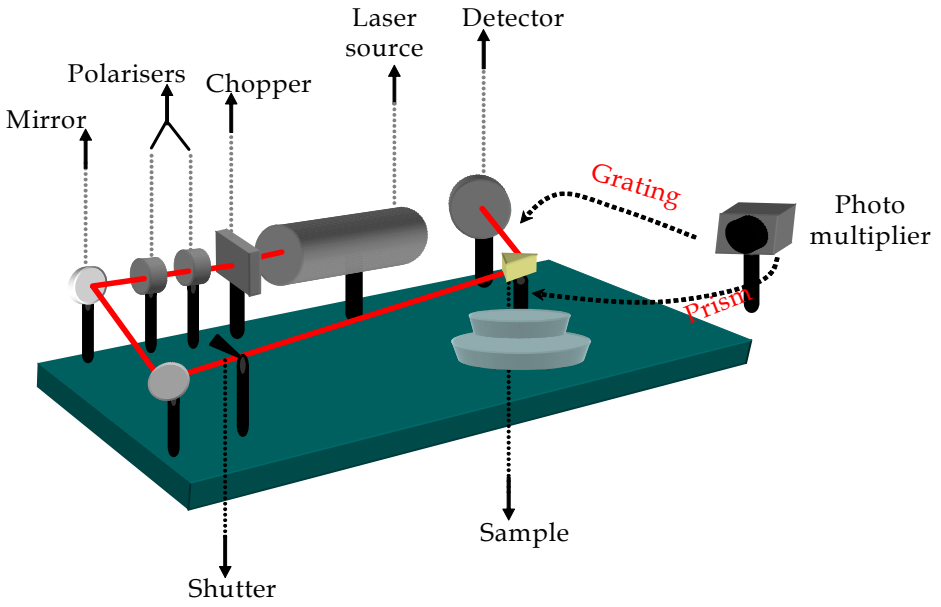

Fig. 2.9 A typical SPR set up, the position of the photomultiplier depends on the kind of sample, in case of gratings, it is placed in the front side, and in case of the prism, it is placed in the back side

Fig. 2.9 is a typical SPR set up, where a He-Ne laser with wavelength λ = 662.8 nm was used. The laser light is passing through a chopper. And then through two polarizers, the first is to control the light intensity and the other is to have P-polarized light. Mirrors are used according to the size of the set up; the light can go directly to hit the sample. In our case, the light passes through two mirrors before hitting the sample. The reflected light is then detected by a photodiode. Both the sample and the photodiode are fixed on a θ-2θ goniometer, where they can move individually or together. A photomultiplier is used to measure the fluorescence intensity. In case of using grating couplers (fig. 2.10), the photomultiplier is fixed in the front side of the sample together with the photodiode, and the definition of the angle is changed according to using any of them. In case of using the prism the SPR elements are placed as in fig. 2.11.

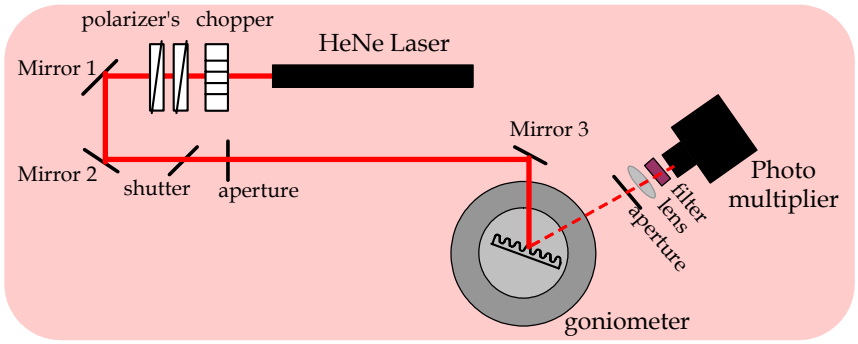

Fig. 2. 10 In plane look to the SPR set up in case of the grating

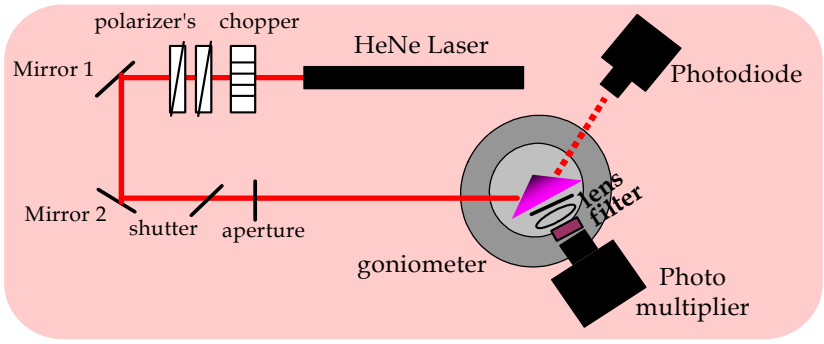

Fig. 2. 11 In plane look to the SPR set up in case of the prism

Chapter -2-

SURFACE PLASMON FLOURESCENCE SPECTROSCOPY

3. GRATINGS; FABRICATION AND CHARACTERIZATION

3.1 Preface

There is a long history behind gratings, starting at 1785 from the American astronomer Rittenhouse, who didn't use it for any serious applications.

In 1821, unaware of the earlier American report, Joseph von Fraunhofer began his work on diffraction gratings. Fraunhofer's persistence resulted in gratings of sufficient quality to enable him to measure the absorption lines of the solar spectrum. He also derived the equations that govern the dispersive behavior of gratings.

About 1870, the scene of grating development returned to America, where L.M. Rutherfurd, a New York lawyer with an avid interest in astronomy, became interested in gratings. In just a few years, Rutherfurd learned to rule reflection gratings in speculum metal that were far superior to any that had been made before. Rutherfurd developed gratings that surpassed even the most powerful prisms.

In 1947, Bausch & Lomb decided to make precision gratings available commercially. In 1950, they succeeded in producing their first high quality grating. A high fidelity replication process was subsequently developed, which was crucial to making replicas, duplicates of the tediously generated master gratings. A most useful feature of modern gratings is the availability of an enormous range of sizes and groove spacings (up to 10,800 grooves per millimeter), and their enhanced quality is now almost taken for granted. In particular, the control of groove shape (or blazing) has increased spectral efficiency dramatically [3-1].

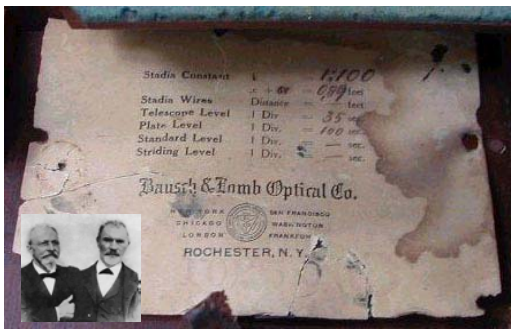

Bausch & Lomb, 1947

As shown in fig. 3.1, gratings can be of different shapes, they can be sinusoidal, square, rectangular…etc. They can also be a group of grooves on a substrate or a group of hole arrays.

3-1. Palmer, C. *Diffraction Grating Handbook* Fifth Edition, THERMO RGL http://www.gratinglab.com/

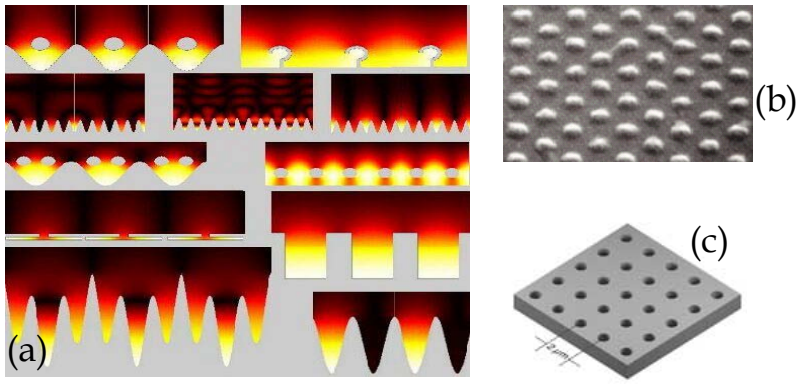

Fig. 3.1 (a) Different shapes of gratings, (b) Group of grooves on a substrate, (c) Group of hole arrays

When monochromatic light is incident on a grating surface, it is diffracted into discrete directions. Each grating groove can be pictured as being a very small, slit-shaped source of diffracted light. The light diffracted by each groove combines to form a diffracted wave front. The usefulness of a grating depends on the fact that there exists a unique set of discrete angles along which, for a given spacing *d* between grooves, the diffracted light from each facet is in phase with the light diffracted from any other facet, so they combine constructively.

Gratings have many advantages:

- They have a light weight and they are easy to install.
- They can be fabricated by an easy and cheap way.
- They have wide applications in the field of spectroscopy.
- They have sensitivity to meet sensing demands.

3.2 Grating Preparation

Many different methods can be used to fabricate gratings, like e-beam lithography [3-2], x-ray lithography [3-3], contact printing [3-4], but hot embossing on polymers [3-2] is known to be the method that perturbs the polymer the least.

3.2.1 Ion Beam Etching

Ion beam etching technique is one of the most reliable methods to fabricate gratings. The principle of this method is based on transferring the structure to the glass substrate through a thin photoresist layer. Fig. 3.2 shows concisely the ion beam procedure, the procedure goes as follows:

3-2. Poppeller, M. et al. *Microelectronic Engineering* 1999, 46, P. 183-186
3-3. Steward, K. J. et al. *J. Vac. Sci. Technol. (B)* 1989, 7(6), P. 1734-1739
3-4. Branch, D. W. et al. *Med. Biol. Eng. and comput.* 1998, 36, P. 135-141

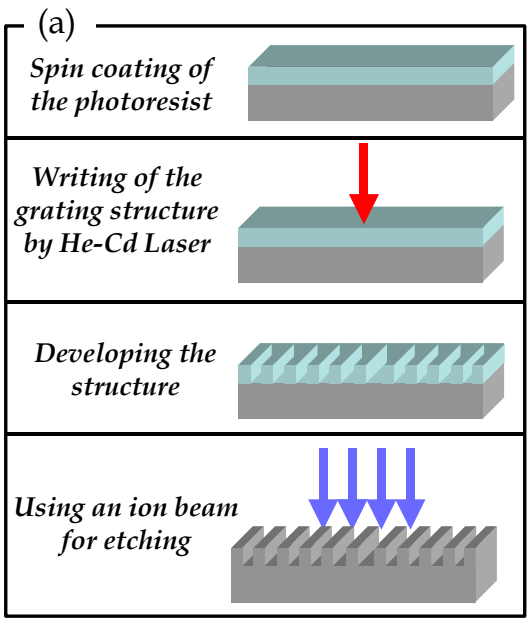

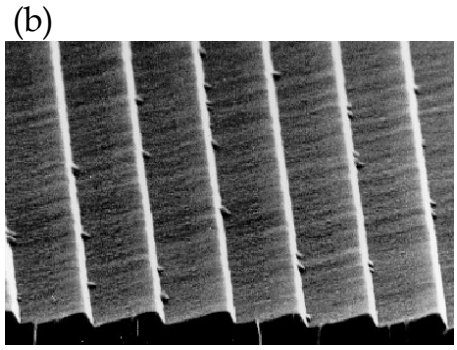

Fig. 3.2 (a) Ion beam etching procedure, (b) an example of saw-tooth grating in silicon fabricated with lithography and ion beam etching.

- A photoresist is spin coated above the glass substrate.
- Using He-Cd laser, the structure is written on the photoresist by using a mask with the desired structure, and let the laser light hit the sample for sometime. Then, the structure is developed.
- The last step is exposing the sample to the ion beam, where the structure is being transferred to the glass substrate.

This method is not as easy as it seems from this fast description, rather it is difficult, expensive, and takes a lot of time. In addition to that, the most important problem is that it is difficult (almost impossible) to get two samples with the same parameters even with taking care of that. This makes the comparison for a series of experiments not easy and the only option is to use the same sample more than one time for many experiments, which is not preferable.

From the last disadvantage about ion beam etching, there was the idea of embossing, where one of the etched gratings can be used to fabricate a large number of embossed gratings, where all have the same parameters. This makes the comparison for a series of experiments easier and also these samples can be used as disposable samples.

3.2.2 Embossing Technique

The embossing principle is based on transferring the structure to the polymer by softening. Softening is achieved by both temperature and pressure. So, to imprint a surface, three basic components are required:

a. A stamp with suitable feature sizes, prepared by, for example, ion-beam etching.

b. The material to be printed, like a layer of polymer of few hundred nanometers, with suitable glass transition temperature (T_g) and molecular weight.

c. The equipment for printing, with adequate control of temperature, pressure, and parallelism of the stamp and the substrate.

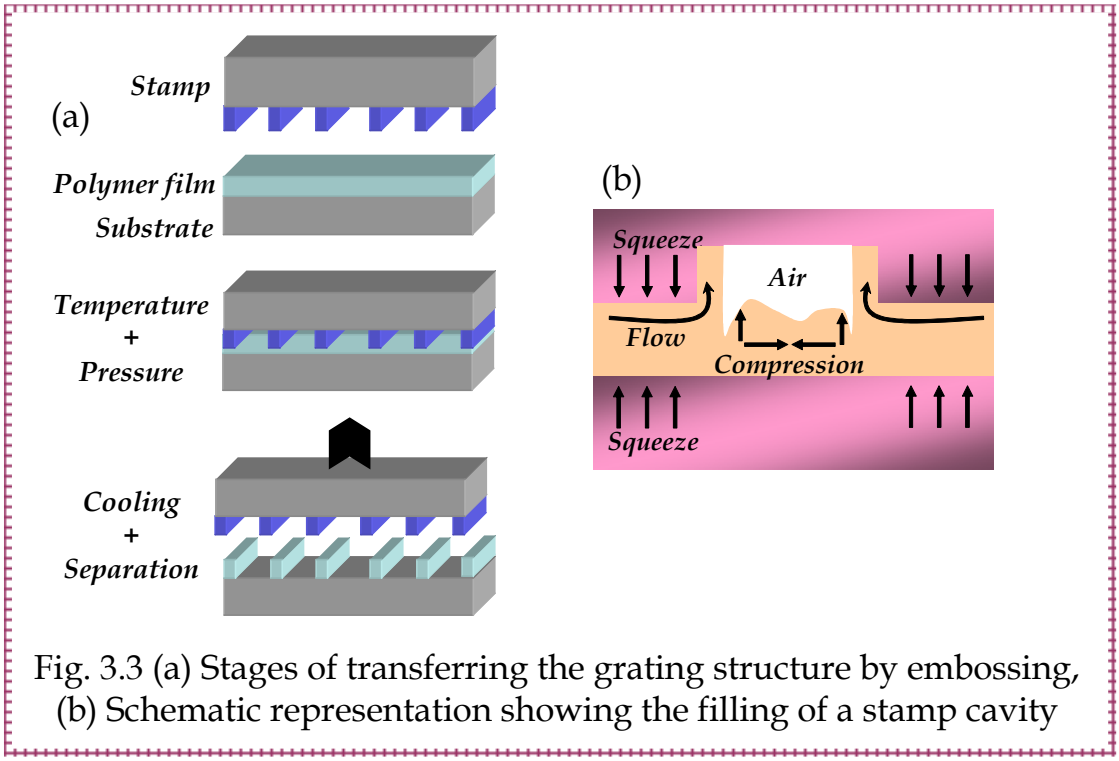

Fig. 3.3 (a) Stages of transferring the grating structure by embossing, (b) Schematic representation showing the filling of a stamp cavity

Fig. 3.3 (a) shows the embossing procedure, which has two basic steps. The first is the imprint step in which a stamp (with the structure on its surface) and the polymer thin film on a substrate are heated up above the T_g of the polymer and then the stamp is pressed into the polymer film. As the stamp is compressed, the viscous polymer is forced to flow into the cavities. The important parameters in this procedure are (1) the temperature, (2) the pressure, and (3) the embossing time, three of them have to be chosen so that the polymer completely fills the cavities of the stamp during embossing. This step duplicates the structures on the stamp in the polymer film. The second step would be cooling the polymer to a temperature below T_g so that it is sufficiently hard to be demoulded.

In this case, both the temperature and the time depend on the polymer layer thickness. Notice also that both the stamp and the polymer film have to be heated.

3.3 Embossing on Polymer Substrates

In this work, the hot embossing principle was used, but instead of using a polymer thin film on glass substrates, polymer substrates were used. Using polymer substrates have some advantages such as:

- Only the stamp has to be heated, and with pressing it into the polymer substrate, the structure can be easily transferred.
- Embossing temperature can be lowered to be slightly higher than the T_g of the polymer. This is because decreasing the polymer thickness requires increase in the temperature, which could be due to the adhesion of the polymer film on the substrate and the stamp surface which hinders the movement of the polymer chains, this retarding effect will increase as the polymer thickness decreases [3-5]. Since the polymer substrates are already too thick (1 mm), so this problem does not exist.
- Very short embossing time (few seconds) is enough to transfer the structure.
- And a technical advantage, as these samples can be prepared in a short time in a cheap way; they can be used as disposable samples. This is important for a series of experiments that require results comparison.

The polymer substrates used in this work are Poly-methyl methacrylate (PMMA); the chemical formula is shown to the right. This polymer is amorphous, and the glass transition temperature is 110°C. The surface energy is 41 dyne/cm, and it adheres well to gold.

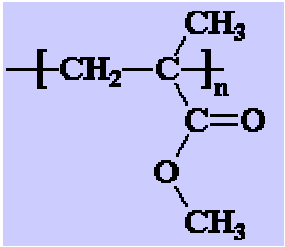

The embossing procedure was carried out as follows:

- Both the grating stamp and the polymer substrates (PMMA) were cleaned by washing with ethanol before using. The PMMA substrates were cleaned without sonification.

- An anti-adhesive layer was applied on the surface of the stamp to lower its surface energy and prevent it from sticking to the substrate. The anti-adhesive layer was applied by immersing the stamp in Dimethyldichlorosilane (chemical formula to the right) for 30 min. and then baking at 110° C for 10 min. to fix the silane layer.

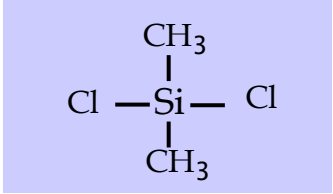

3-5. Heyderman, L. J. et al. *Microelectronic Engineering* 2000, 54, P. 229-245

The silane layer was checked by measuring the contact angle, in this case the contact angle was 98°, which means that the surface is hydrophobic enough to prevent the stamp from sticking to the polymer. (*For contact angle measurement, see Appendix A-3*).

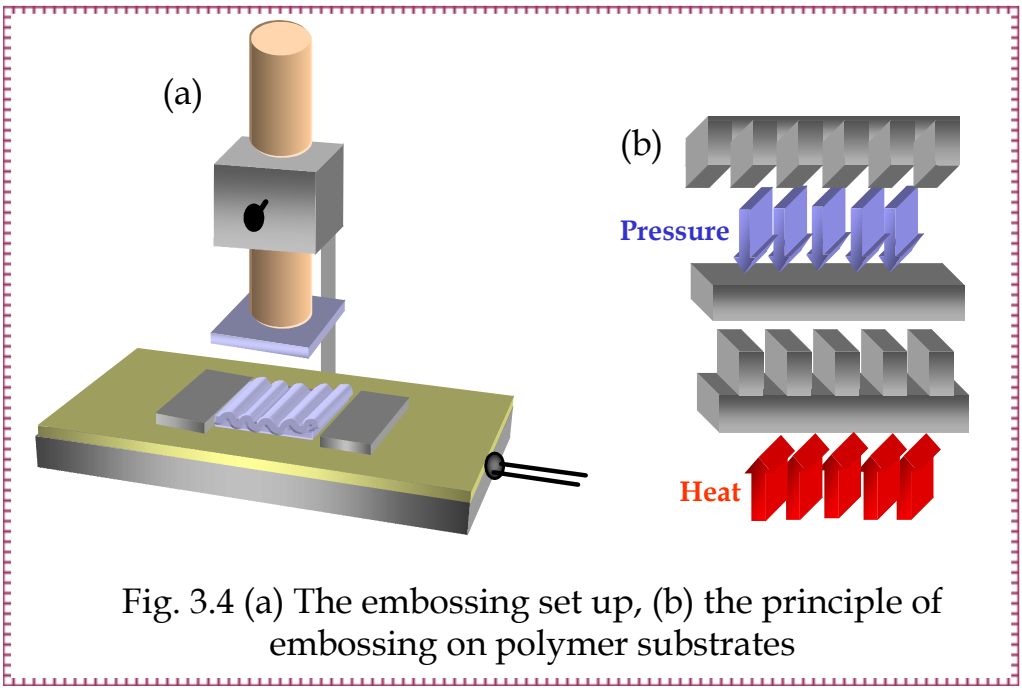

Fig. 3.4 (a) The embossing set up, (b) the principle of embossing on polymer substrates

The idea of the technique was to use a hot master and a cold substrate. The set up, and the technique are shown in fig. 3.4. The stamp is placed on a hot plate to be heated up, and the polymer substrate is held to be pressed over the stamp. The temperature used was 140°C, unfortunately, the pressure was not specified. The substrate was pressed for few seconds and then both the master and the substrate were removed to cool down, so separating them would be easier (*it takes few seconds to separate them*), and this helps the moulding to be better.

3.4 Characterizations of the Embossed Gratings

Since the aim of fabricating the embossed gratings is to use them for surface plasmon resonance applications, two techniques were used for characterization.

The first one was AFM imaging (*see Appendix A-4*) to compare the structures of both the stamp and the replicas, also to see the effect of embossing time on the grating periodicity, the grating constant, and the grating amplitude.
The other one was SPR measurements which were done after evaporating a thick gold layer on top of the grating.

3.4.1 AFM imaging

An AFM image (*see Appendix A-4*) of the stamp that was prepared by ion beam etching, as previously mentioned, was taken. As shown in fig. 3.5, the periodicity of this grating is about 520 nm and the amplitude was about 40 nm, as expected according to the preparation conditions.

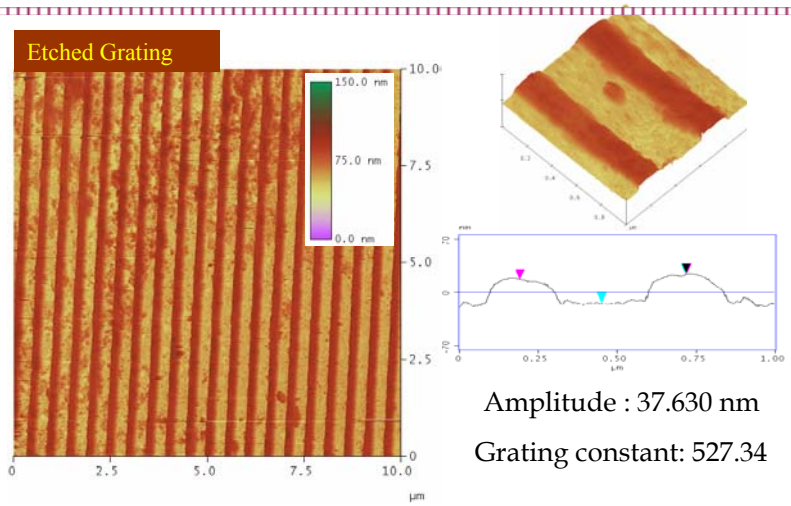

Fig. 3.5 An AFM image of the etched grating used as a stamp showing the grating constant and the grating amplitude

The stamp was used at 140°C for three different embossing times: a few seconds, 1 minute and 2 minutes. AFM images for three of them were used for comparison. The results are shown in fig. 3.6. As can be seen in the figure, increasing the embossing time from few seconds to 1 and 2 minutes caused an increase in both the grating constant (the distance between two grooves) and the amplitude or the depth of the gratings. The figures also show that the profile of the embossed gratings has a convex shape. The morphology of the grooves and ridges can be explained by the mechanics of the mold filling (refer to fig. 3.3 (b)) [3-5].

According to Heyderman et al, the convex profile of the ridges occurs because of the compression of the expanding polymer within the mold cavity by the polymer as it climbs the stamp walls. The polymer that is squeezed into the cavity is under shear stress. The internal friction can cause the polymer to drastically heat up resulting in a lower viscosity, which results in a further flow of polymer into the cavity.

This can also explain the increase in the depth and the distance between the grooves with increasing the embossing time, where at longer periods of time, more of the polymer enters the cavity in a flow and more is pushed into it, and this might increase both the grating constant and the grating depth.

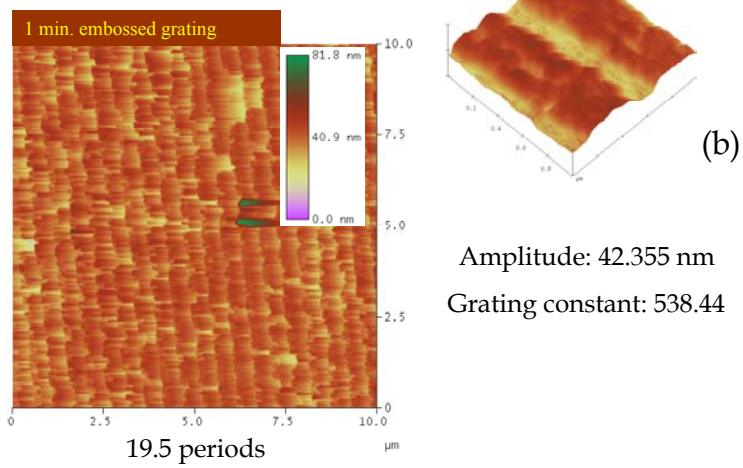

19.5 periods

(b)

Amplitude: 42.355 nm

Grating constant: 538.44

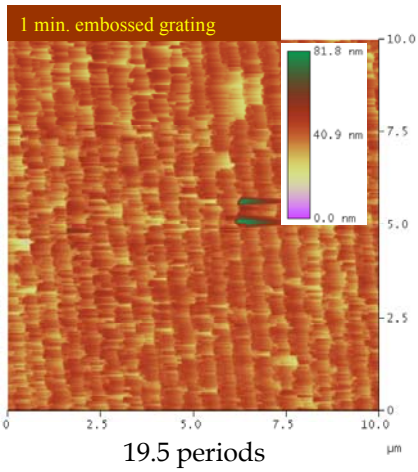

19.5 periods

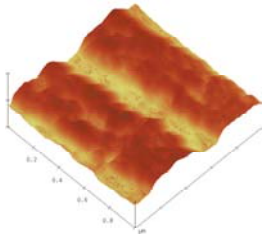

(b)

Amplitude: 42.355 nm

Grating constant: 538.44

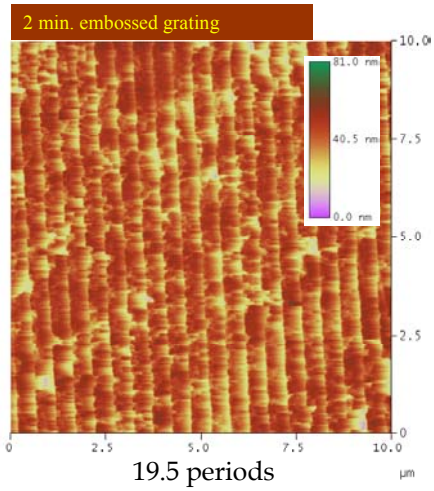

19.5 periods

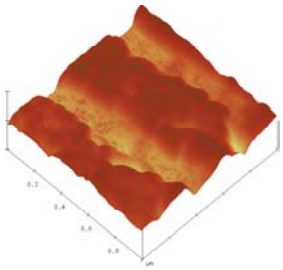

(c)

Amplitude : 45.825 nm

Grating constant: 632.94

Fig. 3.6 AFM images of the gratings embossed for (a) few seconds, (b) 1 minute, (c) 2 minutes. The images show the increase in both the grating constant and the amplitude with increasing the embossing time

3.4.2 Surface Plasmon on Embossed Gratings

In chapter 2, we explained the excitation of surface plasmons by gratings. After preparing our gratings with the embossing technique, and imaging them with the AFM, it was convenient to measure the SPR of these samples, as they would be used in SPR applications. Fig. 3.7 (a) shows SPR scan of our first embossed grating on polymer substrate. The grating constant of this one was 520 nm and the amplitude was 20 nm. The measurement was done against air, and as shown, it gives very high coupling efficiency.

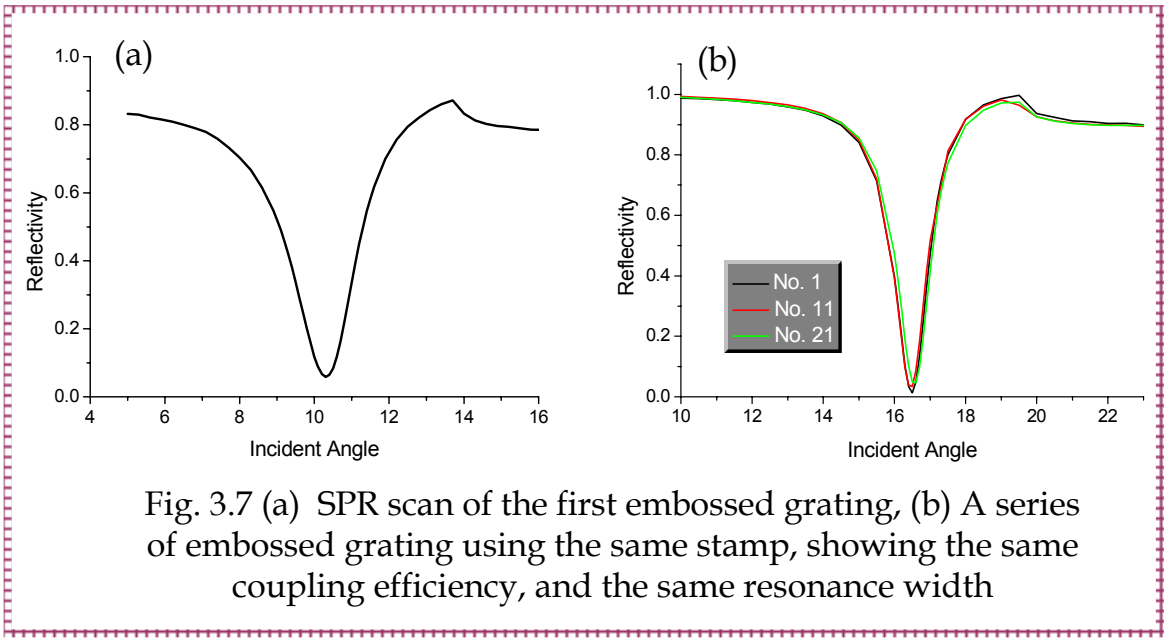

Fig. 3.7 (a) SPR scan of the first embossed grating, (b) A series of embossed grating using the same stamp, showing the same coupling efficiency, and the same resonance width

To check the ability of using the stamp for a long time, a stamp of 480 nm grating constant and 20 nm amplitude was used to emboss a series of gratings, and then an SPR scan was done for samples number 1, 11, and 21. As shown in fig. 3.7 (b) the series of measurements show that all the samples have the same coupling efficiency and the same resonance width, this means that the same stamp can be used to emboss a large number of gratings, in a short time before being deteriorated. The stamp was cleaned with ethanol every few times of embossing, and the silane layer seems to be stable during the procedure time.

As AFM imaging was done to compare etched and embossed gratings, and to see the effect of the embossing time on the grating profile and periodicity, the same was done using the SPR scan curves against air and against water. This is shown in fig. 3.8. We can see that the SPR profile looks similar, however, against air, there is a small shift in the resonance angle and the same applies for the measurement against liquid, where we see that the resonance is broader.

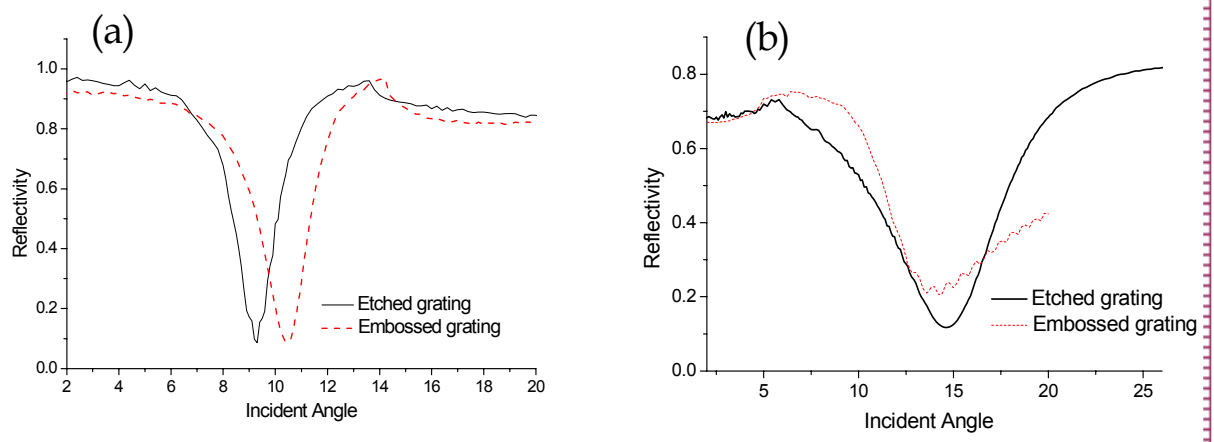

Fig. 3.8 A comparison of SPR scan between etched and embossed gratings (a) against air, and (b) against liquid

SPR scans were also done for gratings embossed at different times to see the effect of the change of the grating constant and the amplitude on the SPR signal together with the AFM, the change seen by AFM can be also seen in SPR, as shown in fig. 3.9. The measurements were also done against air and against liquid.

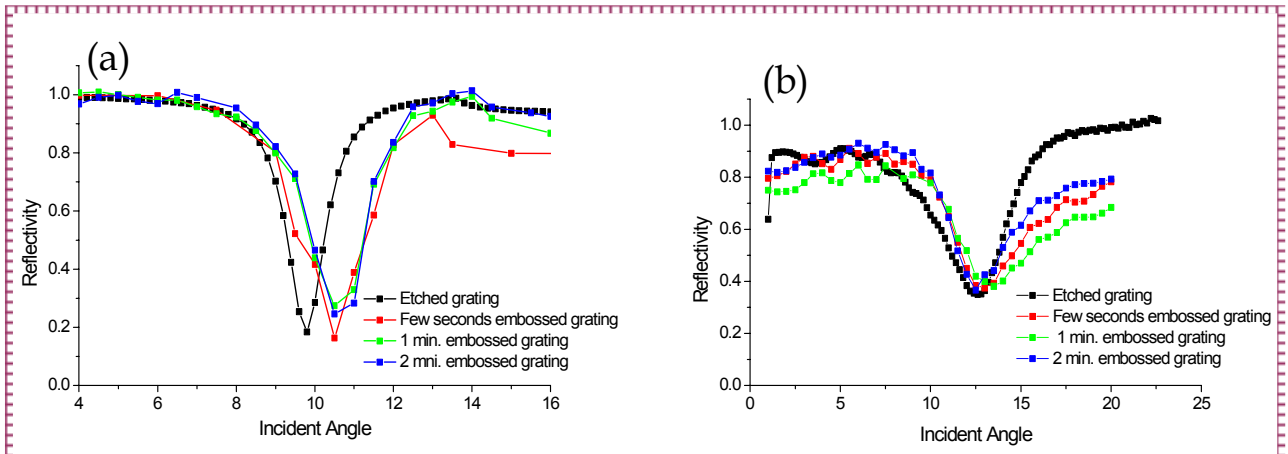

Fig. 3.9 SPR scans of embossed gratings with different embossing times (a) against air, and (b) against liquid

From the previous results, it is clear that the embossing process on polymer substrate was a successful way to fabricate gratings that can be used in SPR applications, and to try one of these applications, one of these embossed gratings was used in a standard DNA experiment to observe the binding on the surface and also the fluorescence signal as a function of both the incident and the emission angle.

3.5 Embossed Grating as a Biosensor

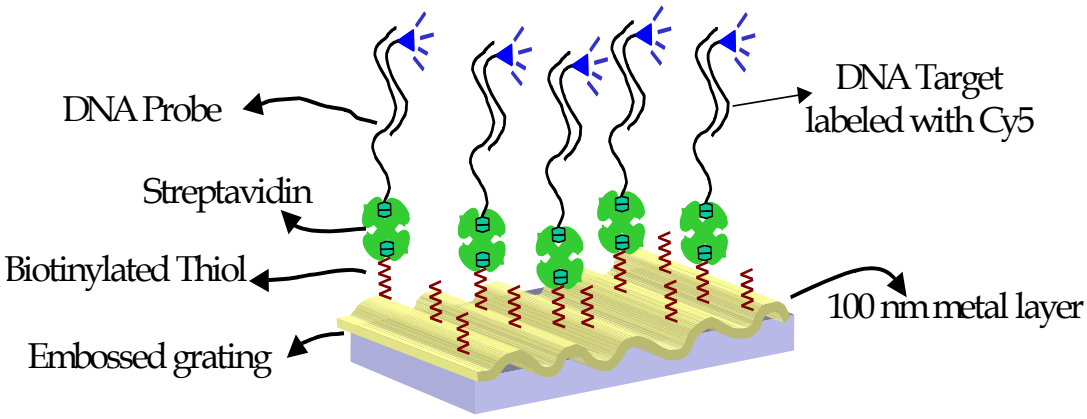

Fig. 3.10 The standard DNA system used to check the ability of the embossed grating to be used as a biosensor

There are some examples of using gratings as biosensors; one of them is using gratings in the field of optical waveguide lightmode spectroscopy which was proved to be a highly sensitive system capable of real time monitoring of biomolecular interactions [3-6].

The system chosen here is a simple DNA matrix. The DNA system was developed in our group (*the system is explained in details in chapter 5*), where the metal layer was modified by a linkage layer (Biotinylated thiol), and then the Streptavidin was bound to the surface through the biotin, the SA binding was monitored by measuring the change in the reflectivity with time (fig. 3.11 (a)). The reflectivity scan was also done after the SA binding and it shows the resonance angle shift which corresponds to the kinetic curve (fig. 3.11 (b)). The next step is the DNA probe binding, and then the DNA target, labeled with Cy5 was injected; in this case, the fluorescence signal was monitored (notice the big bulk jump), this is shown in fig. 3.11 (c). The fluorescence as a function of the emission angle was also measured. As one can see in fig. 3.11 (d), two fluorescence peaks can be seen which are due to the back coupling. As this was shown as an example to document that the embossed gratings can be used as a biosensor. But in the next two chapters, more details will be introduced about the back coupling, the DNA system, and the big bulk jump in case of the gratings.

3-6. Vörös, J. et al. *Biomaterials* 2002, 23, P. 3699-3710

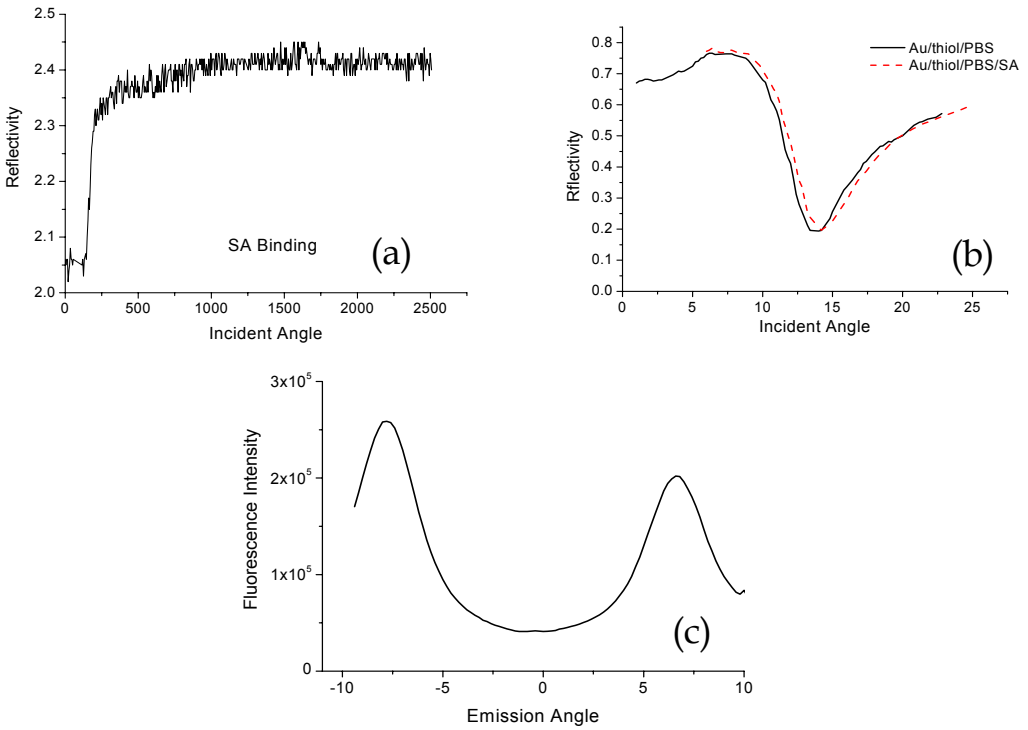

Fig. 3.11 (a) Streptavidin binding, (b) The resonance angle shift after SA binding, (c) The fluorescence scan as a function of the emission angle

3.6 Conclusions

This chapter introduced the fabrication of gratings by the embossing technique that was proved to be a successful way to fabricate gratings with a fast, easy and cheap way. These embossed gratings were characterized by AFM imaging to find the best parameters to be used for the embossing procedure, and also by SPR to prove the ability of these gratings to be used as a biosensor.

DNA experiment was done where the kinetic of the target binding was monitored to show the capability of using the grating for real time measurements and also the fluorescence signal showed the enhancement signal also proved this ability. The fluorescence scan showed clearly the back coupling between the emitted light and the surface plasmons.

In the next two chapters, the back coupling efficiency and the bulk jump will be discussed in more details.

Chapter -4-

BACK COUPLING EFFICIENCY

4.1 Preface

Back coupling efficiency is a very general title, describing the reverse process of surface plasmon excitation, where SP propagating along a grating surface can reduce their wavevector so that they can be transformed into light (*refer to chapter 2 (fig. 2.4)*). Also in chapter 2, we talked about field enhancement at the interface due to surface plasmons and how this field enhancement can be used to excite a chromophore placed near the interface. Before explaining how this back coupling can be observed, we will give a short survey of what was done concerning studying fluorescence excited by grating couplers.

In 1996, Kitson et al. studied the emission of a thin dye layer on a silver grating [4-1]. They found that the emission is dominated by the light re-radiated by SPPs, and that the direction and the polarization of the emission depend on the azimuthal angle between the emitted light and the grating grooves. Their results were explained according to the additional decay routes that a metallic surface can introduce (SPPs), and surface corrugations allow these SPPs to couple to radiative modes. They also found that the emission is concentrated in well-defined directions corresponding to the resonant coupling between the SPPs and photons.

In another work Kitson et al studied the intensity of photoluminescence from a thin layer of laser dye on a metallic grating and how does it depend on the polarization and angle of incidence of the incident beam of light [4-2]. They calculated the field intensity above a silver grating when SPP is resonantly excited by an incident beam (fig. 4.). The field peaks at the metal surface and falls off exponentially with distance, with decay lengths of the order of the wavelength of light in the airside and of the order of the skin depth in the absorbing metal. The intensity of the fluorescence emission from a layer of dye molecules is directly proportional to the energy absorbed by the molecule, and for a weakly absorbing dye, the amount of energy absorbed depends linearly on the local filed intensity.

4-1. Kitson, S.C. et al. *Optics Communications* 1996, 122, P. 147-154
4-2. Kitson S. C. et al. *Journal of Modern Optics* 1996, 43 (3), P. 573-582

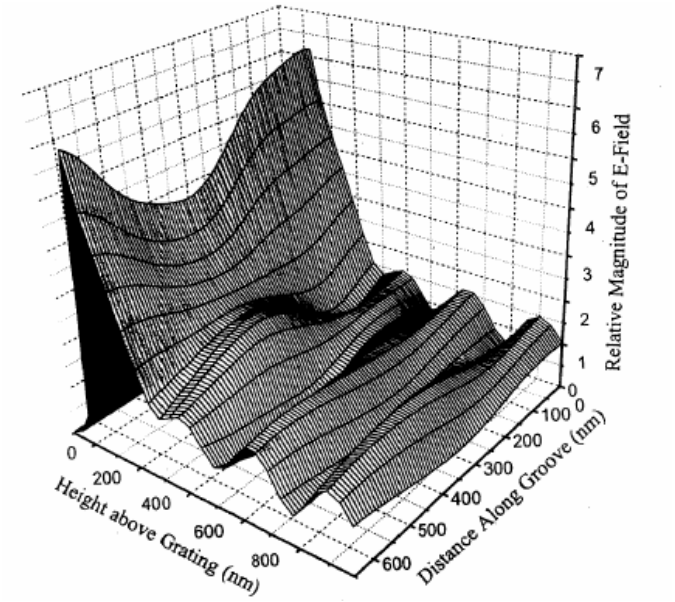

Fig. 4.1 The normalized magnitude of the electric field above a grating when an SPP is resonantly excited [4-3]

For a dye molecule above a metal, a non-radiative decay channel is created which is the direct coupling of the excited molecule to SPPs; this decay channel becomes dominant at a spacing of around 20 nm [4-3]. The SPPs excited by the dye can couple out to bulk radiation by scattering from the grating and the emitted light comes off at certain well-defined directions, and this may allow the light to be collected more efficiently. In this work, it was not yet clear how the coupling strength between the excited dye molecules and the available decay routes could depend on the dye-metal separation.

Our interest was to study the back coupling efficiency, which could be defined as the amount of energy transferred from the emitted light to SPPs. The scattering of SPs from the grating and the back coupling between emitted light and SPs is shown in the dispersion curve in fig. 4.2. This is a not to scale dispersion curve showing that the corrugation of the grating causes the surface plasmons to scatter. Via this scattering, they can couple back to the emitted light provided the chromophores are close enough to the metal surface.

4-3. Pockrand, I. et al. *Chem. Phys. Lett.* 1980, 69, P. 499

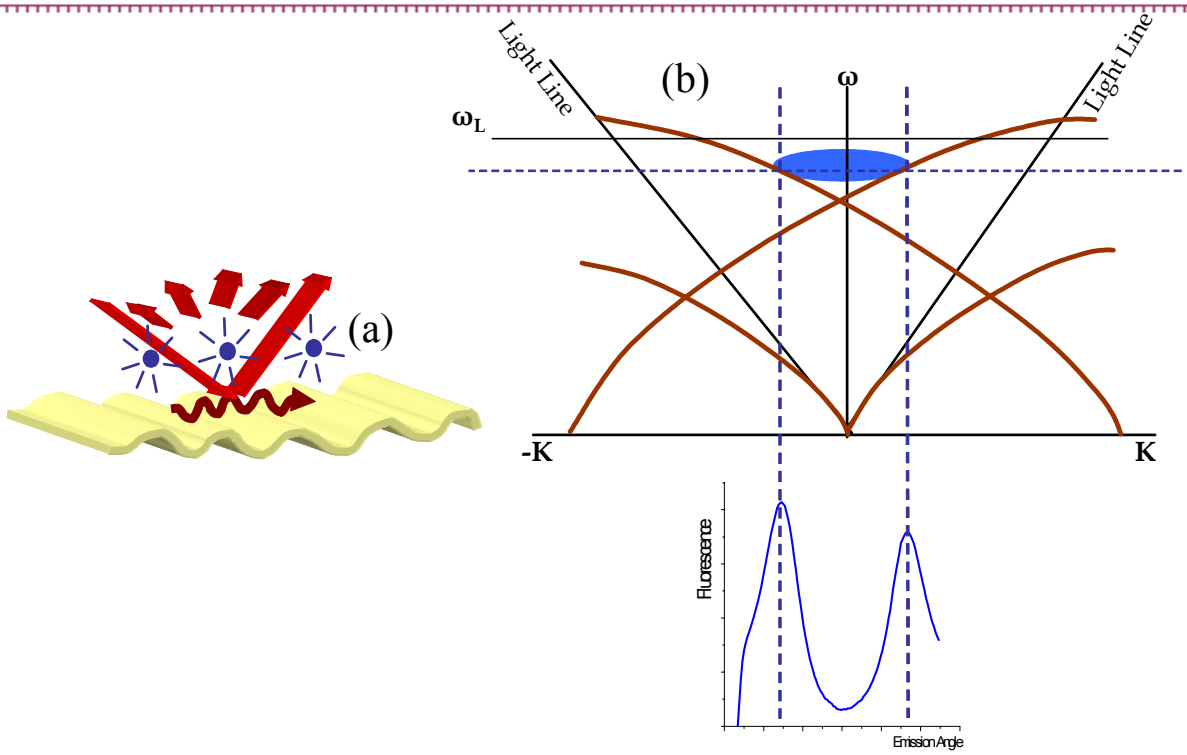

Fig. 4.2 (a) The scattering of the surface plasmons from the grating surface, (b) Not to scale dispersion curve shows the back coupling between the emitted light and the surface plasmons

4.2 Coupling Efficiency Dependent

Several parameters affect the back coupling efficiency, as shown briefly in fig. 4.3, the grating profile, the grating periodicity, the grating amplitude and the dye metal separation.

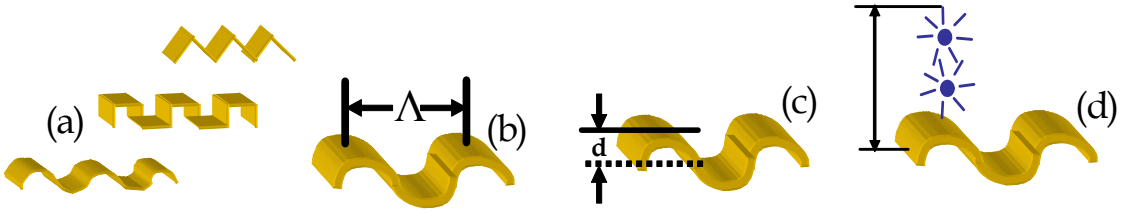

Fig. 4.3 The parameters affecting the back coupling efficiency, (a) the grating profile, (b) the grating periodicity, (c) the grating amplitude and (d) the dye metal separation

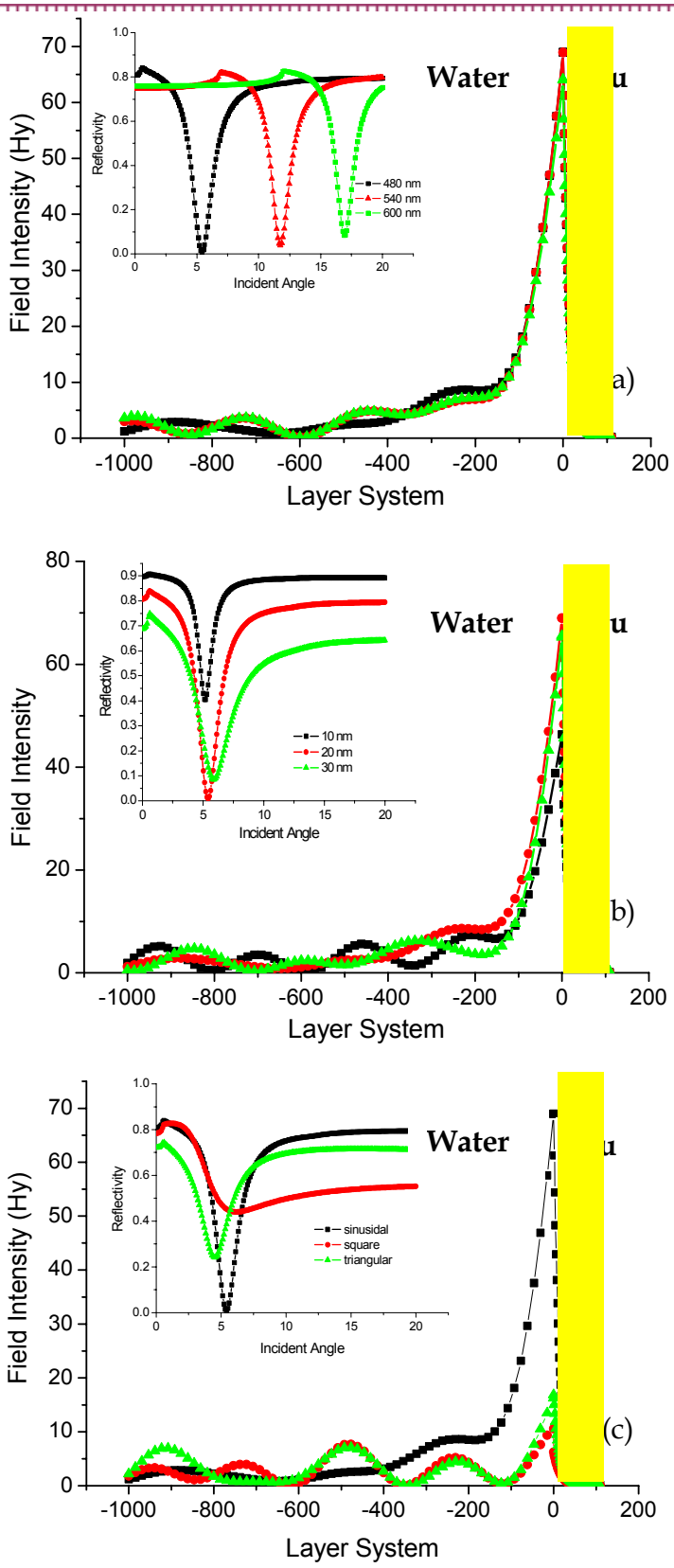

Fig. 4.4 Theoretical simulations showing the change of both the reflectivity and the evanescent field with changing the grating parameters (a) different grating periodicity (b) different grating amplitude, (c) different grating profile

In fig 4.4, theoretical simulations for the reflectivity and the field intensity are shown; these simulations were done using a program developed in our group based on Fresnel equations. All the simulations were done at λ = 633 nm and in a liquid medium.

While the grating periodicity does not have a great effect on the reflectivity signal or the field intensity, with only the position of the resonance angle changing (fig. 4.4 (a)), we see that both the grating amplitude and the grating profile modify the field intensity.

Simulations with changing the grating amplitude were done at Λ = 480 nm grating constant (fig. 4.4 (b)). For 10 nm amplitude, the coupling efficiency is low and also the field intensity. Increasing the amplitude to 20 nm, increases the coupling efficiency and the field intensity. Further increase of the amplitude to 30 nm broadens the resonance and decreases the field intensity again. So, 20 nm is the optimum amplitude for this grating constant.

The grating profile seems to have the greatest effect on the coupling efficiency, with 480 nm periodicity and 20 nm amplitude, both the coupling efficiency and the field intensity are the highest in case of a sinusoidal grating, while using the same parameters in case of a square and a triangular grating decreases both of them significantly.

These simulations were done to figure out the effect of changing these parameters on the coupling efficiency that, in turn, will have an effect on the back coupling efficiency, and also on the field intensity, which will affect the fluorescence signal.

The parameter that was of interest for us was the distance between the dye used for monitoring the fluorescence intensity and the metal surface where two important factors were to be studied here:

- The fluorescence intensity at different distances from the interface in the aqueous medium; this intensity of the fluorescence emitted from a dye in the vicinity of the evanescence field was studied before in our group for planar surfaces [4-4], and its value was found to be in the range of 30-50 nm.

- The most important aspect to be studied related to the coupling efficiency was loss in the back coupling efficiency for large distances and its angle dependence (fig. 4.5).

4-4. Vasilev, K. et al. *J. Chem. Phys.* 2004, 120, 3439-3445

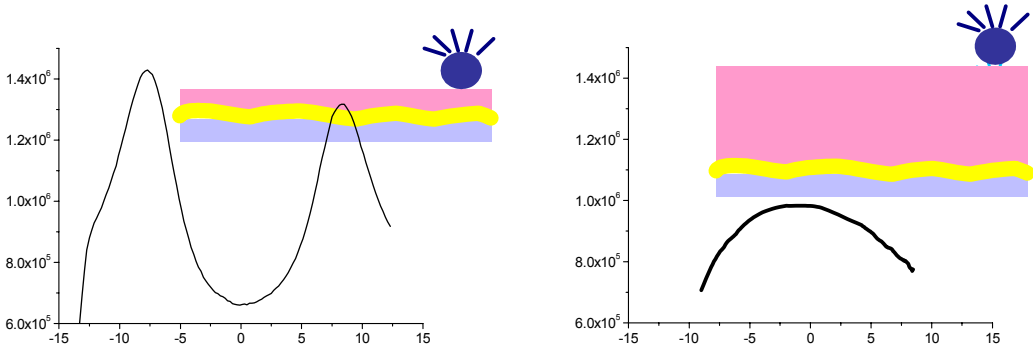

Fig. 4.5 A scheme showing the interest to know if the back coupling will be lost at higher distance from the grating surface.

In the earlier study of the fluorescence intensity at different distances from a planar surface (as mentioned before), electrolyte bi-layers were used [4-4]. In this work, another system was used for this purpose. A system of protein layers was applied above the grating as will be explained in details in the next section.

4.3 Protein Layer System as a Spacer

It has been reported that multi-layer thin films can be fabricated by alternatively depositing two layers of molecules that can bind to each other. This technique is called layer-by-layer (LBL) deposition. Protein deposition can be done by means of antigen antibody interaction [4-5], biotin-avidin interaction [4-6] or sugar-lectin interactions [4-7]. LBL techniques offer a way to control the separation distance between the molecules of interest to the base surface, which is of particular interest for investigating the distance behavior of fluorescence yield by SPFS [4-4]. This also matches exactly with our aim at studying the fluorescence intensity at different distances from the grating and also to see the change in the back coupling efficiency.

Streptavidin and biotinylated IgG were choosed as the alternating molecules according to a strategy reported previously [4-8]. The layers can be selectively decorated by applying labeled streptavidin. The depositing procedure was done with the following steps:

4-5. Bourdillon, C. et al. *J. Am. Chem. Soc.* 1994, 116, P. 10328-10329
4-6. Hoshi, T. et al *Anal. Chem.* 1995 34, P. 770-774
4-7. Anzai, J-I. et al. *Sens. Actuators B.* 2000, 65, P. 94-96
4-8. Cui, X. Q. et al *Biosens. Bioelectron.* 2003, 18, P. 59-67.

- The gold layer was modified by self assembling a monolayer of Di-Thio-di-propionic acid ($C_6H_{10}O_4S_2$), with the the thiol being attached to the gold surface through an S group and a COOH group at the other side.

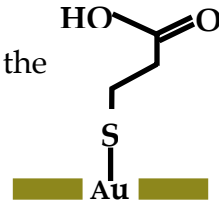

- To covalently attach streptavidin, the surface was activated by active ester chemistry. A fraction of the carboxyl groups on the SAM surface was activated to form reactive N-hydroxysuccinimide esters using a solution of 0.2 (EDC) and 0.05 (NHS) in water ordered from Biacore.

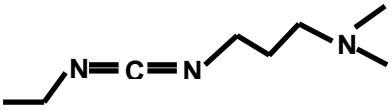

EDC
N-ethyl-N'-(3-dimethylaminopropyl) carbodiimide hydrochloride

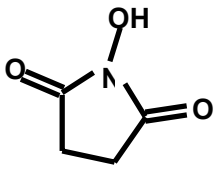

NHS
(M N- hydroxysuccinimide)

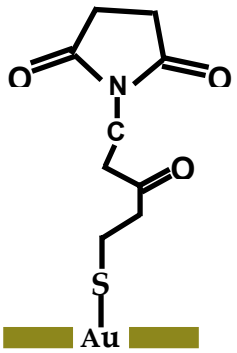

The surface after activation

- After this activation, Streptavidin prepared in sodium acetate, pH 5.0, was immobilized via the reaction of its nucleophilic groups (mainly the ε-amino groups of the lysine residues).

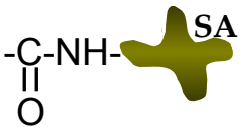

- The excess esters were then deactivated using 1 M ethanolamine hydrochloride adjusted to pH 8.5 with sodium hydroxide, this also desalted loosely bound protein.

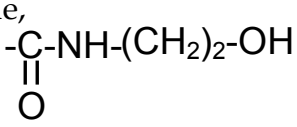

- 20 µg/mL of biotin IgG was immobilized to the streptavidin by injecting the solution in the flow cell for 15 minutes; the binding was monitored by SPR and after rinsing with pure buffer, the SPR resonance was checked by monitoring an angular scan.

- The same was done to immobilize a layer of AFSA (SA labeled with Alexa-Fluor dye) of 20 µg/mL concentration, the binding was also monitored by SPR.

- These layers were built alternatively and both the resonance and the fluorescence signal were measured after each layer to ensure that the layers are consistently built and also to calculate the layer thicknesses as will be explained later.

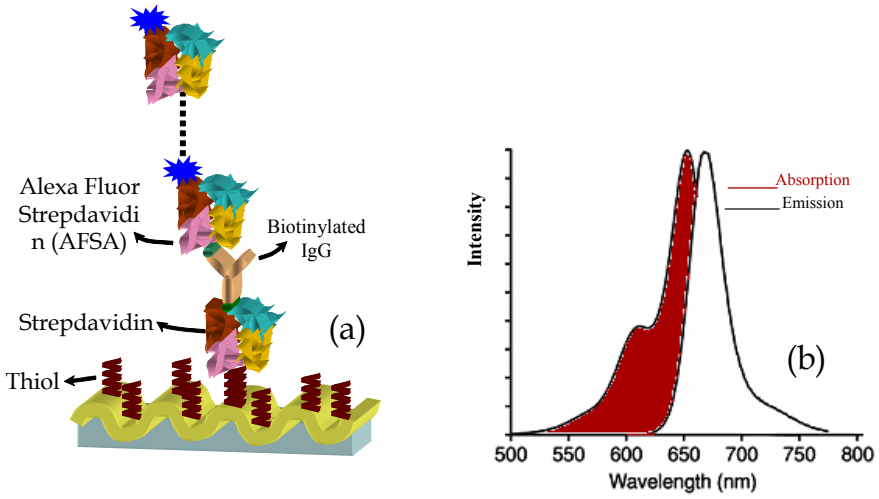

Fig. 4.6 (a) A scheme of the LBL system of alternative SA and IgG, (b) The absorption and emission wavelength of the Alexa Fluor dye used in the experiment

The LBL looks at the end as shown schematically in fig. 4.6 (a). To see the fluorescence signal, the last layer was always AFSA, the absorption and emission wavelength of Alexa Fluor dye is shown in fig. 4.6 (b).

As mentioned before, the reflectivity was measured after each layer binding. The results shown in fig. 4.7 show the gradual shift of the resonance angle which means that the proteins are absorbed, the measurements show a clear shift in the resonance angle for the first 40th steps and then a very small shift after the 60th steps. But the most important step in this investigation was to calculate the thickness specifically to correlate it with the fluorescence signal. In this experiment, 84 binding steps were applied, and the total thickness was about 106 nm, as will be explained next.

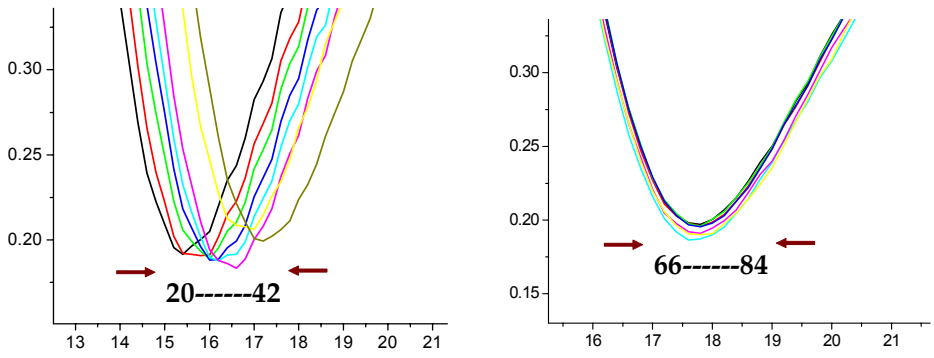

Fig. 4.7 the angle shift measured after depositing each layer showing the significant change at the first 40 layers and then the decrease in the shift after the 60th layer

4.4 Thickness Measurement

As it is well known, simulating the surface plasmon resonance gives the thickness and the refractive index of the layers but not independently, where one of them has to be assumed to find the other. Usually the values of the refractive index are taken from the literature or measured by a refractometer. Because it is essential for our work to find out the thickness more specifically, two different methods were applied to measure and calculate the thickness.

4.4.1 Theoretical Simulations

Using the simulation program mentioned before, theoretical simulations for the angle shift with increasing the distance were done for three different grating profiles, sinusoidal, square and triangular.

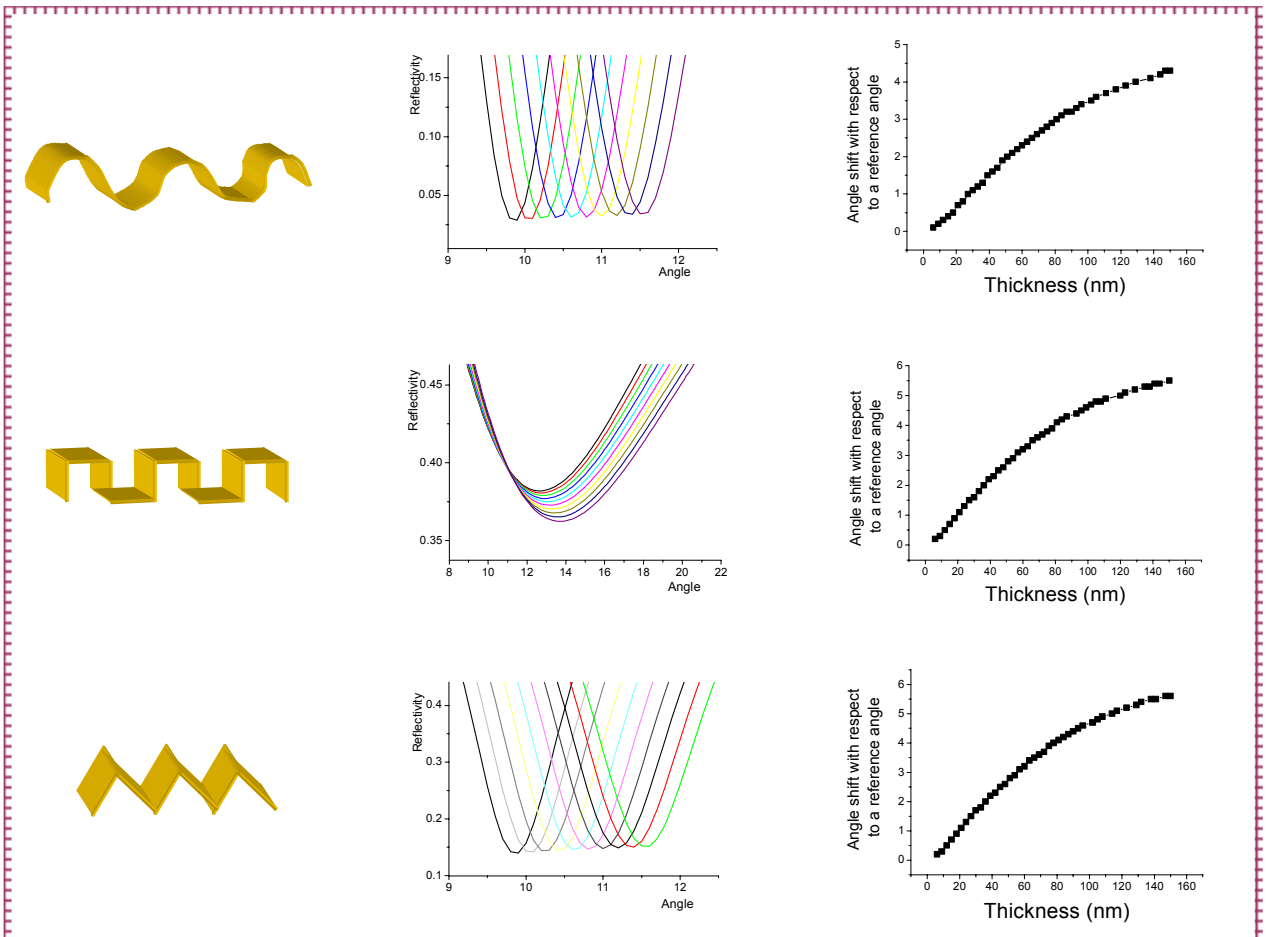

Fig. 4.8 Theoretical simulations for the angle shift for three different grating profiles showing the same trend.

The purpose of doing these simulations was to prove that the grating profile does not affect the angle shift measured for large thicknesses. As shown in fig. 4.8, the thickness as a function of the angle shift gives the same trend for the three different profiles. Our grating has a profile, which is imaged by AFM in fig. 4.9. Since it is proved from the previous simulations that the shift is the same, so the same simulations can apply to our grating.

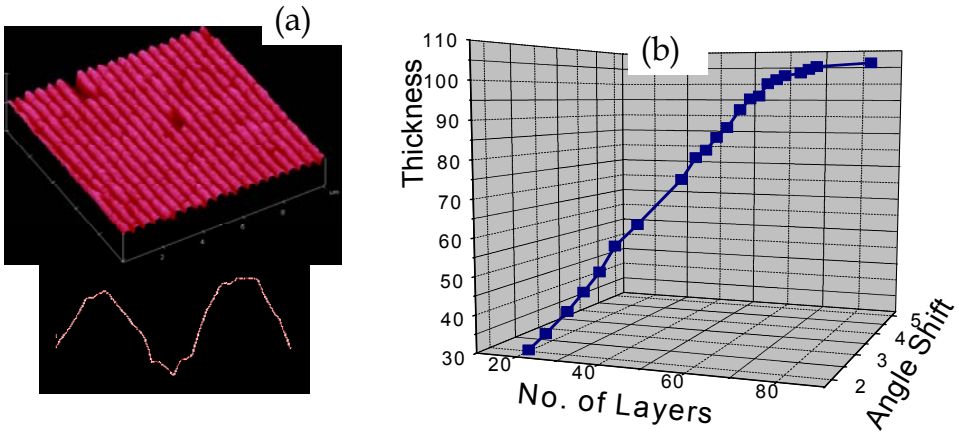

Fig. 4.9 (a) an AFM image showing the profile of the grating used in the experiment, (b) The thickness as a function of both the number of layers and the angle shift assuming the refractive index of the protein to be 1.45

In the previous simulations, the refractive index of the protein was assumed to be 1.45. The thickness was calibrated with the angle shift, and this was used to calculate the thicknesses of our layers. As shown above, each layer gave about 1.5-2 nm thickness.

4.4.2 AFM Imaging for Thickness Measurements

AFM imaging is one of the methods to study protein adsorption on different surfaces (*Appendix A-4*). Imaging proteins can give the possibility to see their crystallization and also to know their thickness. We used AFM as an alternative way to measure the thickness of the protein layers. For this purpose, a multimode AFM machine was used, where imaging can be done in a liquid environment, which matches to our purpose. The gold layer was prepared on Mica and then annealed at high temperature to ensure having a very smooth layer. This was confirmed from the image where the roughness of this layer was about 0.07 nm (fig. 4.10 (a)). This can reduce the error in calculating the thickness of the layers deposited on the surface. Thiol incubation was done in-situ and the adsorption of the layer was followed by taking subsequent images, after rinsing the thiol with ethanol, followed with buffer, the surface was activated (in-situ) with the method explained before, and then the layer by layer system was deposited.

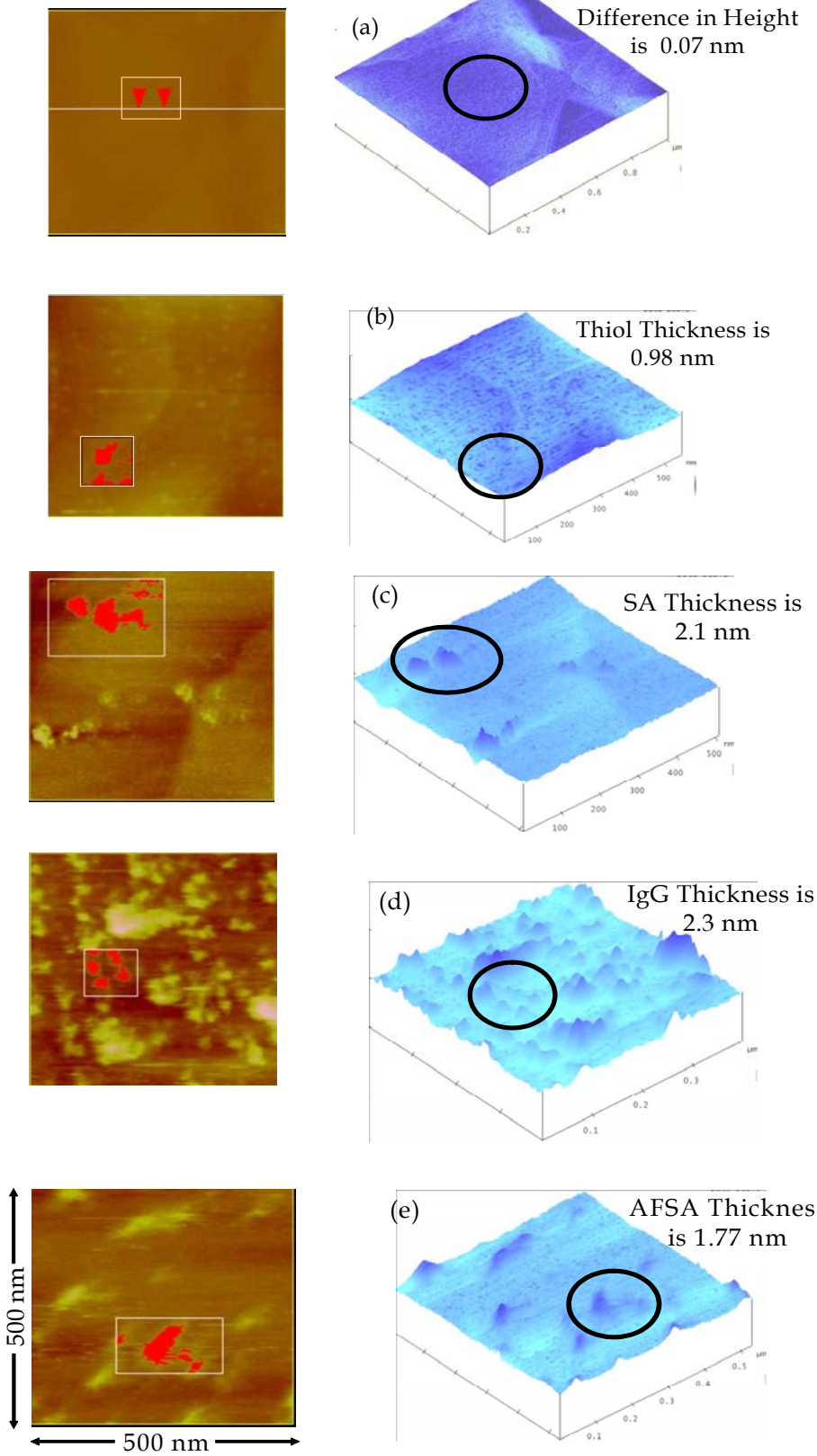

Fig. 4.10 AFM images of the proteins after the deposition of each layer, (a) bare gold on Mica, (b) after thiol modification, (c) after Streptavidin binding, (d) after IgG binding, (e) after AFSA binding. The thickness of each layer is shown next to each image

The disadvantage of this method is that we can not image the same exact area every time after exchanging the solution in the flow cell, where injecting the solution changes the tip positions, so we were trying to reach the same position as exactly as possible.

The AFM results are shown in fig. 10, as shown, the surface roughness is about 0.07nm. For each layer the thickness was calculated by zooming into an area where the protein is seen to be adsorbed (the area highlighted by red and a circle in the figure) and uses the bearing tool to calculate the thickness. The bearing tool provides a method of plotting and analyzing the distribution of surface height over a sample. This form of analysis may be applied to the entire image, or to selected areas of the image, using a rubber band box, an example of the bearing is shown in fig. 4.11

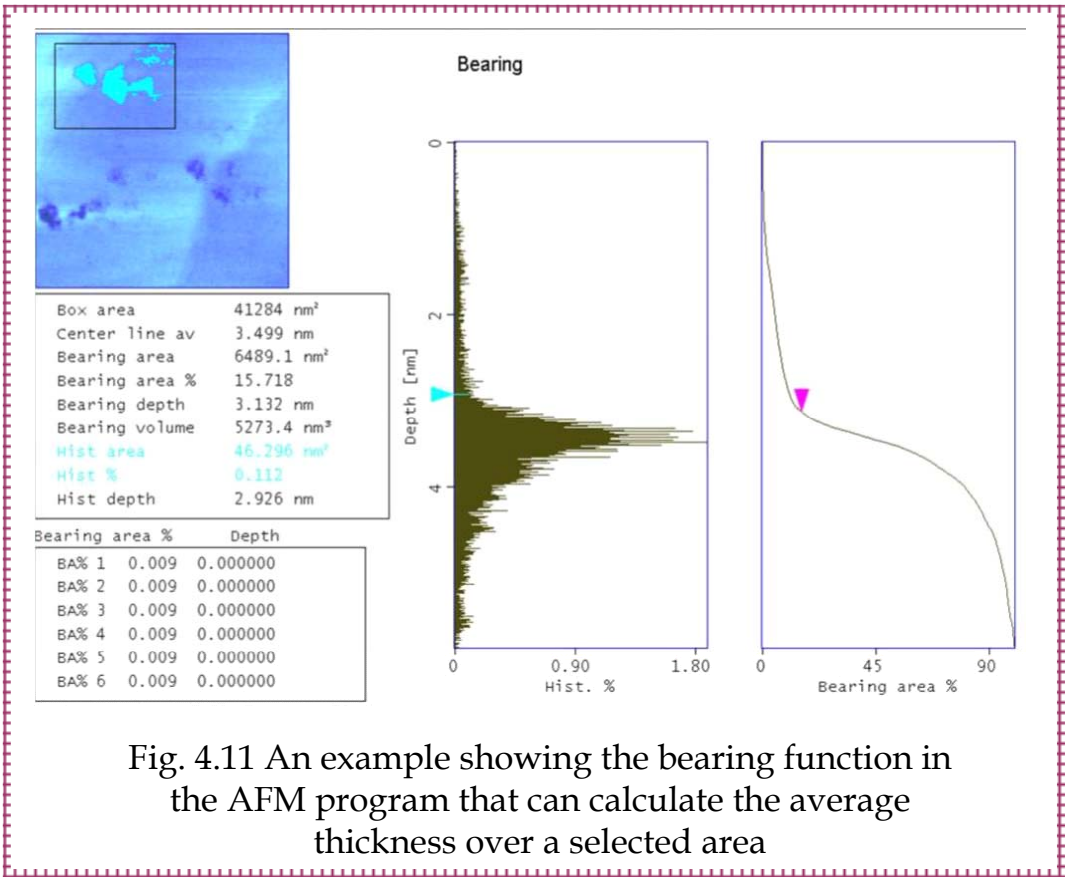

Fig. 4.11 An example showing the bearing function in the AFM program that can calculate the average thickness over a selected area

The layer thicknesses were found to be 0.983 nm for the thiol layer, 2.1 nm for the SA, 2.33 nm for the IgG, and 1.77 nm for the AFSA, these results are very close to the thickness calculated from the theoretical simulations. Fig. 4.12 shows the thicknesses of the layers calculated by both methods.

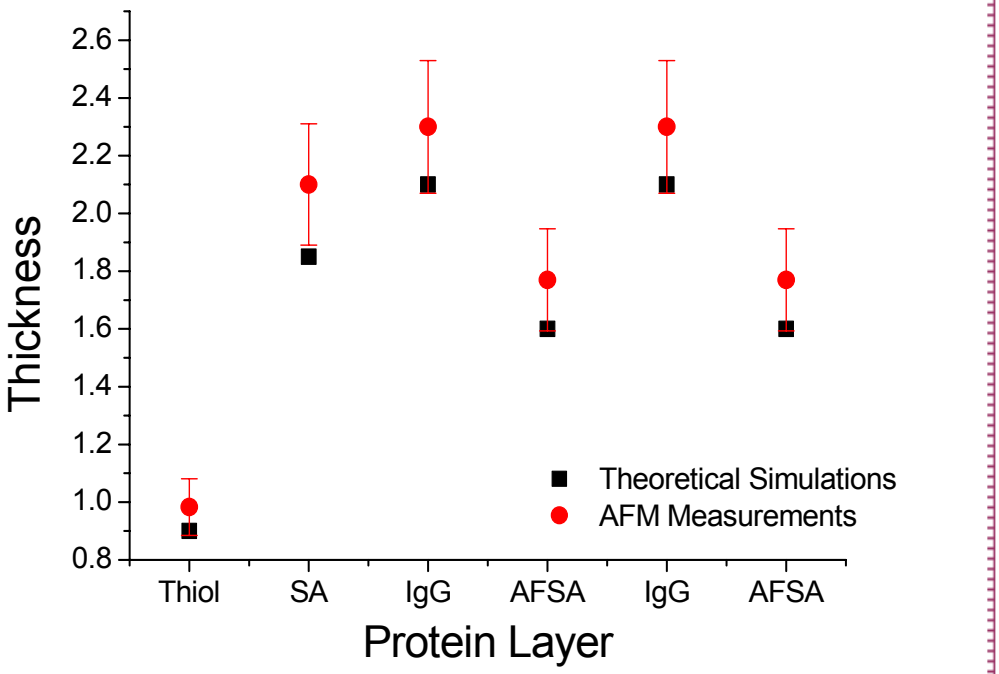

Fig. 4.12 The thickness of the protein layers calculated from the theoretical simulations (at 1.45 refractive index) and from the AFM measurements showing agreement in values

4.5 Back Coupling Distance Dependent

After successfully building the LBL system and calculating the thickness, the back coupling measurements can be analyzed. After each deposited AFSA layer, the fluorescence scan curve was monitored, by fixing the grating and rotating the photomultiplier around the normal to the grating, as shown below.

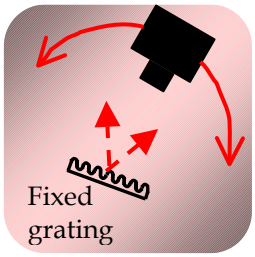

In order to calculate the emission angle with respect to the grating normal, a schematic drawing was done to imagine how we can measure this angle (fig. 4.13).

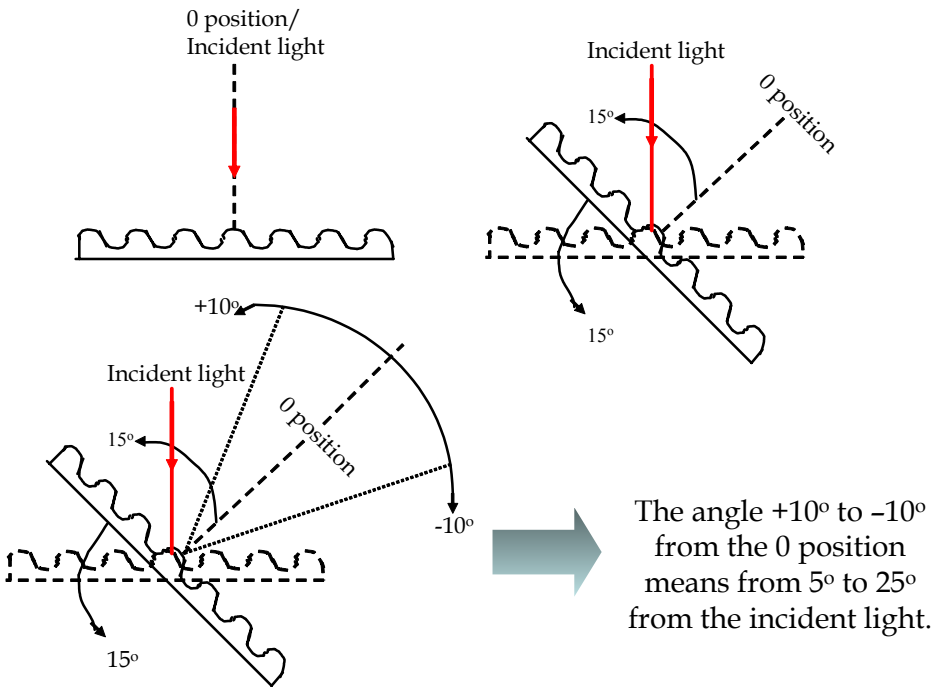

Fig. 4.13 Schematic representation of calculating the angle from to the normal to the grating with respect to the incident angle

As mentioned before, the light emitted from the dye couples back via scattering to surface plasmons and the emitted light comes out in well defined directions (refer to fig. 4.2). The results are shown in fig. 4.14, where two fluorescence peaks appear around the normal to the grating.

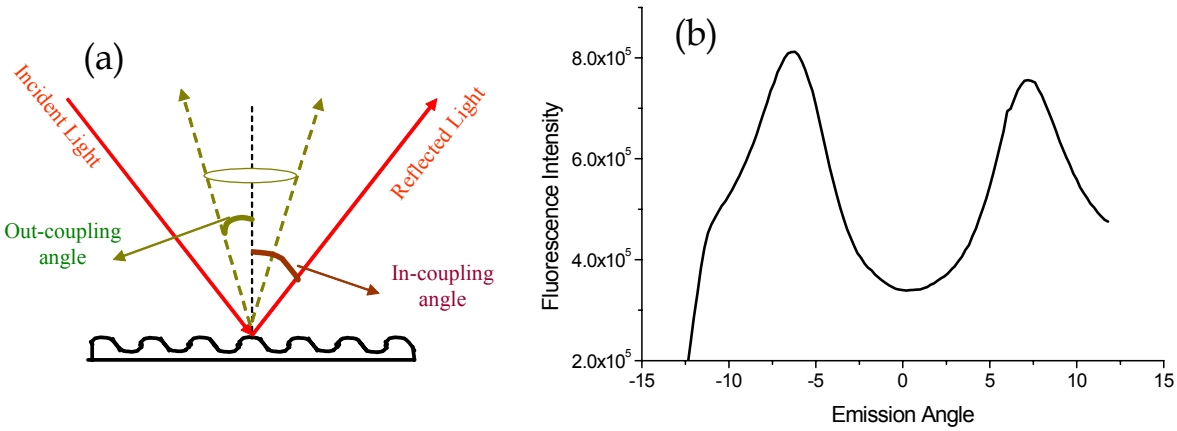

Fig. 4.14 (a) A graph showing the emission angle, (b) The fluorescence intensity measured as a function of the emission angle

Now, to study the back coupling efficiency, the fluorescence intensity was measured at different distances by the protein system explained previously. Fig.

4.12 shows the results, where at the first 5 nm, the fluorescence is quenched being so close to the metal layer, and as the distance increases, both the florescence intensity and the back coupling increase until 50 nm where the fluorescence intensity and the back coupling efficiency start to decrease. Since the fluorescence emission from dye molecules is directly proportional to the energy absorbed by the molecules, the amount of absorbed energy depends linearly on the local field intensity. At distances in the range of 10-50 nm, the dye is still in the vicinity of the evanescent field where it still can experience the enhanced field of the SPP, while at higher distances, the field starts to decay exponentially decreasing the absorbing energy, and as a consequence, the emitted light decreases. Since the coupling efficiency between the emitted light and the SPP determines how efficiently one can be transferred to the other, so the coupling efficiency decreases with decreasing the emitted light. This is shown in fig. 4.15 where the optimum distance above the grating that gives the highest fluorescence intensity is in the range of 30-50 nm.

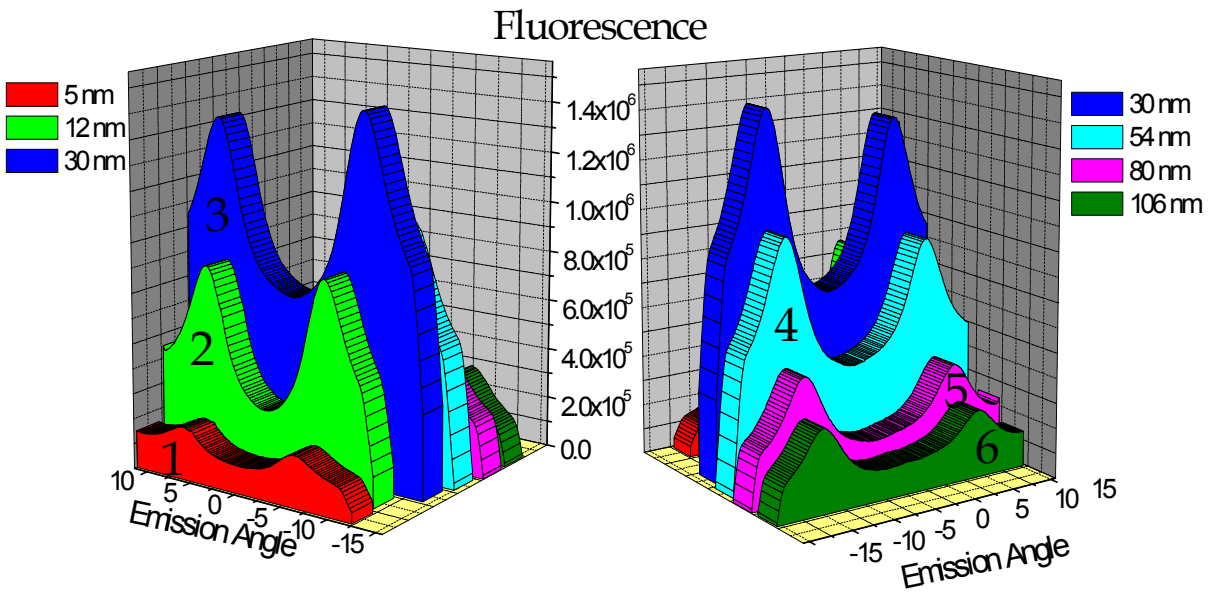

Fig. 4.15 The fluorescence intensity (dominating the coupling efficiency) at different distances above the grating, 1-5 ↔ 5-106 nm

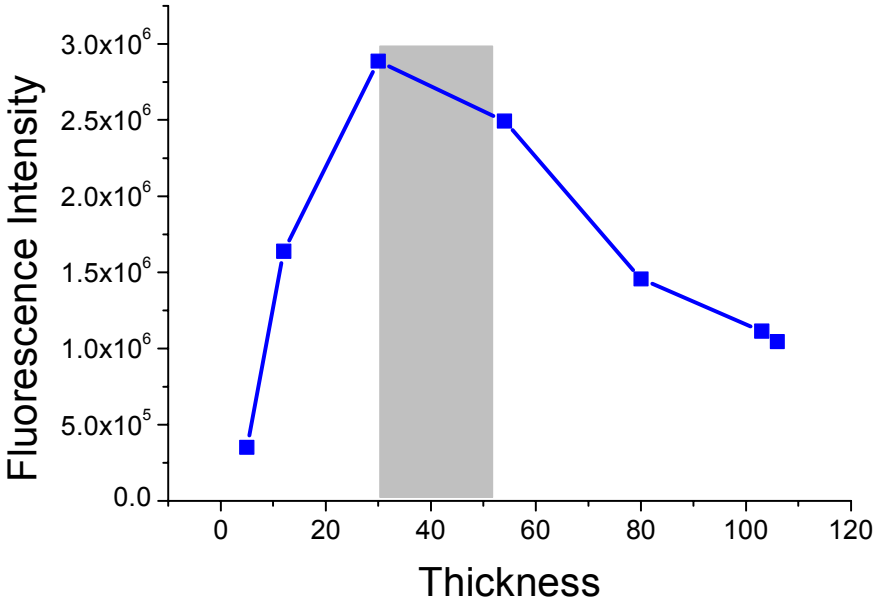

Fig. 4.16. The fluorescence intensity as a function of the thickness above the grating, the grey line emphasize the range of the maximum fluorescence intensity

Fig. 4.14 shows a not-to-scale dispersion curve of the change of the back coupling wavevector with the change of the distance above the grating. With changing the distance from 5 to 30 nm, the positions of the peaks change and for higher distances, the positions are almost the same. This agrees well with the change of the resonance angle with increasing the distance, where at higher distances the shift starts to decrease.

Now, if we go back to the main purpose of running this study, i.e. to find out if the back coupling will be lost at higher distances, it is very obvious that we did not lose the back coupling. At 106 nm, we still could see the back coupling expressed as the two fluorescence peaks around the normal to the grating. This might be explained as the grating is getting shallower at these higher distances, but it still can allow the surface plasmon to scatter and couple back to the emitted light and consequently, the back coupling can be seen.

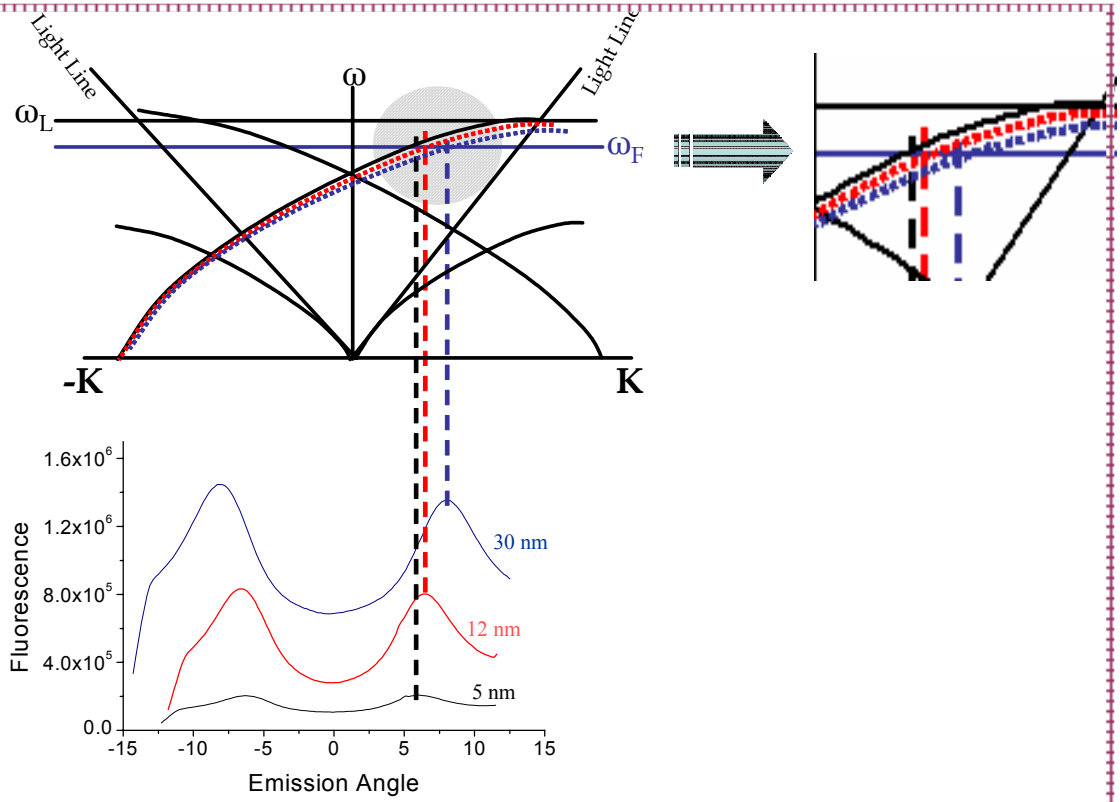

Fig. 4.17. A not to scale dispersion curve showing the change of the back coupling wave vector with changing the thickness above the grating

4.6 Conclusions

In this chapter, back coupling between the emitted light of a chromophore near the surface of a metallic grating and the surface plasmon resonance was studied at different distances above the metal layer using a protein LBL system as a spacer. The results showed that both the fluorescence intensity and the back coupling efficiency increases up to 30 nm where we go above the quenching range. After this both start to decrease due to the decrease of the evanescent field intensity. These results are in agreement with the results determined on a planar metallic surface, and the behavior of the fluorescence was proved to be the same in different media (air or liquid). What was more interesting here is that the back coupling can still be seen at the high distance reached here (106 nm), where the surface plasmon can be considered to scatter till this high distance.

Chapter -5-

BULK JUMP REDUCTION BY CHROMOPHORE QUENCHING

5. BULK JUMP REDUCTION BY CHROMOPHORE QUNCHING

5.1 Preface

In all forms of spectroscopy, there is always a question as to whether it is possible to detect the desired signal above the noise level. In surface sensors, sensitivity is a major problem, where it is important to distinguish between signals from the surface and from the bulk of the sample. Surface sensitive techniques are more sensitive to molecules located near the surface than to those in the bulk (fig. 5.1).

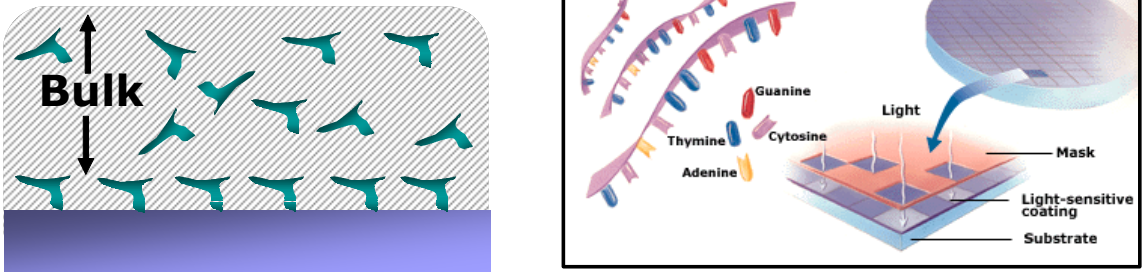

Fig. 5.1 (a) The difference between the species in the bulk and on the surface, (b) a DNA chip where the hybridization in the bulk can lower its sensitivity [5-1]

DNA analysis became very important for the detection of pathogenic microorganisms such as bacteria and viruses by their genetic material and the detection of infectious diseases. Due to the huge amount of genetic information that need to be analyzed in routine medical procedures, there is a high demand on efficient screening methods for point mutations in the patient's genome and DNA detection schemes. DNA arrays and chips provide the possibility to screen DNA samples for various mutations simultaneously and are widely used for the high throughput analysis of DNA samples, but the sensitivity of these chips should be high enough to guarantee a significant and specific signal. Returning to our issue, these chips should have the ability to distinguish between the signal coming from the bulk and that coming from the surface which is the one of interest.

5-1. www.devicelink.com/ivdt/archive/98/09/009.html

The function of deoxyribonucleic acid (DNA) is to carry the genetic information in living organisms from generation to generation and to allow for the expression of that information under appropriate conditions. The information that is stored in DNA is transcribed into RNA sequences and translated into amino-acid sequences.

DNA is a biopolymer which is formed from nucleotide units [5-2, 5-3]. These monomers consist of either a purine base (adenine, guanine) or a pyrimidine base (thymine, cytosine), deoxyribose and a phosphate moiety as shown in fig. 5.2 (a). The 3′ and 5′ hydroxyl group of the sugar is phosphorylated. If nucleotides are coupled together by phosphodiester linkages the typical sugar phosphate backbone of single stranded DNA is formed as shown in fig. 5.2 (b). Due to the numbering of the atoms in the deoxyribose unit one can distinguish the 5′ and the 3′ end of a DNA strand.

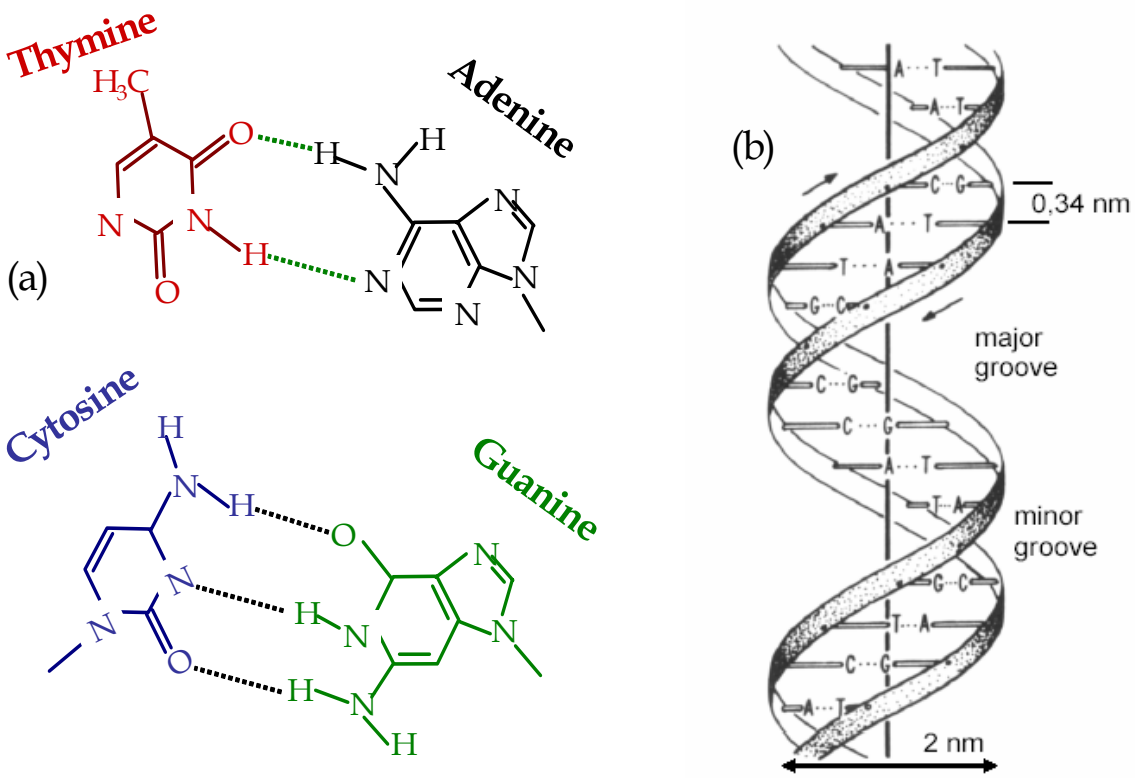

Fig. 5.2 (a) The hydrogen bonding between the base pairs A-T and C-G, (b) the double helix

5-2. Adams, R. L. P., et al. *The Biochemistry of Nucleic Acids* 1992 (Chapman & Hall, London).
5-3. Saenger, W. *Principles of Nucleic Acid Structure* 1983 (ed. Cantor, C.) (Springer, New York).

Two single strands can bind to each other in an ordered manner and form double stranded DNA. This process is called hybridization. The two polynucleotide chains are of opposite polarity in the way that the terminal nucleotide of one strand has a 5′ end, while the complementary one exhibits a 3′ end on the same terminus. The strands are running in opposite directions and are said to be anti-parallel. Different forms of DNA helixes can be formed but the B form of DNA is the preferred one. It is a right-handed helix with a pitch of 3.4 nm and 10 bases per each turn of the helix, such that the distance between one base pair is 0.34 nm.

DNA detection schemes on surfaces are actively investigated. The development of DNA sensors or DNA chips for the automation of the analysis process and the regeneration of the used sensor surface. Most, if not all such nucleic acid detection schemes are designed in a sandwich format. They exploit the specificity of base recognition between DNA strands and the high binding constants of the resulting duplex. The sensor surface is usually modified with probe DNA of known sequence and is exposed to an aqueous solution of the target sequence. Monitoring of hybridization of the target to the modified sensor surface indicates the complementary of probe and target. Thus, from the analysis of the binding processes the target sequence can be deduced. In particular in the case of DNA chips thousands of different probes are immobilized and analyzed simultaneously. This process is called sequencing by hybridization (SBH) and relies on the discrimination between fully matched and mismatched oligonucleotide pairs [5-4, 5-5]. In the next section, the architecture used in this work will be explained.

5.2 The Biological System

A standard streptavidin matrix was used to immobilize the oligonucleotide on the surface as follows:

The gold layer was modified by biotinylated thiol (a mixture of 11-mercapto-(8-biotinamido-4, 7, dioxaoctyl-)-undecanoylamide and 1-mercapto-undecanole with a ration of 1:9). Streptavidin was used as a linkage between the biotinylated thiol and the biotinylated DNA probe; the DNA target was labelled with Cy5. This is a standard DNA system [5-6], where injecting the target results in a high signal as mentioned before. Fig. 5.3 shows the system and the chemical structure of the thiol.

5-4. Bains, S. and Smith, C. G. *J.Theor. Biol.*1988, 135, P. 303-307
5-5. Drmanac, R. et.al. *Science* 1994. 260, P. 1649-1652
5-6. Neumann, T. et al. Advanced Functional Materials 2002, 12(9), P. 575-585

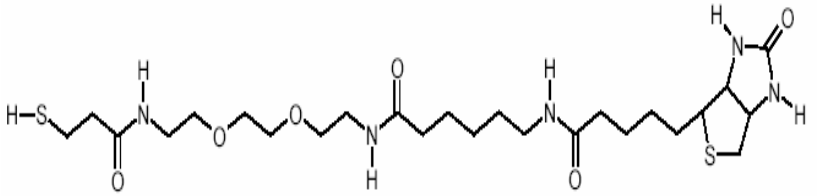

(a) Biotinylated Thiol

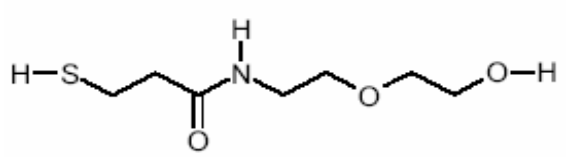

(b) OH-terminated Thiol

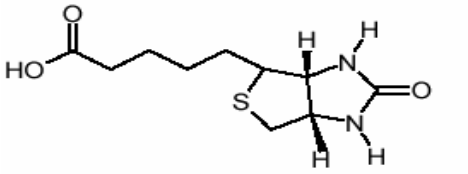

(c) A biotin molecule, the structure formula of biotin (right) exhibits a carboxylic function which can be used to couple biological molecules to the ligand.

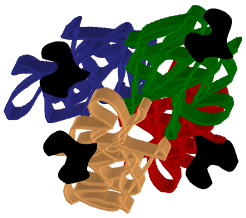

(d) Tetrameric Streptavidin (left) can bind up to 4 biotin molecules (black) with high affinity.

Fig. 5.3 The materials used to build the Streptavidin system

As mentioned before, embossed gratings were used in these experiments. Grating couplers were used in a wide range recently as optical biosensors [5-7-5-10]; surface plasmon fluorescence spectroscopy with grating couplers is an effective method in DNA detection. Injecting the chromophore labelled target of interest results in a major increase of fluorescence signal, coming from both the bulk and from surface- bound species. In the standard DNA system, with the injection of the labelled target, the observed increase in the signal is coming from both the bulk and the surface binding reaction, rinsing results in an instant drop of fluorescence to an intensity level which corresponds to surface-bound population; this is schematically represented in fig. 5.4.

In case of the grating, the fluorescence light is collected from the front side where there is more contribution from the reflected light, leading to a very high bulk signal. This represents a big problem for the sensitivity of the system. This work focuses on finding a way to overcome this problem by eliminating the bulk signal without affecting the surface signal.

5-7. Wittwer, V. et al. *Glass Science and Technology-Glastechnische Berichte* 2000, 73(4), P. 116-118
5-8. Akkoyun, A. et al. *Biosensors and Bioelectronics* 2002, 17(8), P. 655-664
5-9. Duveneck, GL. et al. *Analytica Chimica Acta* 2002, 469(1), P. 49-61
5-10. Cottier, K. et al. *Sensors and Actuators B* 2003, 91(1-3), P. 241-251

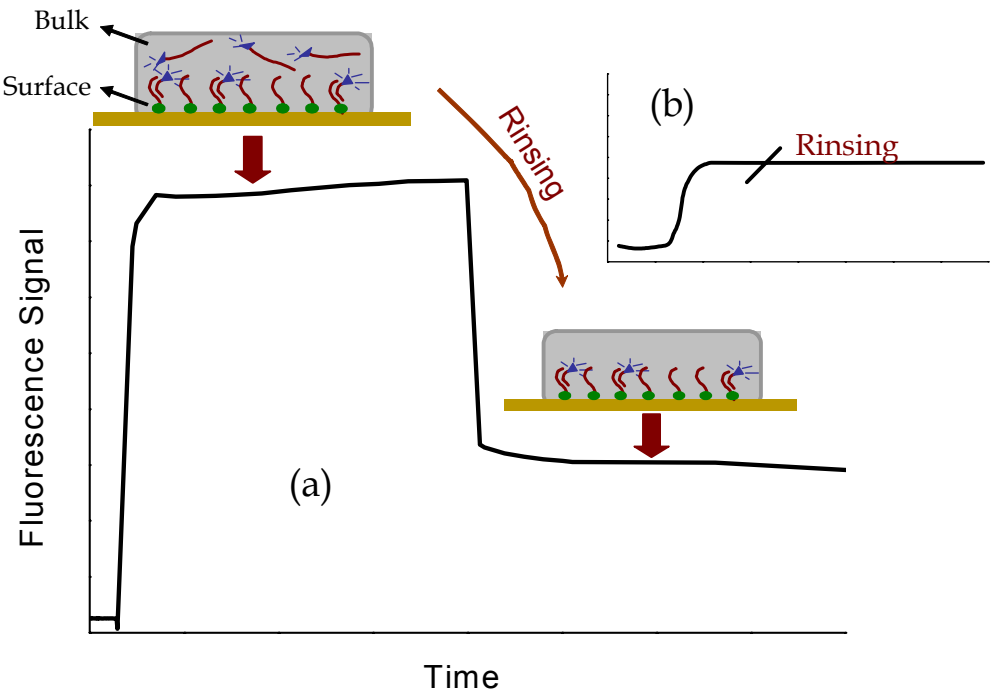

Fig. 5.4 (a) A schematic drawing showing the bulk jump due to injecting the labeled target, and after rinsing, where all the unbind species are removed, (b) the desired signal, where there is no change in the signal after rinsing.

5.3 Bulk Quenching

The principle of fluorescence resonance energy transfer was used, where the target (to be detected) labelled with fluorescence molecules was used as a donor in the presence of another fluorescence molecule (to act as an acceptor), the energy will be transferred from the donor to the acceptor. So, upon injecting a mixture of these solutions, there will not be any bulk jump, and the fluorescence signal in this case is coming from the surface reaction. In this case, rinsing would not change the signal because the target-quencher mixture is washed away with no impact on the fluorescence originating from the surface-bound species.

FRET has wide applications in studying biological molecules [5-11-5-15]. It is a distance dependent procedure whereby the emission energy of a donor chromophore acts as the excitation energy for an acceptor chromophore (*refer to section 2.5.3*).

5-11. Ha, T. et al. *Proc. Nat. Aca. Sci.* USA 1996, 93, P. 6264-6268
5-12. Charreyre, M. et al. *Langmuir* 1997, 13, P. 3103-3110
5-13. Selvin, P. *Nature Structural Biology* 2000, 7(9), P. 730-734
5-14. Widengren, J. *J. Phys. Chem. A* 2001, 105, P. 6851-6866
5-15. Heyduk, T. and Heyduk, E. *Nature Biotechnology* 2002, 20, P. 171-176

In order to eliminate or reduce this signal, the target was mixed with another DNA sequence that exhibits mismatch 1 with the target, the reason for choosing the sequence to be mismatch 1 was to be sure that the target-quencher hybrid is less stable than the target-probe complex, and thus, can not inhibit the surface reaction, fig. 5.5 shows the used biological system. The couple of dyes used in this experiment were Cy 5 and Cy 5.5, with a strong overlap between the absorption and emission spectra of these two dyes. This makes them ideally suited for FRET application (fig. 5.6).

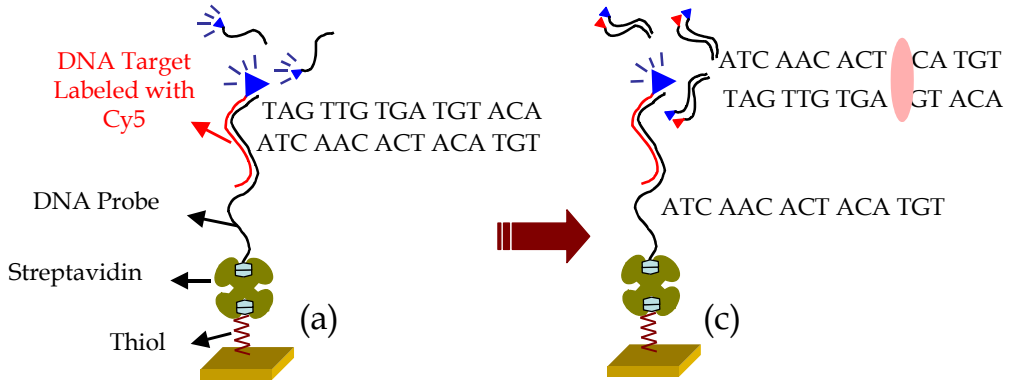

Fig. 5.5 (a) A standard DNA system, the target labeled with Cy5 exhibits mismatch 0 with the probe, and the unbind species emit in the bulk, (b) a mixture of the target and another sequence labeled with Cy5.5 that exhibits mismatch 1 with the target was used, in this case, the unbind species do not emit in the bulk where the energy is transferred from Cy5 to Cy5.5

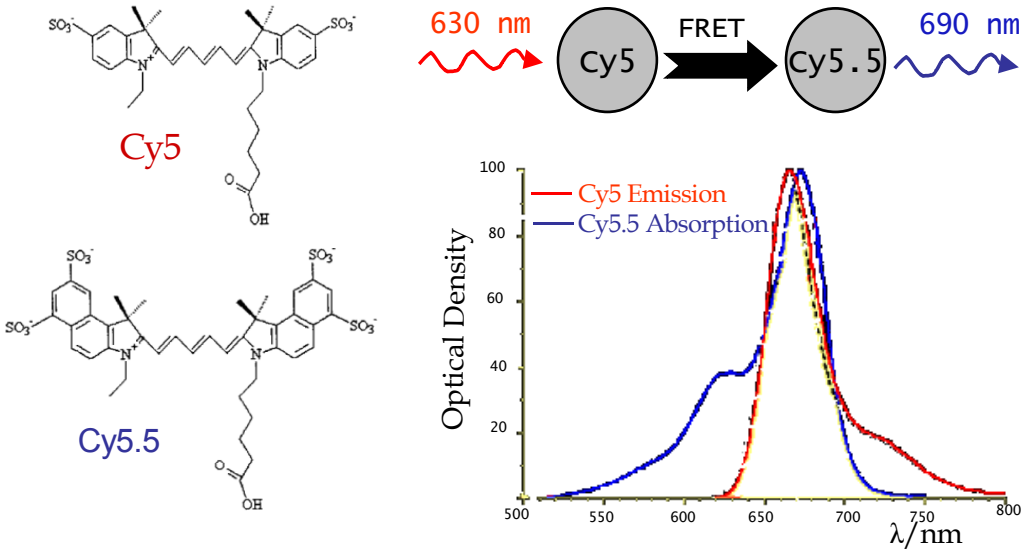

Fig. 5.6 The overlap between the absorption and emission wavelength of Cy 5 and Cy 5.5

Note:

Notice that the volume of the flow cell is very important parameter in this work, where increasing the thickness of the flow cell increases the bulk contribution and might changes the volume of the quencher needed to eliminate the bulk signal. A scheme of the flow cell used in our experiment is to the right.

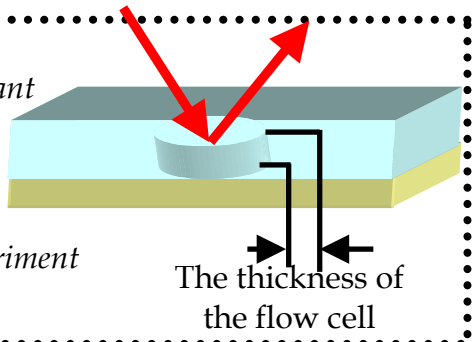

5.4 Mechanism of Energy Transfer

Before using the system explained before on the surface, it was convenient to look to the mechanism of the energy transfer in the bulk. Fig. 5.7 (a) shows the fluorescence emission intensity of a solution of DNA sequence labelled with Cy 5 with adding different concentrations of another solution of DNA labelled with Cy 5.5 (quencher), the fluorescence intensity decreases with increasing the quencher concentration as expected, but the decrease is not linear, and after adding 65% of the quencher volume, the fluorescence intensity is stable.

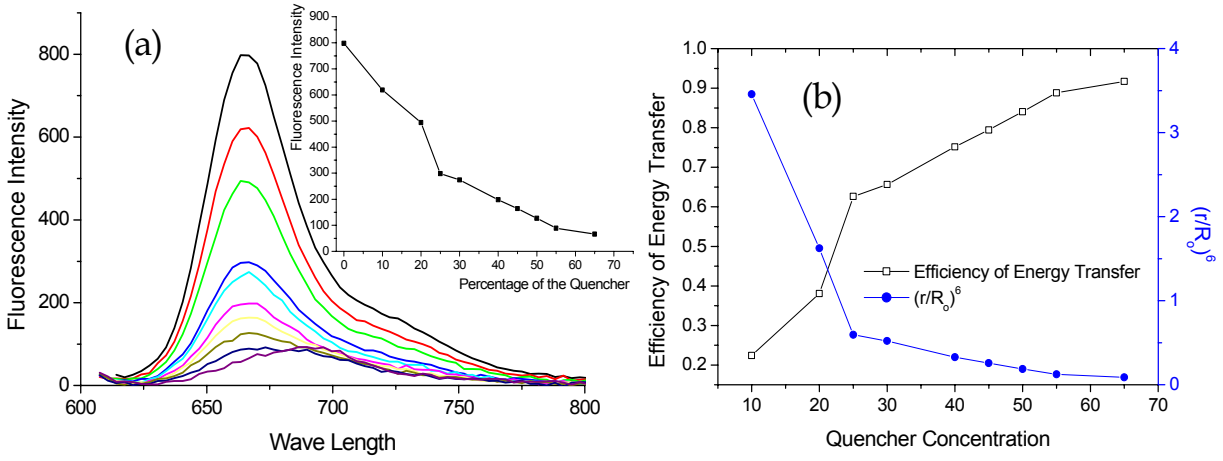

Fig. 5.7 (a) The decrease in the fluorescence intensity with increasing the quencher concentration, (b) The efficiency of energy transfer and the change in the distance between the two dyes as a function of the quencher concentration

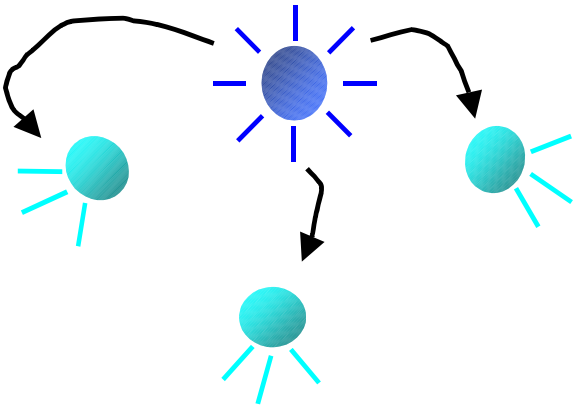

Fig. 5.8 The energy transfer in solution is random, where the orientational factor is randomized rotational diffusion

It is hard with these experiments to find out which mechanism is responsible in this case. In solution, both donor and acceptor are considered to be distributed in three dimensions. In this case, the orientation factor is randomized by rotational diffusion. To declare this more, both the efficiency of energy transfer and the distance between the two dyes were calculated as a function of the quencher concentration (fig. 5.7 (b)) as follows [2-12]:

$$E = (1-F_{da}/F_d)$$

Where F_{da} is the fluorescence intensity of the donor in the presence of the acceptor, and F_d is the intensity of the donor in the absence of the acceptor. E is the efficiency of energy transfer,

$$E = 1/[1+(r/R_o)^6]$$

As shown in the figure the efficiency of energy transfer increases with increasing the quencher concentration at the same time that the distance between the two dyes decreases. The decrease in the distance between the two dyes increases the probability of having strong coupling.

The question now is if immobilizing the two dyes on the surface will show the same behavior. The DNA system explained before was used on the surface. After immobilizing the DNA probe, the target, labeled with Cy5 was injected and the bulk jump was observed. Different concentrations of the quencher were added to the target solution to be circulated with the target, starting from 5% concentration. Fig. 5.9 shows the decrease in the fluorescence intensity with increasing the quencher concentration till 20% where the fluorescence was almost stable with adding more quencher, this means that all the molecules in the bulk were already quenched and the signal in this stage is the real surface signal. At this point, the bulk was rinsed with buffer, and it was noticed that there is a small change in the signal after rinsing. This experiment was repeated few times and the results were the same, this decrease in the signal after rinsing could be explained according to the nature of dyes used here, Cy5 and Cy5.5, where Cy 5.5 still can emit light at 670 nm wavelength which is the window that we looked through.

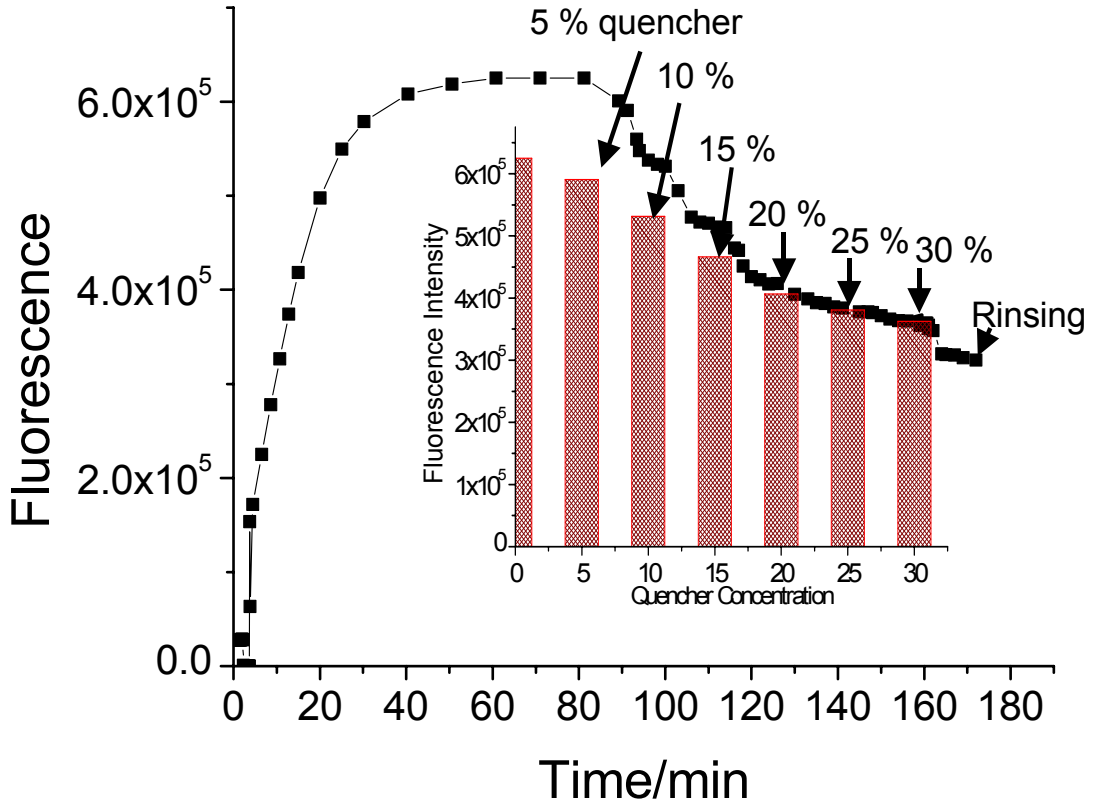

Fig. 5.9 The decrease in the fluorescence intensity with increasing the quencher concentration on the surface using the DNA system explained in the text

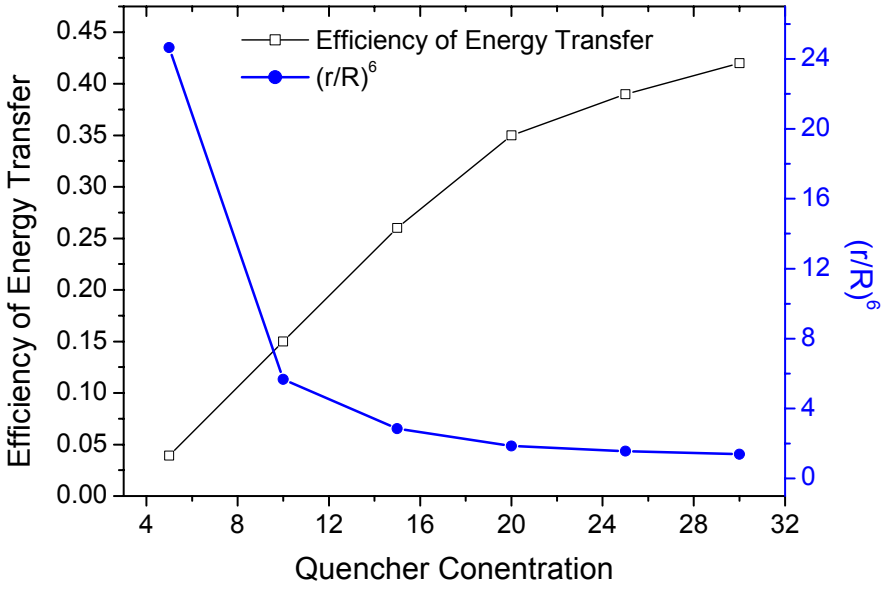

Fig. 5.10 The efficiency of energy transfer and the change in the distance between the two dyes as a function of the quencher concentration in case of working on the surface

In case of working on the surface, the efficiency of energy transfer and the distance between the two dyes were also calculated as a function of the quencher concentration (fig. 5.10). Comparing these results with the one from working on the bulk shows that the efficiency of energy transfer in case of working in the bulk is higher than on the surface (fig. 5.11).

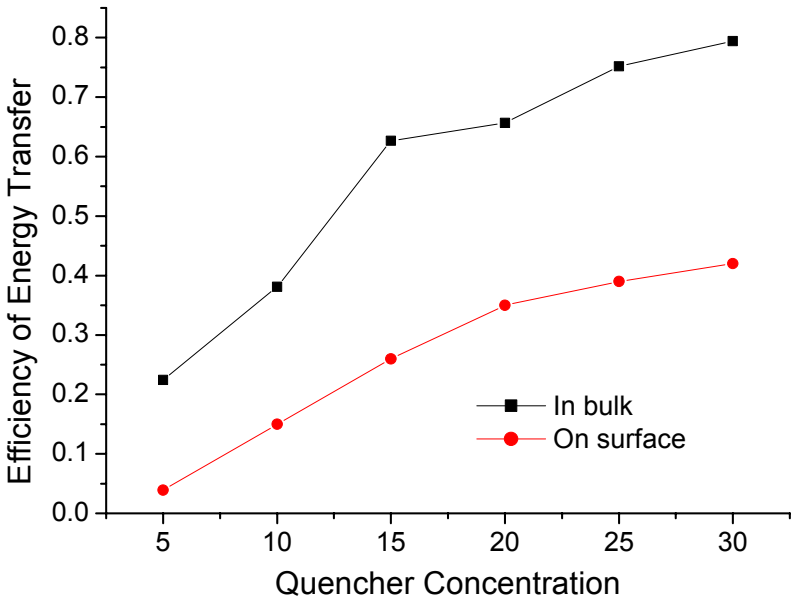

Fig. 5.11 The efficiency of energy transfer and the change in the bulk is higher than that on the surface

The orientaional motion can have significant effect on the rate of energy transfer. The higher rate of energy transfer means lower survival time, so the rotational diffusion of the dipole on chromophores is high (fig. 5.12). This means that rotational diffusion in the bulk is higher than that on the surface.

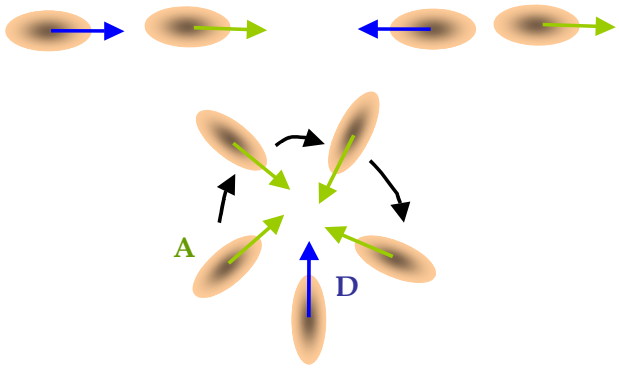

Fig. 5.12 A scheme representing the orientational motion and the rotational diffusion of the dipole of the chromophores

From these results, 20% of the quencher was believed to be enough to quench all the bulk molecules on the surface under our conditions. To confirm these results, the same system was used on the surface but instead of injecting the target, a mixture of the target and 20% of the quencher was injected, as shown in fig. 5.13, the bulk jump was almost eliminated, however the saturation is reached later than in the first case.

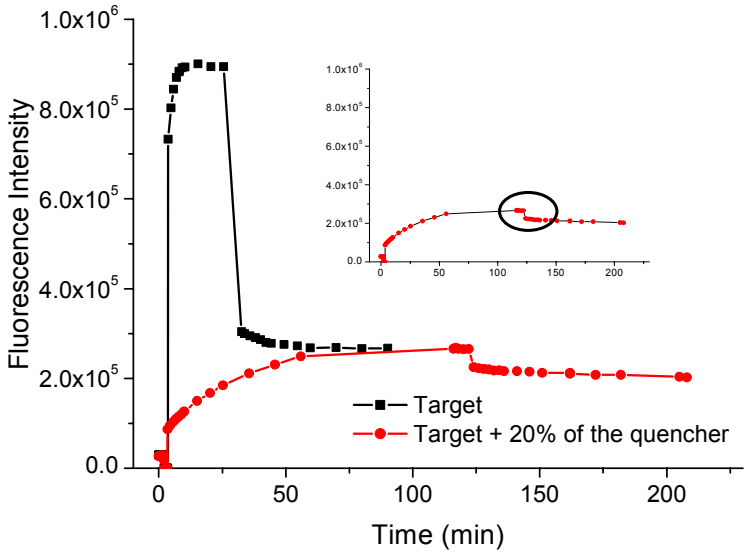

Fig. 5.13 In case of using the target, there is a huge bulk jump, where the signal is coming from both the bulk and the surface, while with using a mixture of the target and the quencher, the signal is coming only from the surface, notice the small change in the signal after rinsing, which could be due to the nature of Cy5.5

5.5 Conclusions

In all the standard optical biosensors, the bulk jump due to the unbound species represents a big problem where it can decrease the sensitivity of these sensors. This work presented an attempt to design architecture to reduce or eliminate the bulk signal. The principle of fluorescence resonance energy transfer was used. The DNA target to be detected was mixed with another sequence that exhibits mismatch one with it. The mixture percentage was studied to quench the unbound species without affecting the surface binding reaction. This can be a way to have higher sensitive DNA sensors where it is easy to detect the signal coming from the surface directly.

The results shows that the rate of energy transfer in case of DNA coupling in the bulk is higher than in coupling on the surface which could mean that the rotational diffusion in the bulk is higher.

Chapter -6-

LONG RANGE SURFACE PLASMON FLOURESCENCE SPECTROSCOPY

6. LONG RANGE SURFACE PLASMON FLOURESCENCE SPECTROSCOPY

6.1 Brief Survey

In 1981, Dror Sarid, University of Arizona, observed a phenomenon, which he called long range surface plasmons [6-1]. While he was solving the equation of injected surface-plasma waves that propagate on thin metal films as a function of the film thickness, he observed the splitting of the modes into two branches, and he predicted that one can reach propagation distances that are more than one order of magnitude larger than observed before.

This was the beginning of the observation of LRSPR, after that many reports have been published to study LRSPR theoretically and experimentally. Graig et al. measured the propagation and attenuation constants of long range surface plasmon polaritons on thin metal films [6-2]. They found that the attenuation constant of the LRSPR mode can decrease by a factor of 63 relative to that obtained with a thick metal film.

Yang et al presented in 1991 an analysis of the surface modes of a thin slab of material surrounded symmetrically by dielectric media [6-3]. They found that the long range surface mode exists almost for any value of dielectric constant.

In 1996, a multilayer system of Teflon-Au-Teflon-air was studied by Manfred Kessler and Elizabeth Hall. They demonstrated the existence of long range SPR and long range SER (Surface Exciton Resonance) theoretically and the practical construction of multilayer with suitable dielectric properties [6-4].

Another try from Wood et al. to excite long range surface plasmon was done by placing nickel films in a symmetric environment to allow coupling to LRSP modes [6-5].

All these tries were mainly concerned of using LRSPR as a high resolution system, or studying some theoretical models to prove the existence of LRSPR in different architectures.

6-1. Sarid, D. *Phy. Rev. Lett.* 1981, 47(26), P. 1927-1930
6-2. Graig A. et al. *Optics Letters* 1983, 8(7), P. 380-382
6-3. Yang F. et al. *Phy. Rev. B* 1991, 44(11), P. 5855-5872
6-4. Kessler, M. and Hall, E. *Thin Solid Films* 1996, 272, P. 161-169
6-5. Wood, E. L. et al. Optics Communications 1996, 132, P. 212-216

Another different way to use LRSPR in sensor applications was reported by Nenninger et al. in 2001 where they used in a wavelength modulated surface plasmon resonance sensor [6-6]. They claimed that LRSPR sensor had a sensitivity of seven times higher than the conventional SPR; their sensitivity was based on the response during a refractometric experiment.

The last work, using LRSPR in biosensor applications, was published recently [6-7]. Wark et al. created a novel bioaffinity sensor based on SPR imaging measurements of a multiple layered structure that supports the generation of LRSPR at the water metal interface.

In our work, we studied LRSPR from a different point of view. For example, as mentioned before, earlier work concentrated on LRSPR as a high resolution system. We will prove here that the high resolution does not add any benefit to this system and for the first time, we will combine LRSPR with fluorescence measurements. We found that LRSPR has a great advantage which is the electric filed at the interface which is much higher than the conventional SPR, and placing fluorescence molecules in the vicinity of this field increase the measured signal by a factor of 7-9. This all will be explained in details in the next sections of this chapter.

6.2 LRSPR against SPR

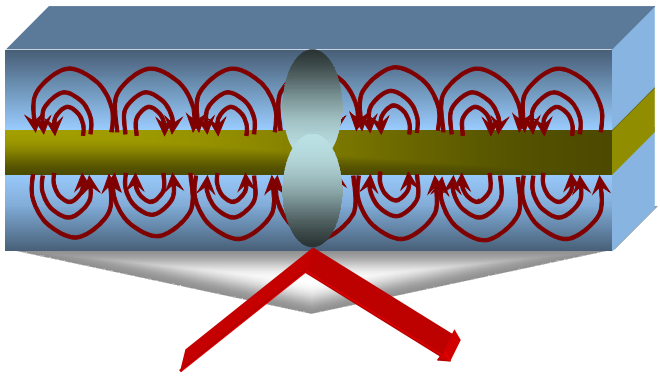

Fig. 6.1 The long range surface plasmon system, the metal layer is surrounded by two symmetric layers, and the surface plasmons are created on the both interfaces leading to the overlapping of the two evanescent fields

6-6. Nenninger, G. G. et al. *Sensors and Actuators B* 2001, 74, P. 145-151
6-7. Wark, A. W. et al. *Anal. Chem.* 2005, 77, P. 3904-3907

Fig. 6.1 shows the architecture that can excite LRSPR, with the metal layer being surrounded by two identical layers. Surface plasmons are excited on both interfaces. Two interfaces and two surface plasmons mean also two evanescent waves extending into both the dielectric medium and into the metal. Depending on the thickness of the metal layer, these two fields can overlap resulting on the establishment of a transverse standing wave. Therefore, this SPW (surface plasma wave) mode splits into one symmetrical and one anti-symmetrical mode, referring to the transverse electric field distributions.

Previous analysis of the dispersion of the SPW that propagate on various combinations of thin films sandwiched between thin dielectric films revealed the existence and splitting of SPW modes as the metal thickness decreases [6-8, 6-9].

With all this work done to figure out the fundamentals of LRSPR, there is no clear definition for it. While some refer the name to the longer propagation length of the magnetic field component inside the dielectric. LRSPR can be best represented by the longitudinal electric field (E_x), where this component of the field is closely associated with the collective longitudinal oscillations of electrons [6-10] (fig. 6.2).

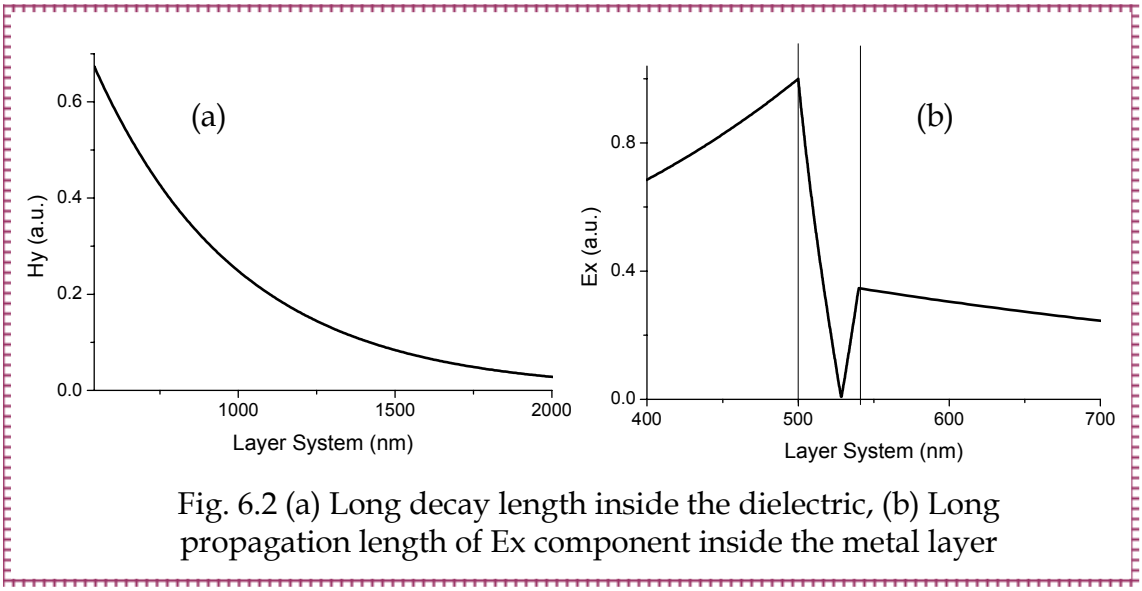

Fig. 6.2 (a) Long decay length inside the dielectric, (b) Long propagation length of Ex component inside the metal layer

As mentioned in the previous survey, the recent studies tried to play with this architecture to excite LRSPR. In our work, we assumed the system: prism/dielectric/gold/buffer.

Because the system is mainly used to prove that it could be of higher sensitivity than the conventional SPR system, theoretical and experimental comparisons were done all over the different points studied about LRSPR. Assuming a complete symmetric system, the first comparisons are shown in fig. 6.3,

6-8. Economou, E. N. *Phys. Rev.* 1960, 82, P. 539
6-9. Kliewer, K. I. and Fuchs, R. *Phys. Rev.* 1967, 53, P. 498
6-10. Pigeon, F. et al. *J. Appl. Phys.* 2001, 90(2), P. 852-859

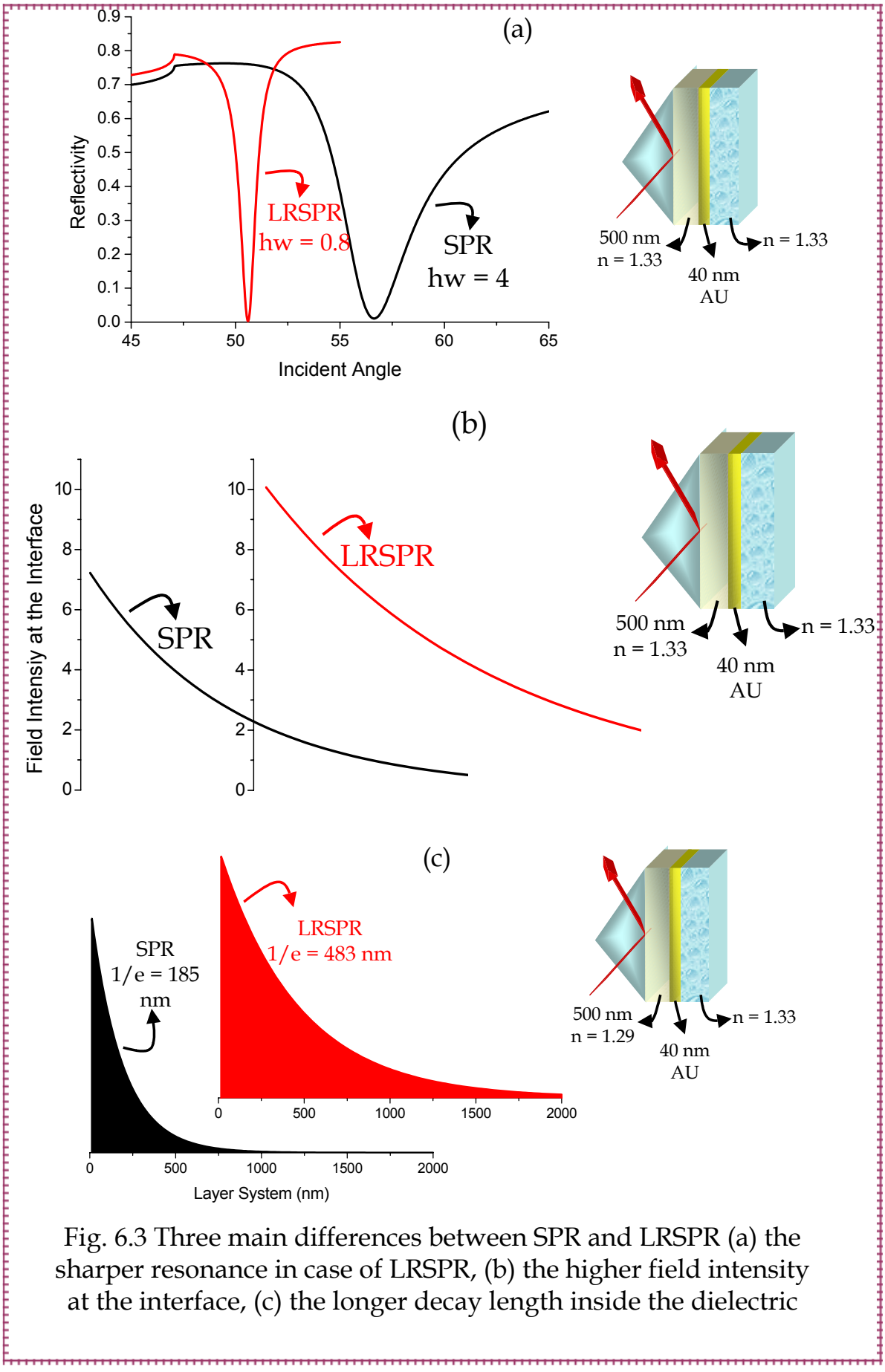

Fig. 6.3 Three main differences between SPR and LRSPR (a) the sharper resonance in case of LRSPR, (b) the higher field intensity at the interface, (c) the longer decay length inside the dielectric

where we can see three differences between SPR and LRSPR. These were the main differences that were believed to give the possibility of the LRSPR system to be of higher sensitivity.

The resonance curves show that the FWHM in case of LRSPR to be 0.3 while in SPR it is 3.4, this means that LRSPR has a very high resolution (*this was the point that all the previous studies were based on*), also as shown in fig. 6.2 (a), the resonance is at much lower angle than that of SPR which could be a could experimental advantage for some set ups.

The other advantage is the higher field intensity at the interface, fig. 6.2 (b) shows this difference and this was the first point that our work was based on, to use this high field intensity to excite a chromophore, expecting the signal to be of much higher intensity than in SPR.

The third difference is the longer decay length which goes in LRSPR to 400 nm inside the dielectric (fig. 6.2 (c)). This is another advantage that we could use to immobilize an extended biological matrix in the range of 500 nm; the longer chain means a lot of available sites for labelled biological molecules that can be detected. In case of SPR, the thickest matrix that could be used was the Dextran matrix which was in the range of 100 nm [6-11]. This is the range that can be used for the SPR, where longer chains will be outside the evanescent field, but in case of LRSPR, this chain can be elongated to more than 500 nm and still can be sensed.

Note:

- *The previous simulations were done in a liquid medium, assuming a complete symmetric system, where the refractive index of the first layer was 1.33 the same as water.*
- *As will be explained later, the field intensity at the interface can not express the exact experimental results, where the system is very sensitive to any small change in the thickness or the refractive index.*

6.3 Optimum Parameters

In order to find the optimum thicknesses of the materials used, theoretical simulations were performed for the highest coupling efficiency and the lowest FWHM, which as a consequence means the highest field intensity. The material used as the first dielectric layer was Teflon AF 1600. The refractive index of this material is 1.29 which is lower than that of water or buffer. As shown in fig. 6.4, the optimum thicknesses were found to be 500 nm for Teflon and 40 nm for gold.

6-11. Yu, F. et al. *J. Am. Chem. Soc.* 2004, 126, P. 8902-8903

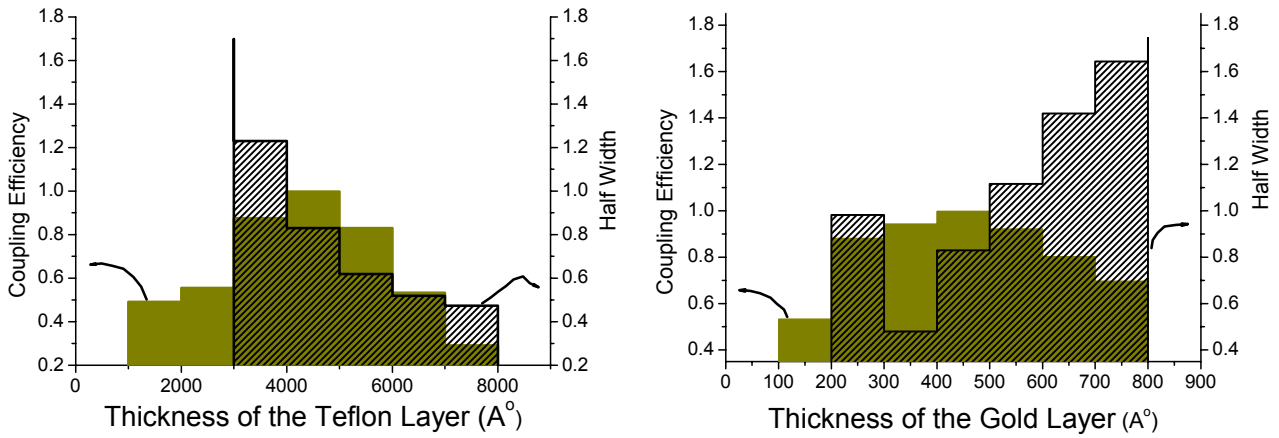

Fig. 6.4 The simulations done to find the optimum thicknesses of both Teflon and Au (a) changing the thickness of the Teflon layer from 100 to 500 nm increases the coupling efficiency and decreases the half width, after 500 nm, the coupling efficiency decreases again, (c) changing the thickness of the gold layer from 10 to 80 nm increases the coupling efficiency and decreases the half width until 80 nm, where the opposite starts to take place.

6.4 Sample Preparation

The architecture chosen was: Prism/Teflon/Au/Buffer. The reason of choosing Teflon was that it has a refractive index close to water or buffer (1.29), and the design was decided to be capable of using it as a biosensor.

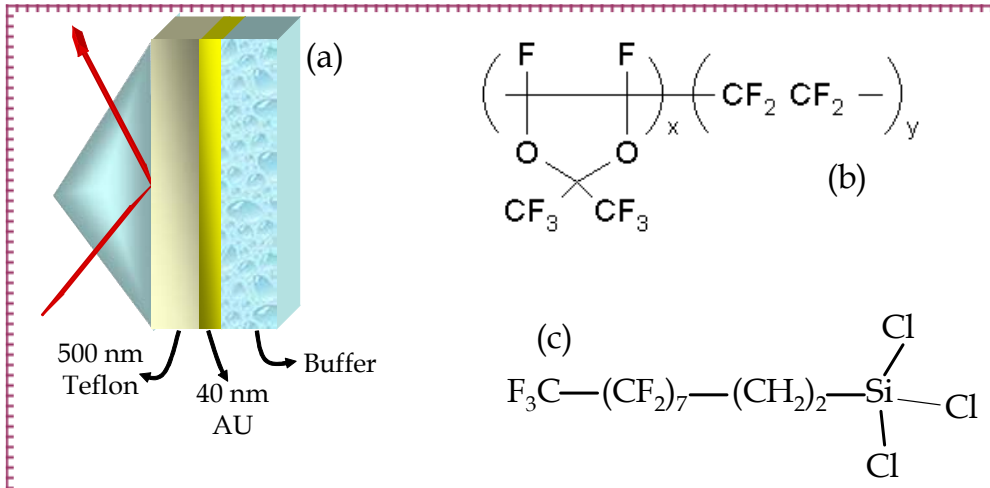

Fig. 6.5 (a) The system used to excite LRSPR, (b) the chemical structure of Teflon, (c) the chemical structure of the Perfluorodecyltrichlorosilane used to silanize the glass before Teflon deposition

Bk7 glass substrates were modified by Perfluorodecyltrichlorosilane (fig. 6.5 (c)) to improve the glass-Teflon adhesion as follows:

- Perfluorodecyltrichlorosilane is sensitive to air, so it was treated in a glove box, 2% solution was prepared using dry Toluene as a solvent.
- The glass substrates were cleaned by boiling in Isopropanol for 10 minutes and then dried by Nitrogen, as recommended by the Teflon manufacturer.
- Then, the substrates were immersed in the silane solution for one hour.
- The substrates were washed with toluene and dried with Nitrogen.

After modifying the glass slides with a silane layer, 3 % solution of Teflon 1600 was spin coated with 500 rpm for 30 sec. to have a thickness of 500 nm, the thickness was checked by a surface profiler (see Appendix A-2). Teflon 1600 was purchased from DuPont, and a fluorinated solvent (FC-77, purchased from Across) was used for dilution. The substrates coated with Teflon were baked at 110°C for 10 minutes.

The next step was gold deposition by thermal evaporation. The adhesion between Teflon and gold was proved to be good enough for our applications.

6.5 Figuring out some fundamentals

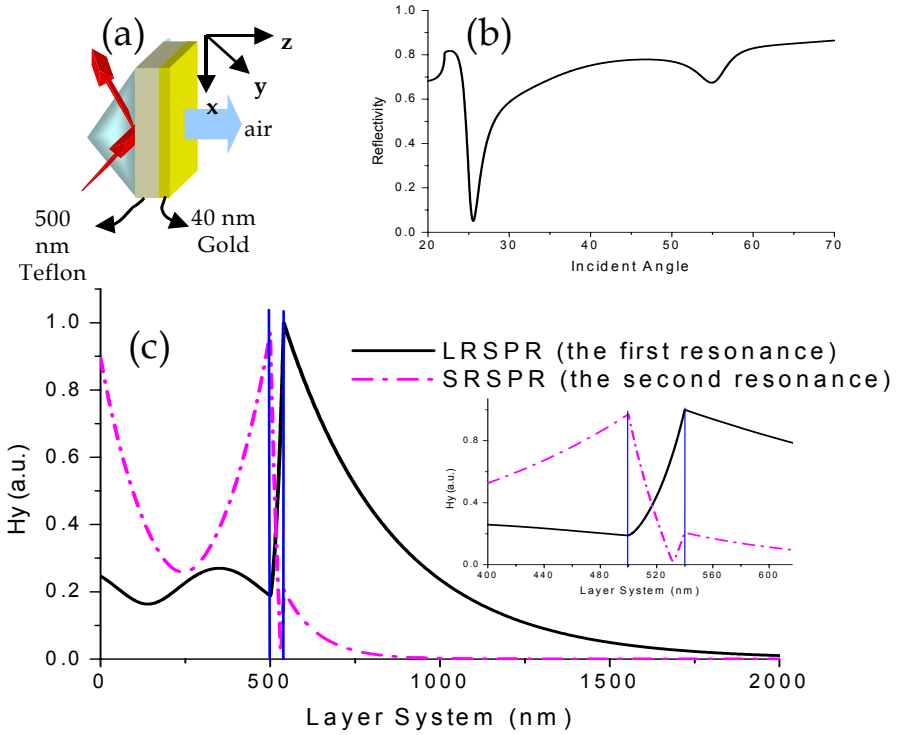

Fig. 6.6. (a) The system used for the simulation, the metal layer is surrounded by the Tefoln and air, (b) the reflectivity, shows two minima, the first one is due to the LRSPR, and the second one is due to SRSPR, (c) the magnetic field distribution of both LRSPR and SRSPR.

We started here with studying the system where the metal layer is exposed to air. Fig. 6.6 shows the system used; 500 nm of Teflon before 40 nm of Gold. In this case, two minima were observed as a result of the splitting of the mode to short and long range surface plasmons. From the simulations of the magnetic field distribution, it was confirmed that the first minimum is due to the LRSPR, where the field propagates to about 1500 nm in the air side, while for the second minimum, the field propagates to about 500 nm, which is nearly the same as in the conventional SPR, this is shown in fig. 6.6 (c).

The main idea of this work is to use the LRSPR as a biosensor, the metal layer must be exposed to buffer solution or water, as shown in fig. 6.7 changing the medium above the metal layer to water, changes the resonance angle which is due to LRSPR (as confirmed by the field distribution) to higher angle, while the second resonance (SRSPR) disappears. This means that in case of water, only one surface plasmon resonance could be excited. This mode has the same character as the LRSPR where the decay length of the magnetic field is about 310 nm, and the electric field propagates to zero inside the metal layer.

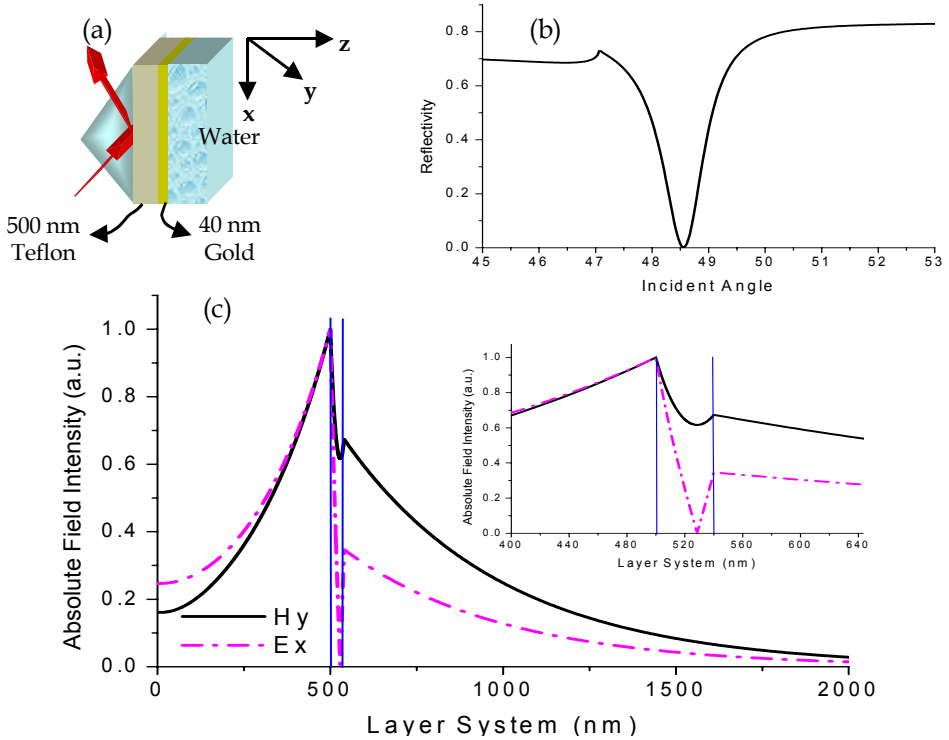

Fig. 6.7 (a) Changing the medium above the metal layer to water, (b) the reflectivity shows only one minimum, where the first resonance, due to the LRSPR, changes to higher angle and the second resonance disappears, (c) the magnetic field and the x-components of the electric field distributions for the LRSPR.

6.6 High Resolution is not Advantage!

Most of the previous studies about LRSPR were mainly concentrated on using it as a high resolution system because of the very sharp resonance, but the sharp resonance does not give any significant additional benefit for the LRSPR. This is because as the resonance width gets less, the angle shift becomes less. Theoretical simulations and experiments were done to calculate the sensitivity of both SPR and LRSPR based on the shift in the resonance angle, and as seen in fig. 6.8(a), theoretically, the shift in the resonance angle makes LRSPR a poor sensitive system where the sensitivity calculated for SPR is much higher.

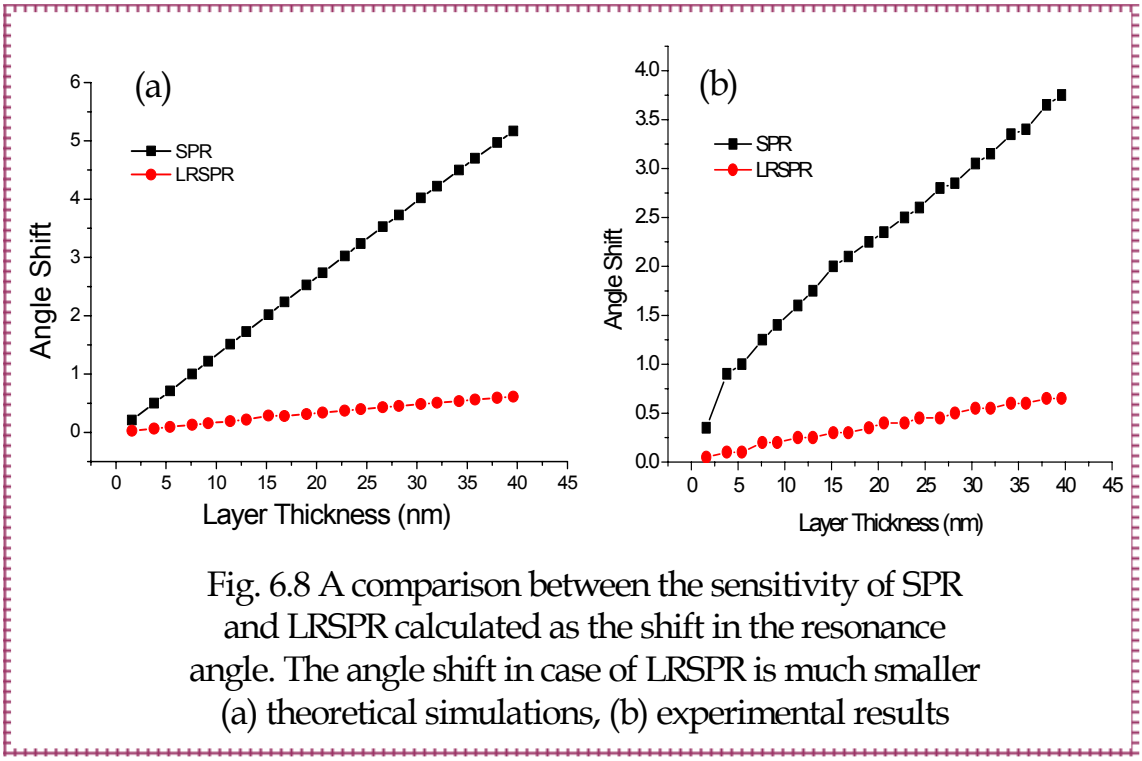

Fig. 6.8 A comparison between the sensitivity of SPR and LRSPR calculated as the shift in the resonance angle. The angle shift in case of LRSPR is much smaller (a) theoretical simulations, (b) experimental results

To prove this experimentally, a layer-by-layer system of Streptavidin and anti-body were built on the surface *(the same system used in chapter 4)*. From the simulations, the thickness of each layer can be found, the experimental angle shift as a function of the layer thickness is shown in fig. 6.8(b), and it agrees well with the theoretical simulations.

The sharp resonance in case of LRSPR is combined with a smaller angle shift. Fig. 6.9 shows that the ratio between the full width of half maximum and the angle shift is almost the same for both systems. So, the high resolution of this system does not make it more sensitive.

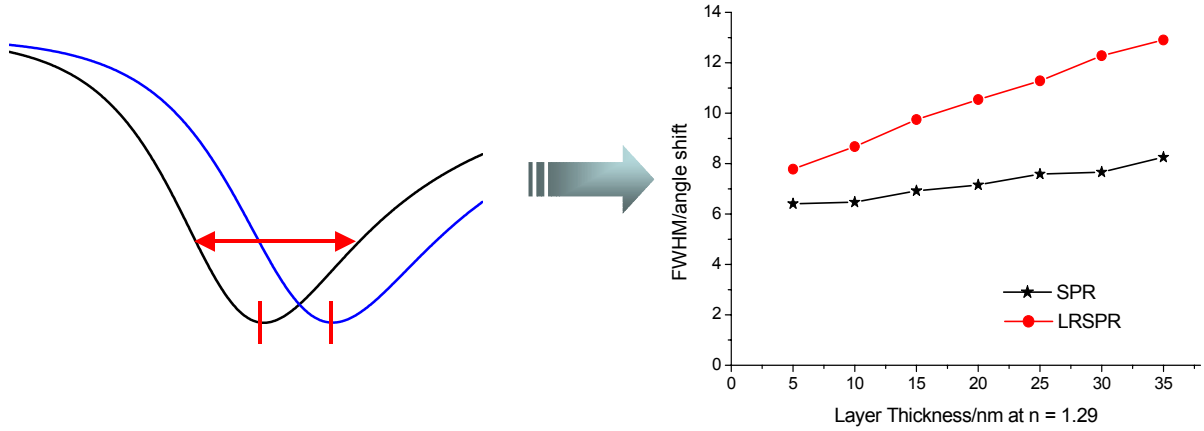

Fig. 6.9 The ratio between the full width of half maximum and the angle shift is almost the same for both SPR and LRSPR

6.7 Field Intensity and Fluorescence signal

6.7.1 Sensitivity Comparison

Since LRSPR was proved to be less sensitive if we look into the angle shift, so, it was more important to look to the field intensity and if we can use it. The idea of having higher field intensity at the interface was used to excite fluorescence; we wanted to compare the sensitivity of SPFS and LRSPFS using labeled molecules. As a first try, the system shown in fig. 6.10 was used to study the fluorescence intensity.

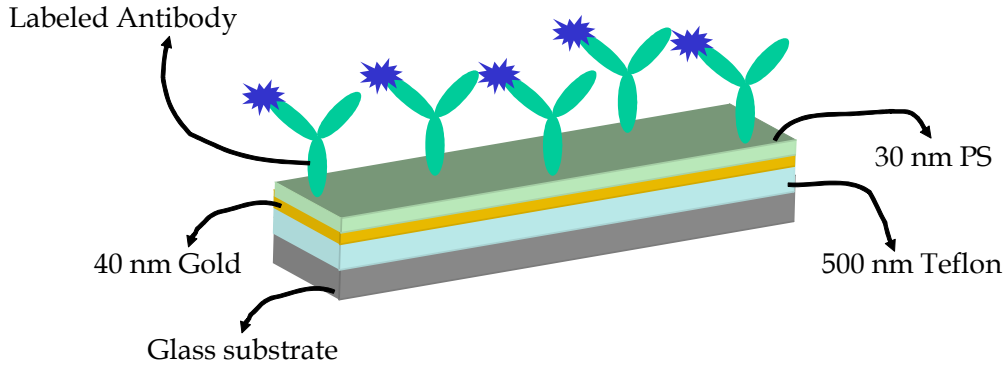

Fig. 6.10 The system used to compare the fluorescence intensity of SPFS and LRSPFS, 30 nm of polystyrene is spin coated above the gold layer to ensure a hydrophobic surface for the antibody to be physisorbed.

To compare the fluorescence intensity for both SPR and LRSPR, 30 nm of polystyrene was spin coated on top of the gold layer for both the samples of conventional SPR (*glass/2 nm Cr/ 50 nm Au/PS*) and those of LRSPR (*glass/500 nm Teflon/40 nm Au/PS*). The experiments were done under the same conditions. The reason for using 30 nm Teflon was to ensure a hydrophobic surface for the anti-body to be physisorbed and also to avoid quenching, as known from before; the optimum distance to have the highest fluorescence intensity is 30 nm. The results are shown in fig. 6.11; the fluorescence intensity in case of LRSPR is about 10.8 times higher than the conventional SPR.

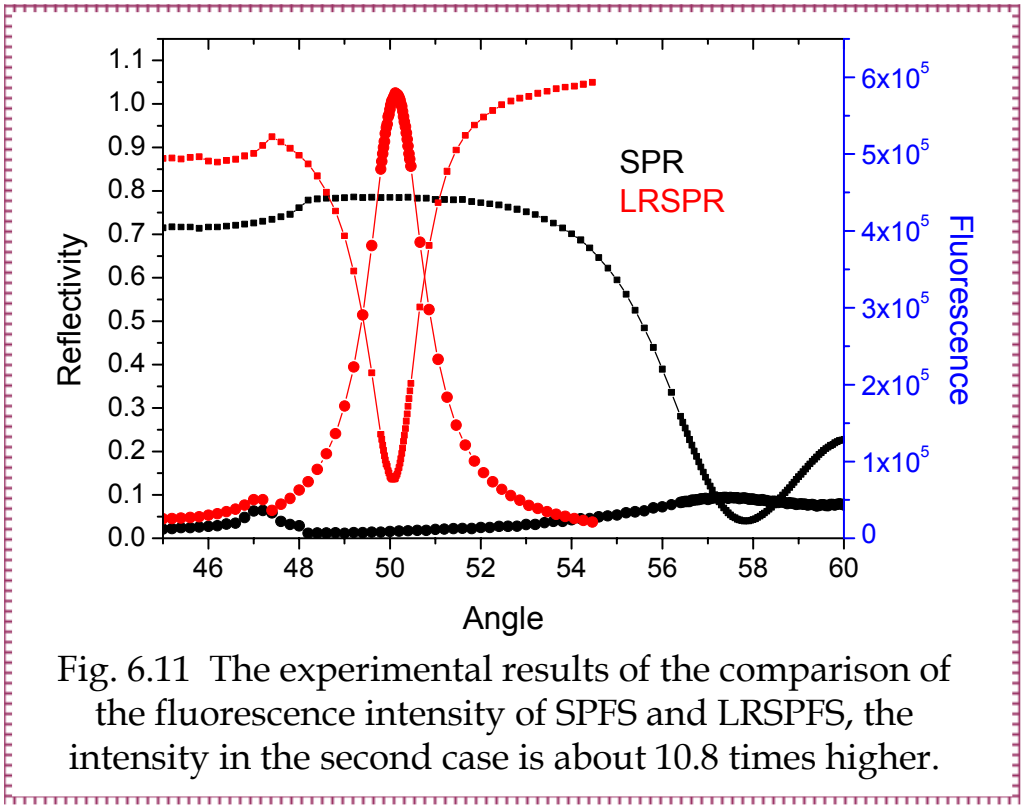

Fig. 6.11 The experimental results of the comparison of the fluorescence intensity of SPFS and LRSPFS, the intensity in the second case is about 10.8 times higher.

6.7.2 Roughness Effect

Teflon is a very rough material, especially at high thickness. As it is well known, the higher roughness might increase the amount of materials on the surface. Because of this, it was taken into account that the higher signal in case of LRSPR might be a contribution of both the field intensity and also the amount of chromophores on the surface.

To be sure that the fluorescence signal is mainly due to the field intensity of the LRPR, two experiments were done:

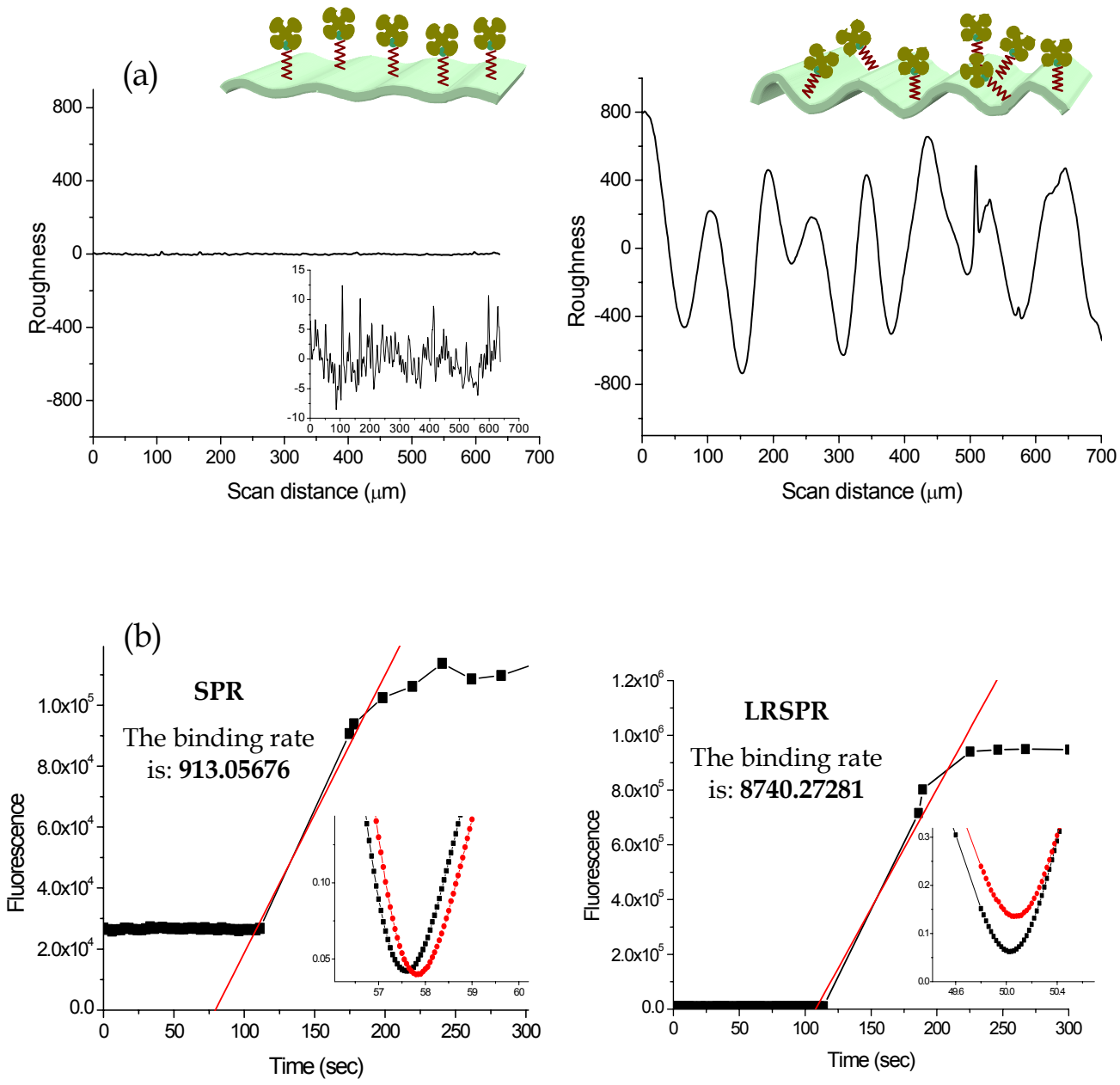

Fig. 6.12 (a) The roughness of the surface in case of the SPR system is in the range of 10-15 nm, but in the LRSPR system is in the range of 800 nm; the higher roughness means more material on the surface (b) the binding rates and the resonance angle shifts of SPR and LRSPR show that the LRSPR surface has an amount of material 1.1 times higher than that of SPR

- After preparing the SPR and the LRSPR samples with the system mentioned before, the surface of these samples were scanned by surface profiler (*see Appendix A*-2), as shown in fig. 6.12 (a), the roughness of the SPR system is in the range of 10-15 nm, while that of the LRSPR system is in the range of 80-100 nm. The higher roughness suggests having more material on the surface.

- The kinetics of the protein binding to the surfaces were monitored to calculate the binding rate, described as dR/dt [6-11], where R is the response that increases linearly with time t. the binding rate in case of LRSPR was higher than that of SPR. From the reflectivity scan, the angle shift shows that the LRSPR sample has an amount of material 1.1 times higher than that on the SPR sample surface (fig. 6.12(b)).

Comparing these results with the previous results that show the 10 times higher fluorescence signal, we can easily see that the contribution of the signal coming from the amount of chromophores on the surface is much smaller than that coming from the field intensity. Subtracting the factor of the material amount, we can predict that the signal in case of LRSPR is about 9 times higher than that of SPR.

We have to mention here that there were some variations in the fluorescence intensity in different experiments. Due to the very thick layer of the first dielectric layer, the system is very sensitive to very small changes in the thickness and the refractive index. These changes are very small that they can be in the error range, which is difficult to control experimentally. However, these variations do not diminish the principle of the higher sensitivity of the LRSPR system.

As an example for that, fig. 6.14 shows the fast change in the field intensity at the interface with very slight changes in the refractive index of the first dielectric layer.

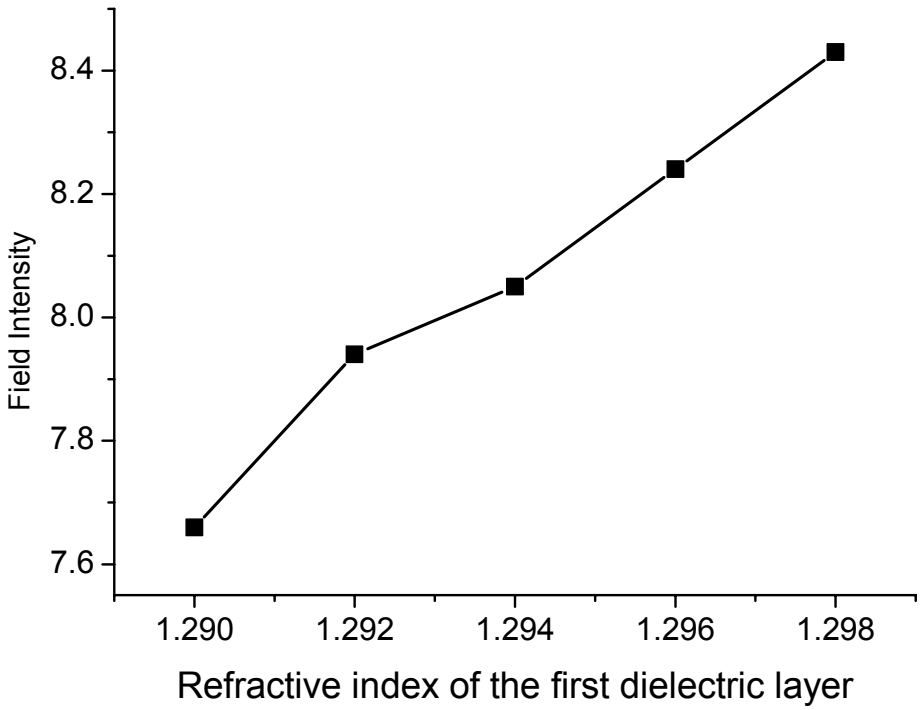

Fig. 6.13 The fast change of the field intensity at the interface with very slight change in the refractive index of the first dielectric layer

6.8 Effect of the Distance from the Metal Layer

In the previous experiment, the chromophore was placed about 30 nm above the metal layer, as we wanted to use this system in different biological system, like standard DNA system (*used in chapter 2*), or a layer by layer system (*used in chapter 4*). In these systems, the chromophore could be at very small distances from the metal surface, typically from 5-10 nm. What we have found is that the fluorescence signal in case of LRSPR was lower than the SPR one which contradicts with the previous results. In fig 6.15, two comparisons are shown, the first was done using a DNA system, and in this case, the distance is about 10 nm. The other one was done using the physisorption on 30 nm of PS. The only difference here was the separation between the fluorescence molecule and the metal layer.

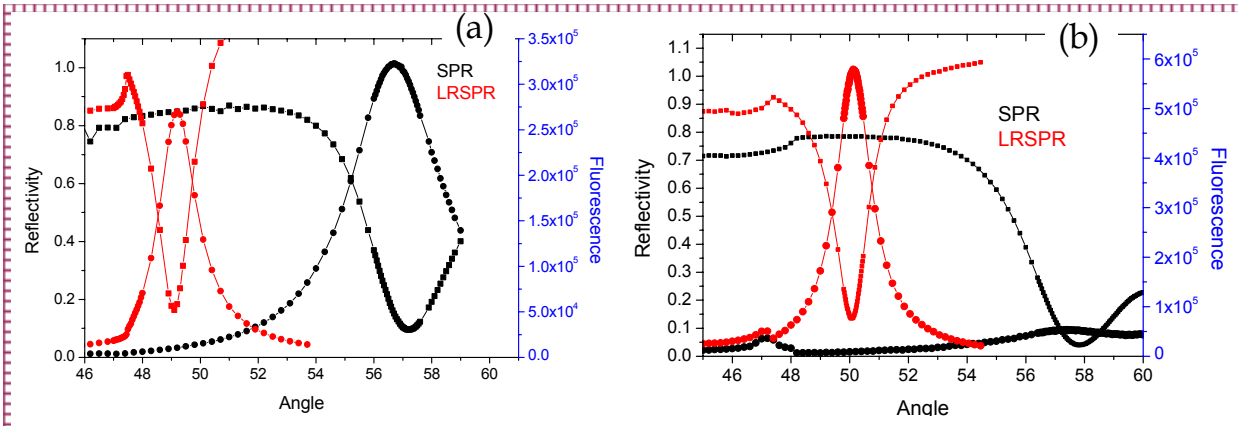

Fig. 6.14 (a) At small distances from the metal layer (glass/500 nm Teflon (1.29)/40 nm Au/DNA system), the fluorescence intensity for LRSPFS is lower than in SPFS, (b) but at higher distances from the metal layer (glass/500 nm Teflon (1.29)/40 nm Au/30 nm PS (1.58), the fluorescence intensity for LRSPFS is much higher than in SPFS

To find out what is the effect of the distance on the fluorescence signal. Theoretical simulations of the field distribution for SPR and LRSPR were done (fig. 6.16). In these simulations, the dielectric layer was supposed to be Teflon with 1.29 refractive index. As shown in the figure, at very short distances from the metal layer, the field intensity is almost the same, but it increases for LRSPR as the distance increases. This might explain the lower fluorescence signal for LRSPR at distances close to the metal layer, where at these small distances the field is not higher than in case of SPR, so the fluorescence signal is also not higher.

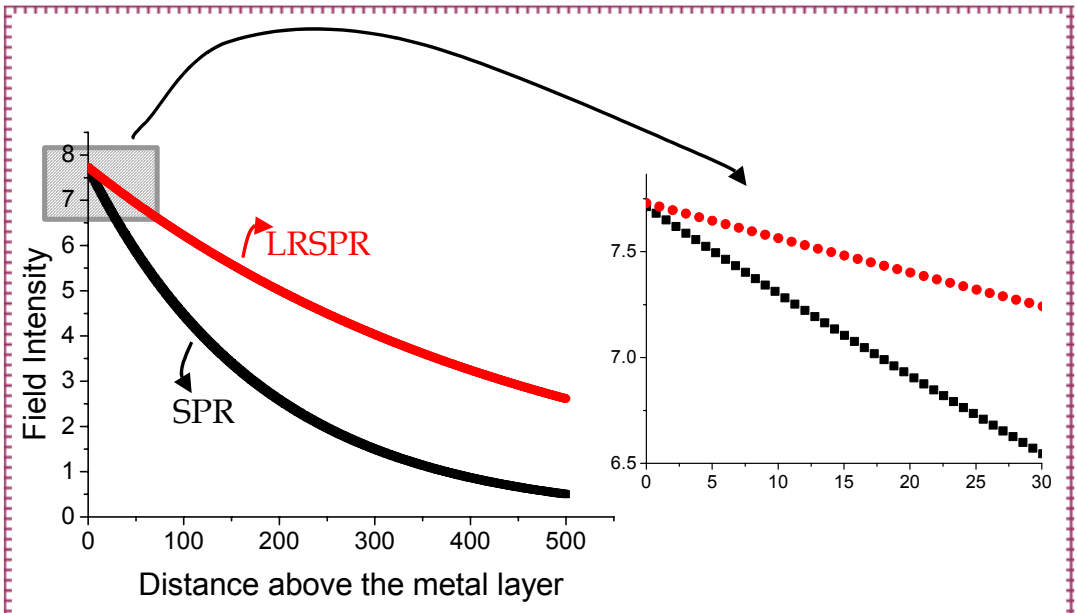

Fig. 6.15 The field distribution for SPR and LRSPR where the first dielectric layer has a refractive index of 1.29 shows that the difference in the fluorescence intensity increases with increasing the distance above the metal layer

To prove this in an experimental way, the layer by layer system (*used in chapter 4*) was applied on both the SPR and LRSPR systems, where with this system we can start from low distance and go to further distances. Fig. 4.17 shows the results where it is clear that at the first layers where the distance is less than 10 nm, the signal for LRSPFS is lower and then it starts to increase at distances about 13 nm above the metal layer.

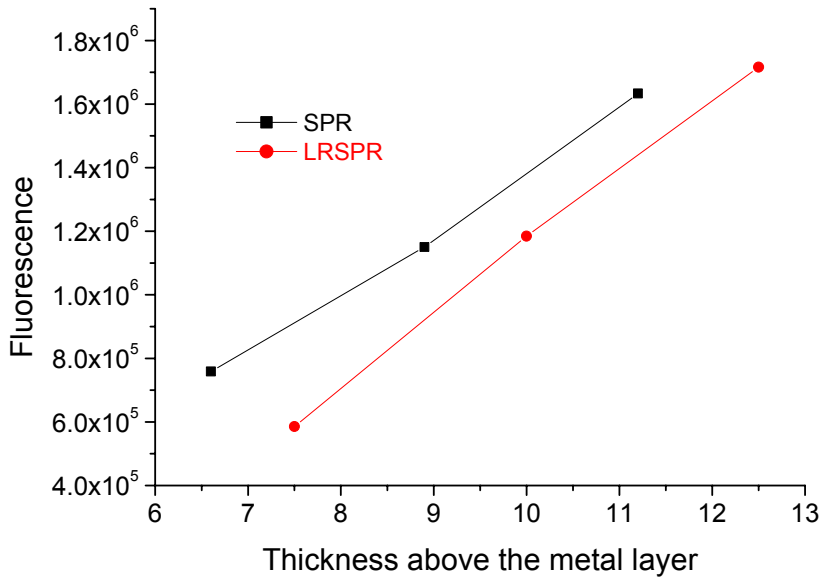

Fig. 6.16 A layer by layer system was used to monitor the fluorescence at different distances. At the first layers the fluorescence intensity for LRSPFS is lower and then starts to increase at about 13 nm

6.9 Effect of the Refractive Index of the First Dielectric Layer

The effect of the distance from the metal layer took us to discuss the effect of the refractive index of the first dielectric layer supporting LRSPR on the filed intensity at the interface and consequently on the fluorescence signal. Theoretical simulations were done for the field distribution (fig. 6.18(a)). From these simulations, it was found that the field intensity at the interface increases with increasing the refractive index of the first dielectric layer till 1.34 when the field intensity starts to decrease again, but surprisingly, as the field intensity increases due to increasing the system symmetry, the decay length decreases from 460 nm to about 350 nm, these results are shown in fig. 6.18(b). This concludes that the optimum refractive index of the first dielectric layer is 1.36, at this value, the decay length is 280 nm which is still higher than that of the conventional SPR (150 nm).

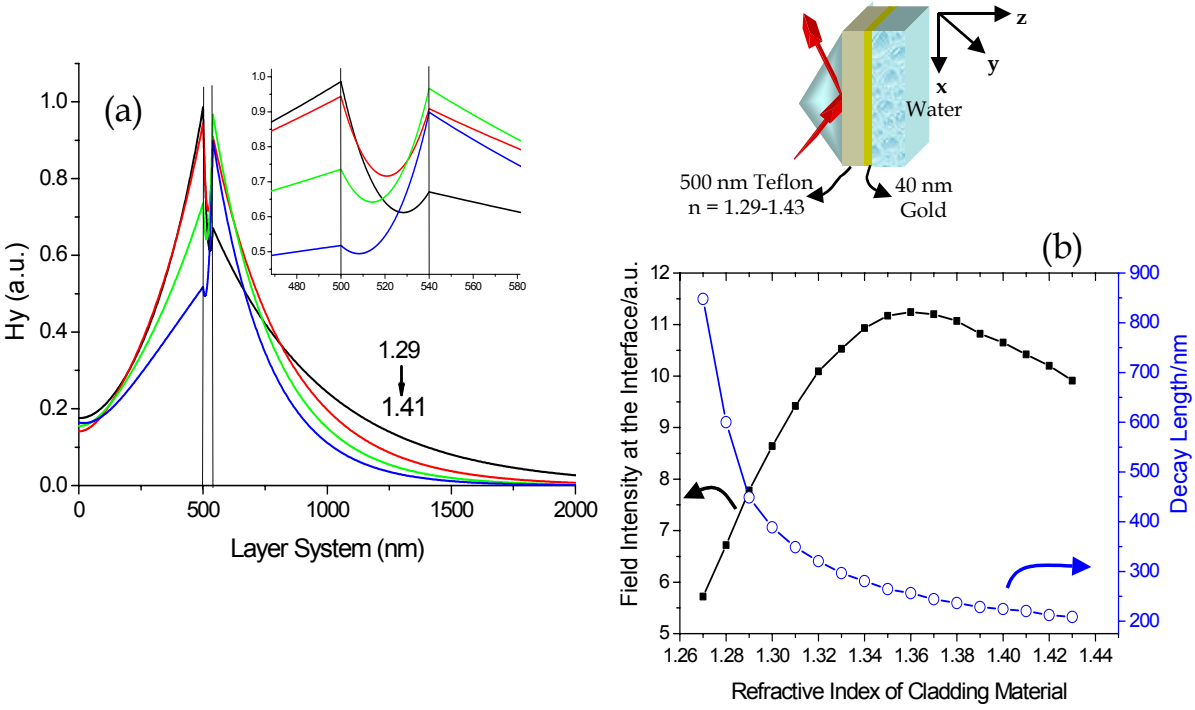

Fig. 6.17 The change in both the field intensity at the interface and the decay length with the change of the refractive index of the first dielectric layer

Unfortunately, there is no natural material that has a refractive index of this range, but some other materials that were synthesised to have a refractive index of about 1.34, like Cytop, from Asahi glass company (Japan) and a porous material manufactured by IBM (USA). Till the point of writing this thesis, trying to use these material in a biosensor configuration was not successful, however, the results with using Teflon was satisfying in the matter of the fluorescence signal and also in the long evanescent field that we tried to use it as a big advantage as will be explained in section 6.11.

Note

The optimum refractive index is 1.36 not 1.33 as was expected to make the system completely symmetric, this could be a consequence of the prism existence, where the light has to pass through the prism that has a different refractive index leading to disturbing this symmetry taking into account the relation between the wave vector and the field intensity.

6.10 Fluorescence Phase Shift

Studying the fluorescence with LRSPR leads to find out an interesting difference between SPFS and LRSPFS. It is known from before that in case of SPFS, the fluorescence peak is at a slightly lower angle than the resonance angle, and this is referred to the phase difference between the surface mode and the driving photon field due to the damping (loss) in the metal (*as explained in chapter 2*). In case of LRSPFS, this shift was found theoretically and experimentally to be at slightly higher angle at the metal analyte interface. This was proved theoretically from the simulations and to prove this experimentally, the fluorescence signal was studied at the metal analyte interface using the same system explained before. The results are shown in fig. 6.19, at the metal analyte interface, the fluorescence peak is at higher angle than the resonance angle, if the difference in the angles is referred to the phase shift, this means that the driving photon field is pushed to the other direction due to the first dielectric layer.

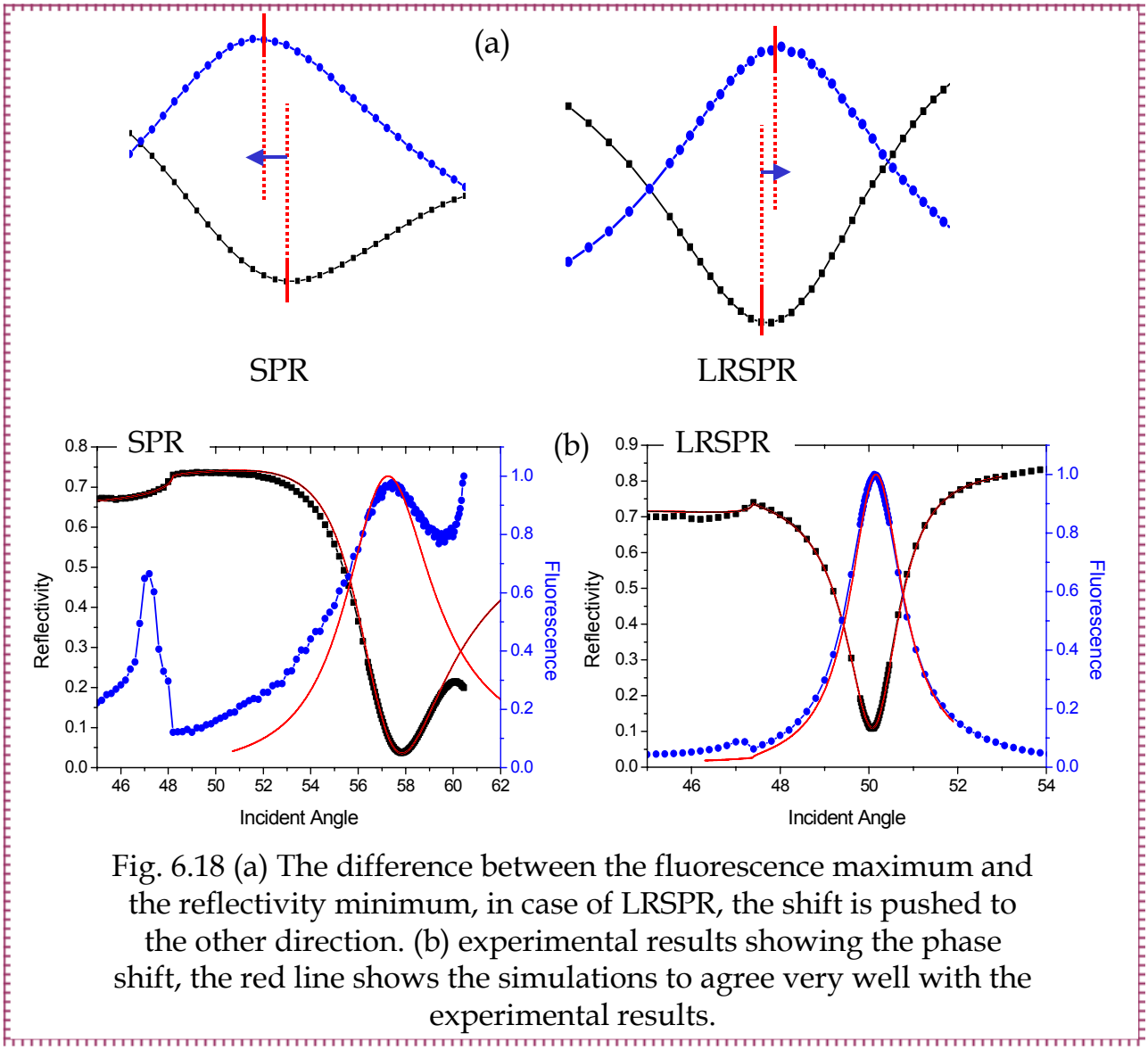

Fig. 6.18 (a) The difference between the fluorescence maximum and the reflectivity minimum, in case of LRSPR, the shift is pushed to the other direction. (b) experimental results showing the phase shift, the red line shows the simulations to agree very well with the experimental results.

For further investigation about this phase shift, we figured the difference between the resonance angle and the angle of the maximum fluorescence at the interface between the first dielectric layer and the metal, and at the interface between the metal and the analyte. This was done by mixing the Teflon layer that supports the long range SPR with a dye (DiIC1 (5) dye), after gold evaporation, the fluorescence signal was measured as a function of the incident angle. This is shown in fig. 6.20, where there is almost no angle shift.

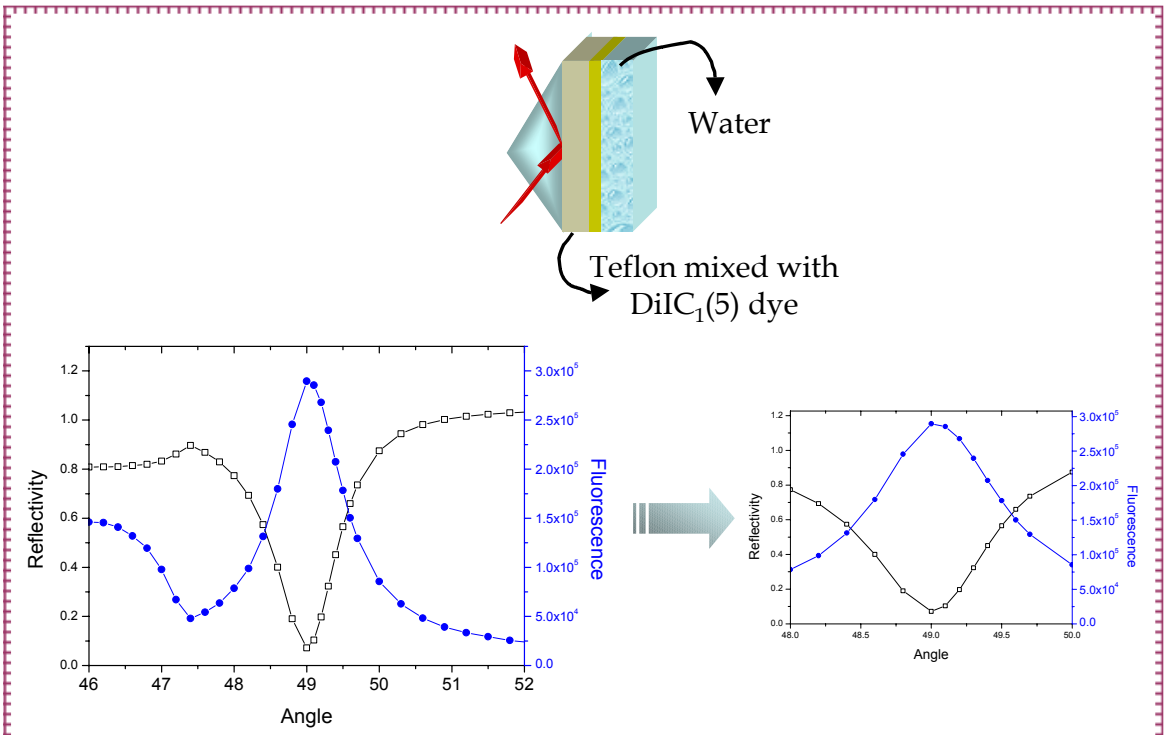

Fig. 6.19 The fluorescence signal scanned as a function of the incident angle showing that there is no phase shift at the dielectric metal interface.

These results were also confirmed theoretically by making theoretical simulations for both the reflectivity and the fluorescence intensity at the two interfaces (fig. 6.21). These results mean that the shift is due to the damping in the metal layer.

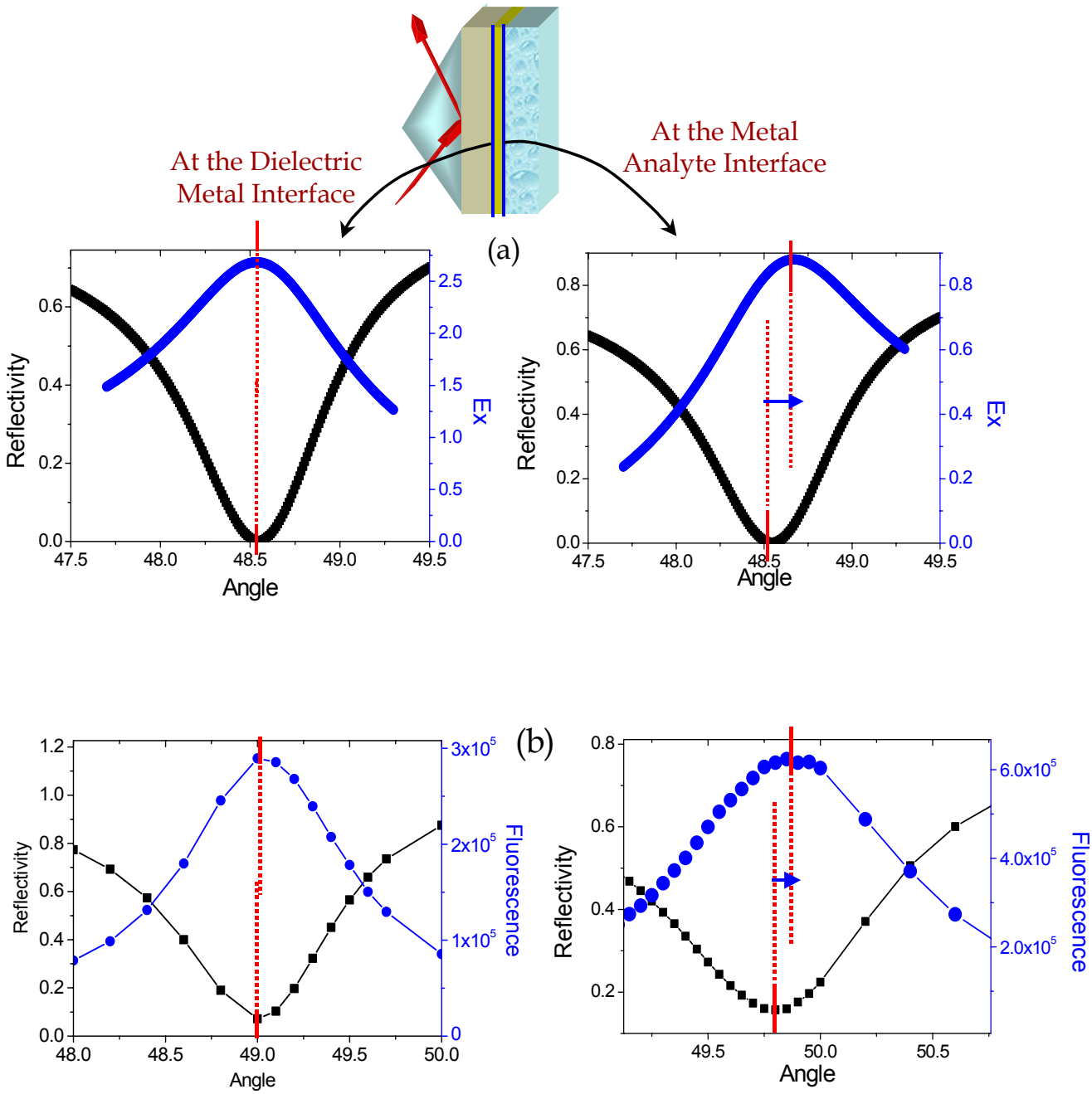

Fig. 6.20 (a) Theoretical simulations of the reflectivity and the fluorescence intensity showing no shift at the dielectric metal interface, and a shift of the maximum fluorescence to higher angle at the metal analyte interface, (b) the same effect was seen experimentally

6.11 Working at high distances above the metal layer

As explained previously, the decay length of the evanescent field is in the range of 150 nm, and that of the LRSPR is 1000 nm (in case of using Teflon). This suggests that it is possible to work at higher distances in case of LRSPR and still being in the vicinity of the evanescent field. This was seen experimentally by spin coating of 500 nm of Teflon above gold in both the SPR and the LRSPR samples. As shown in fig. 6.22, in case of LRSPR the fluorescence signal can be easily seen where it is comparable to the signal of SPR inside the evanescent field, but for SPR, there is almost no signal where this distance is already outside the evanescent field.

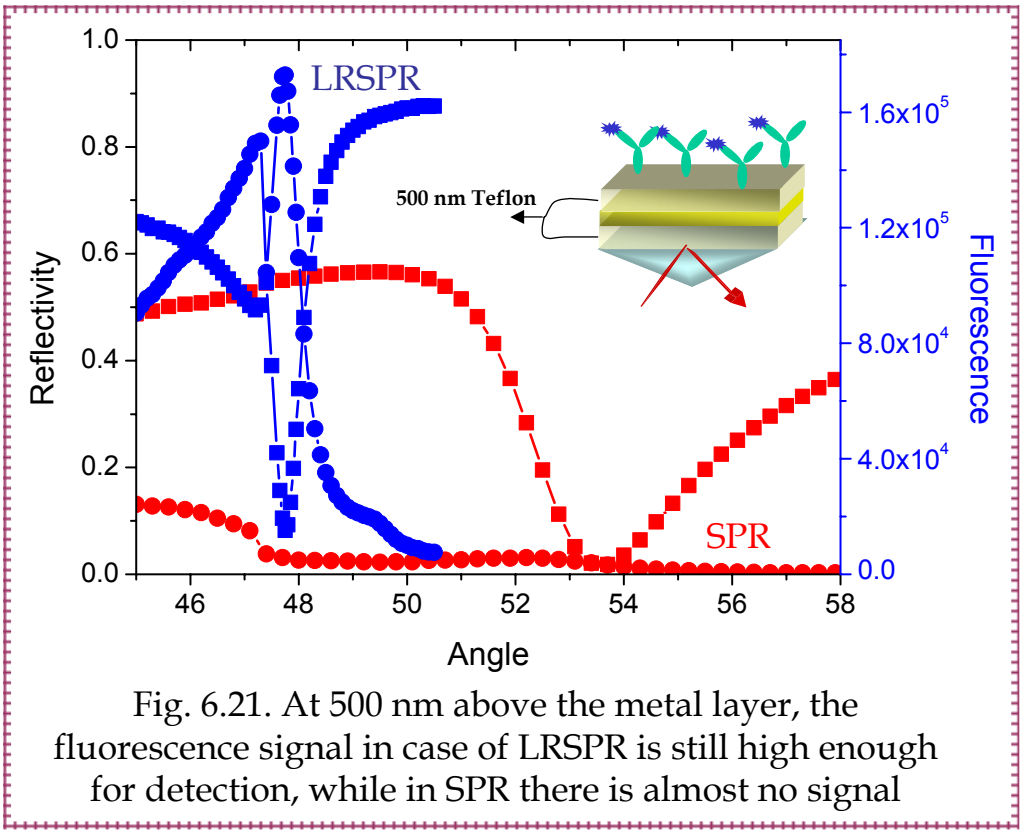

Fig. 6.21. At 500 nm above the metal layer, the fluorescence signal in case of LRSPR is still high enough for detection, while in SPR there is almost no signal

Being able to see a high signal at this distance could be of great interest if a thick matrix, in the range of 100-500 nm, is to be synthesized, having many binding sites. This makes it possible to detect small molecules with very low concentrations.

As in the Biacore chip, where a Dextran matrix in the range of 100 nm is synthesized above the gold layer and could be used to detect 500 aM of an antibody, we tried to imitate this system but with longer chain. Synthesizing this matrix was working but could not be reproduced regularly. However from the previous results, we believe that synthesizing such a matrix can be of great benefit to have a biosensor with extremely high sensitivity.

6.12 Conclusions

We started studying LRSPR to understand some of its fundamentals, but this took us to find out very interesting differences between SPR and LRSPR.

- Looking to the sensitivity, as the angle shift does not give any advantage to this system, as found that the high resolution due to the sharp resonance decreases the angle shift.
- The field intensity at the interface is higher than SPR, and this give this system the higher sensitivity if combined with fluorescence. The fluorescence intensity was found to be about 9 times higher than the SPFS.
- This fluorescence intensity depends on the electric field intensity which is very sensitive to any small change in the thickness or the refractive index of the first dielectric layer, and this is shown as some variations in the fluorescence signal from one experiment to the other.
- The lower refractive index of the Teflon layer was found to have an effect on the fluorescence signal, where the optimum field intensity at the interface was found to be 1.34-1.36, so if a material of this range of refractive index is to be found, we will guarantee a very high fluorescence signal.
- Another interesting difference between SPFS and LRSPFS is the phase shift between the surface mode and the driving photon field. In case of LRSPFS, the shift was found to be in the opposite direction.
- Beside the higher field intensity, one important thing is the decay length of the evanescent field, which is in the range of 400-800 nm in case of LRSPR; this makes it very interesting when using a very long chain matrix for bio-sensing purposes.

Chapter -7-

Summary

7. Summary

Based on surface plasmon resonance spectroscopy and surface plasmon fluorescence spectroscopy, we tried in this work to introduce some ways to develop optical biosensors to be of higher sensitivity. Two main aspects were studied to achieve this purpose.

The first part was concerning grating couplers in biosensors; we started with fabricating of gratings by the embossing technique, which is a fast and cheap way to obtain gratings in a short time. These gratings were checked by AFM and SPR to prove that they can be used as a biosensor.

The next step was to study the back coupling efficiency from a grating coupler and figuring how this back coupling efficiency can depend on the distance between the chromophores and the metal layer. A layer by layer protein system was used to build a spacer between the metal layer and the dye, and it was found that the optimum is about 30 nm above the metal which agrees well with the previous work done on a planar surface.

Measuring the fluorescence signal in case of DNA experiments with grating couplers can decrease the surface sensitivity because of the high bulk signal due to the high contribution of the reflected light with the measured fluorescence signal. In order to overcome this problem, we designed a DNA architecture based on the fluorescence resonance energy transfer. The target to be detected was mixed with another sequence that exhibits a mismatch with the target and which was labelled with another dye that can show FRET effect with the first one. The mixture was immobilized on the surface, where the target was bound to the probe at the same time that all the unbound species in the bulk were quenched. In this case the monitored signal would be coming only from the surface not from the bulk and the surface.

The second part of this work was a systematic investigation of long-range surface plasmons. LRSPR was studied before theoretically and sometimes experimentally with different architectures, but it was never before combined with the fluorescence measurements. Doing this let us find very interesting informations about LRSPR. The idea was using the high field intensity at the interface, which is higher in case of LRSPR than in the conventional SPR, to excite the chromophores. We found that the fluorescence signal in this case is about 9 times higher, which give this system the ability to be used as a very high sensitive device for detection of small molecules with low concentrations.

Having a deeper look into this system, we found that it is very sensitive to any small change in the thickness or the refractive index of the dielectric layer used to support the LRSPR, which was very important to increase the field intensity as possible. A refractive index of 1.36 was found to be the optimum one in this case, which is difficult to get.

The most important aspect about LRSPFS, beside the high field intensity, is the very long evanescent filed that can reach 400-800 nm. The fluorescence signal measured at 500 nm was comparable, if not higher, than the conventional SPFS signal in the vicinity of its field. This means that a very thick matrix can be used having a lot of binding sites to capture proteins, which can increase the fluorescence signal.

Chapter -8-

APPENDICES

8. APPENDICES

Appendix A;

EXPERIMENTAL FACILITIES

A-1. Thin Film Deposition

A-1.1 Thermal Evaporation

The vacuum thermal evaporation deposition technique consists of a heating unit for the material to be deposited. The material vapour finally condenses in form of thin film on the cold substrate surface and on the vacuum chamber walls.

Usually low pressures are used, about 10^{-6} or 10^{-5} Torr, to avoid reaction between the vapour and atmosphere. At these low pressures, the mean free path of vapour atoms is the same order as the vacuum chamber dimensions, so these particles travel in straight lines from the evaporation source towards the substrate. This originates 'shadowing' phenomena with 3D objects, especially in those regions not directly accessible from the evaporation source (crucible).

Besides, in thermal evaporation techniques the average energy of vapour atoms reaching the substrate surface is generally low (tenths of eV). This affects seriously the morphology of the films, often resulting in a porous and little adherent material.

This method was used for preparation of the gold layer used in all the experiments included in this work.

Fig. A-1.1 shows a scheme of the thermal evaporation method.

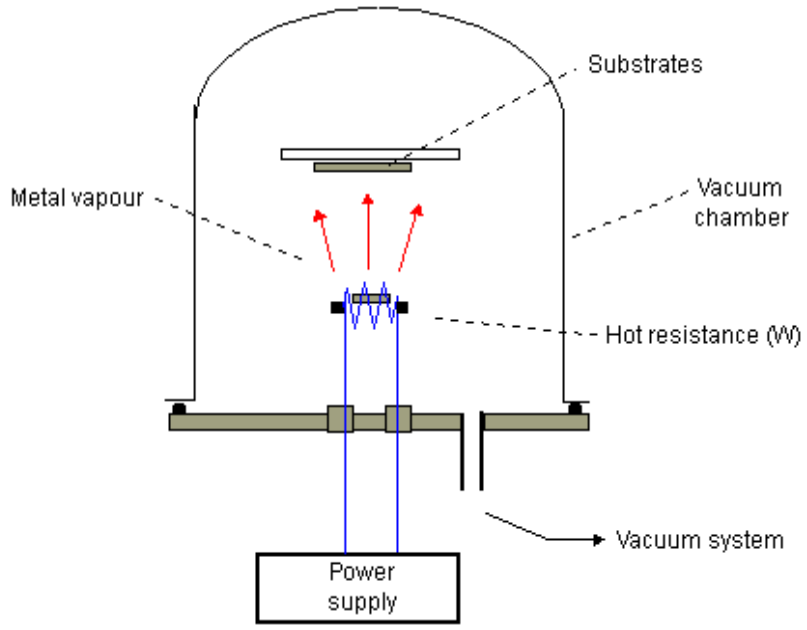

Fig. A-1.1 A scheme of the thermal evaporation method

Evaporation machine

Edwards Auto 305

A-1.2 *Spin Coating*

Spin coating is the preferred method for application of thin, uniform films to flat substrates. An excess amount of polymer solution is placed on the substrate. The substrate is then rotated at high speed in order to spread the fluid by centrifugal force. Rotation is continued for some time, with fluid being spun off the edges of the substrate, until the desired film thickness is achieved. The solvent is usually volatile, providing for its simultaneous evaporation (fig. A-1.2).

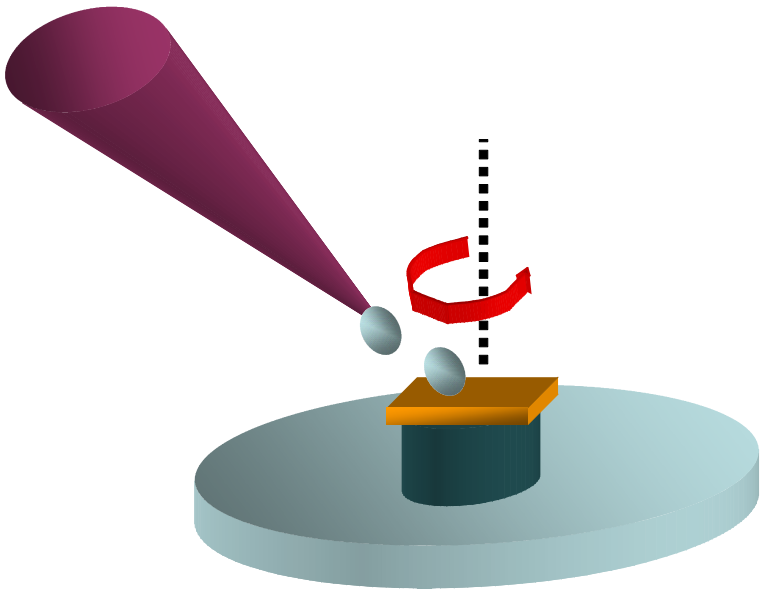

Fig. A-1.2 A scheme of the spin coating technique

A-2. Thickness Measurement by Surface Profiler

The measurement technique used by these instruments is that of optical triangulation, whereby a beam of laser light is focused onto the surface of the sample. A position sensitive detector then collects the diffusely scattered light, and measures the relative height of the sample surface to the sensor (z-height).
These systems measure surface features with a resolution ranging from 0.01 μm to 6.0 μm according to the selected measuring range. They can scan surfaces up to 100x100 mm with a Z travel of 35 mm. Images are displayed in colour on a high resolution screen. Optional CCD camera and a video screen facilitate alignment and visual inspection of small surfaces. Software provides 3D isometric view of scanned area with relative height shown in color bands, 2D view with relative height shown in color shades, and cross section profiles. They can also calculate volume, surface area, surface roughness and perform measurement of special features including length, angle, range etc. Measurements and isometric view can be stored as ASCII exportable data files and processed with PC and Macintosh TM software. Optical surface profiling has several significant advantages over other methods. It is non contact as so preserves the surface integrity of the sample, a crucial issue when the study of unique and often alterated organic materials is concerned. Therefore originals objects can be analyzed without need of taking replicas of the zones of interest as currently done in SEM analysis and when traditional profiling systems are used.

Surface Profiler

KLA-TENCOR P-10

A-3. Contact Angle Measurements

Contact angles of liquids on polymer surfaces are widely used to predict wetting and adhesion properties of these solids by calculating their solid-vapor surface tension. While the theory is based on the equilibrium of an axisymmetric sessile drop on a flat, horizontal, smooth, homogeneous, isotropic, and rigid solid, it is generally found in practice that a whole range of contact angles is accessible experimentally causing wetting or contact angle hysteresis. The reason is that contact angle phenomena are very complicated. Contact angles on polymer surfaces are not only influenced by the interfacial tensions according to Young's equation but also by many other phenomena, such as surface roughness, chemical heterogeneity, sorption layers, molecular orientation, swelling, and partial solution of the polymer or low-molecular constituents in the polymer material. These effects have to be considered when contact angle measurements are used to calculate the solid surface tension of polymers.

The hydrophobicity/hydrophilicity of a solid surface is usually expressed in terms of wettability which can be quantified by contact angle measurements.

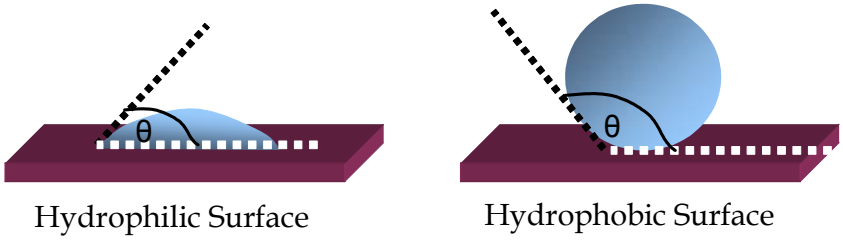

Fig. A-1.3 The difference between the contact angles of hydrophilic and hydrophobic surfaces

For Contact Angle Measurements

Drop shape analysis system DSA10-MK2

A-4. Atomic Force Microscopy

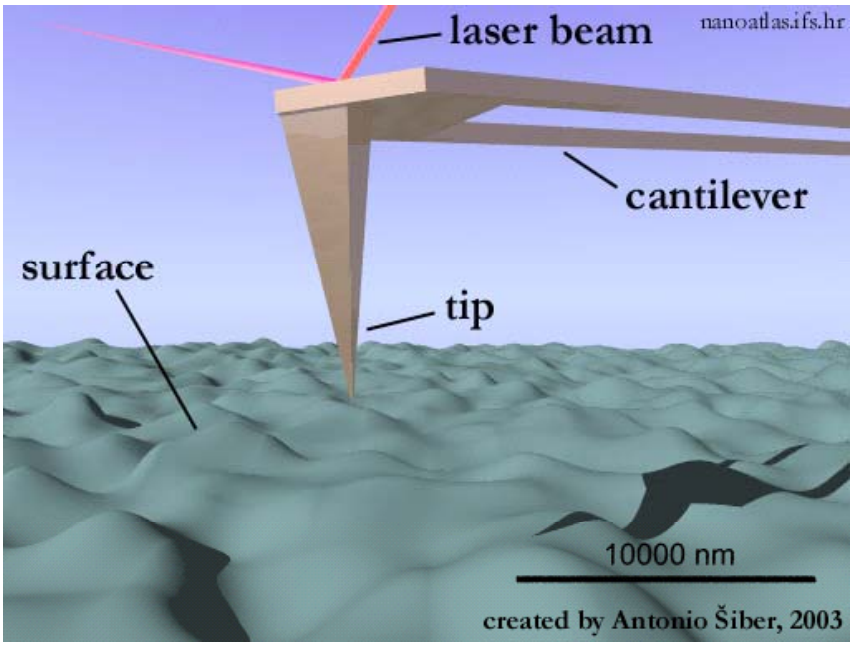

Fig. A-1.4 A picture taken from the internet showing the principle of AFM

The atomic force microscope (AFM), sometimes also called scanning force microscope, was invented by Gerd Binnig, Calvin Quate and Christoph Gerber in 1986. With the AFM conducting and insulating samples can be imaged. Thomas Albrecht and Calvin Quate were the first who imaged an insulator, boron nitride, and could see the periodic structure at atomic resolution. AFMs can be operated in vacuum, air or liquids including water. This opened a wide range of applications. Polymers and biological objects have been studied. Electrochemical processes or the dissolution of crystals can be imaged with atomic resolution.

In the AFM the sample is scanned by a tip, which is mounted to a cantilever spring. Alternatively the sample is scanned underneath the tip. Like in the STM the sample is scanned by a piezoelectric translator. In normal operation the tip actually touches the sample surface, much like the stylus of a record player.

For the AFM, however, the tip is sharper and the tracking force is smaller: typical forces are 0.1 nN to 100 nN. To obtain such small forces the spring constant of cantilevers used must be small. Typical spring constants are 1 N/m. Hence, if an atom while being scanned deflects such a cantilever by 0.1 nm, a force of only 0.1 nN is required.

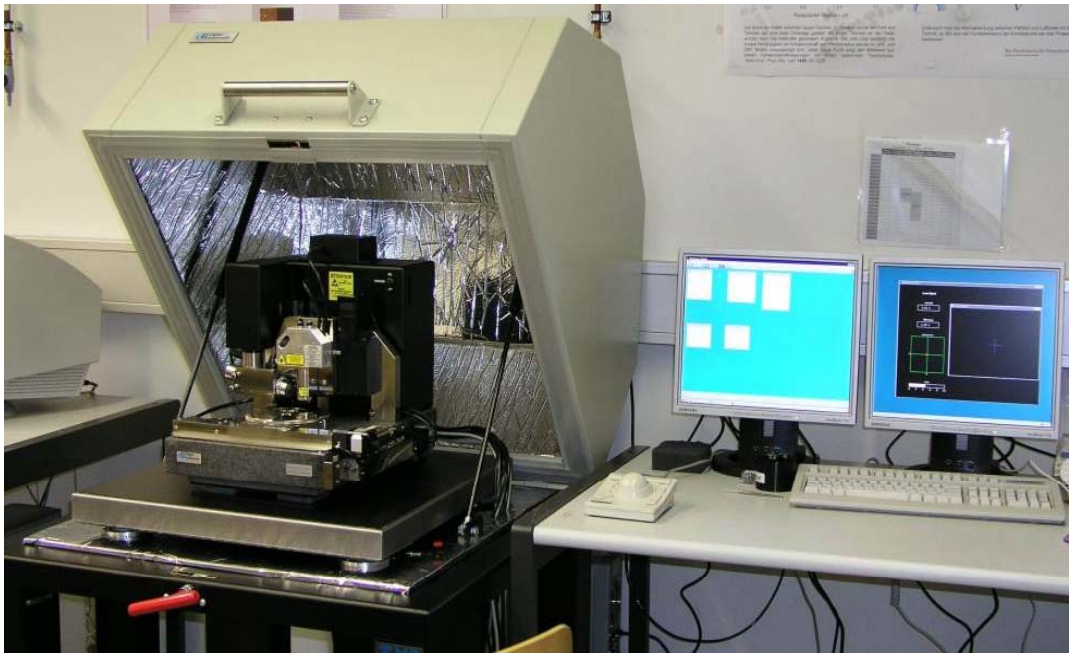

For AFM Measurements

Veeco-Dimension 3100

Appendix B;

LIST OF FIGURES

Chapter 1

Chapter 2

Chapter 3

Chapter 4

Chapter 5

Chapter 6

Chapter 8

Appendix C;

ABBREVIATIONS

AAGR----------Average Annual Growth Rate
AFM----------Atomic Force Microscopy
DNA----------deoxyribonucleic acid
EDC----------carbodiimide hydrochloride
FRET----------Fluorescence Resonance Energy Transfer
FWHM----------Full Width of Half Maximum
IgG----------Immunoglobulin
IR----------Infra Red
LBL----------Layer by Layer
LRSPFS----------Long Rage Surface Plasmon Fluorescence Spectroscopy
LRSPR----------Long Range Surface Plasmon
NHS----------N-hydroxy-succinimide
PBS---------- phosphate buffered saline (buffer)
PMMA----------Poly-methyl methacylate
PMT---------- photo multiplier tube
PS----------Polystyrene
RET---------- Resonance Energy Transfer
rpm----------Round per Minute
SA----------Streptavidin
SER----------Surface Exciton Resonance
SLD----------Scattering Length Density
SPFS---------- Surface Plasmon Fluorescence Spectroscopy
SPPs----------Surface Plasmon Polaritons
SPR ----------Surface Plasmon Resonance
SPW----------Surface Plasmon Wave
TIR----------Total Internal Reflection

CURRICULUM VITAE

Amal Sayed Kasry Female, Born in Bani Suef city, Egypt, 1971, Egyptian

EDUCATION

2003-2006
Johannes Gutenberg University and Max Planck Institute for Polymer Research, Mainz, Germany
PhD in Material Science, Biology Department
"Surface Plasmon Fluorescence Spectroscopy; New trends in Optical Biosensors".

1998-2001
Faculty of Girls, Ain- Shams University, Cairo and the National Centre of Research, Giza, Egypt
M.Sc. in Solid State Physics, Physics Department
"Preparation and Characterization of Thin films for Detection of some Toxic and Flammable Gases".

1995
Minia University, Egypt
Post Graduate Studies for the Partial Fulfilment of the M.Sc. Degree

1989-1993
Beni-Suef Faculty of Science, Cairo University, Egypt,
B. Sc. Physics Department

PUBLICATIONS

1. Long Range Surface Plasmon Fluorescence Spectroscopy as a New Trend in Optical Biosensors
Amal Kasry and Wolfgang Knoll
In Preparation

2. Distance Dependent Back Coupling Efficiency of Metallic Gratings
A. Kasry, Susana Moreno Flores and W. Knoll
In Preparation

3. Bulk Jump Reduction by Chromophore Quenching as a Surface Sensitive System
Amal Kasry and Wolfgang Knoll
In Preparation

4. In-situ Polypeptide Formation on Gold Surface for Biosensor Applications
Hatice Duran, Amal Kasry, Anke Lübbert and Wolfgang Knoll
In preparation

PRESENTATIONS

- **Bulk Jump Reduction by Chromophore Quenching as an Effective Tool for Sensitive DNA Detection,** *Associate European Labs (LEA) meeting, Strasburg, France, December 2005.*
- **Employing Long Range Surface Plasmon Fluorescence Spectroscopy in Biosensors,** *15th IUPAB & 5th EBSA International Biophysics Congress, Montpellier, France, August 2005.*
- **New Trends in Optical Biosensors**, *Internal MPIP seminar, Naurod, Germany, May 2005.*
- **Employing Grating Couplers in Biosensors**, *Associate European Labs (LEA) student meeting, Strasburg, France, December 2004.*
- **Bulk Jump Reduction by Chromophore Quenching** *'The 5th International Conference on Biological Physics ICBP2004 Gothenburg, Sweden, August 2004.*
- **Distance Dependent Coupling Efficiency Between Chromophores and Surface Plasmon Polaritons on Gratings,** *Mainz-Twente-Bath joint seminar, Mainz, Germany, February 2004.*
- **Studying the Fluorescence of Chromophores at Different Distances From a Grating Fabricated by Embossing Technique**, ***Associate European Labs (LEA) student meeting, Strasburg, France, December 2003.***
- **Preparation and Characterization of ZnO thin films for Gas Sensor Applications,** ***The 1st International Material Science and Engineering Conference, Cairo University, Beni-suef, Egypt, 2002.***